CHEMICAL ENGINEERING SCIENCE
GENIE CHIMIQUE

VOL. 13 1960 No. 3

Drying wheat in a spouted bed*

On the continuous, moisture diffusion controlled drying of solid particles in a well-mixed, isothermal bed

H. A. BECKER and H. R. SALLANS
National Research Council of Canada, Prairie Regional Laboratory, Saskatoon, Saskatchewan

(*Received* 9 *March* 1960)

Abstract—The continuous drying of wheat in a spouted bed is idealizable as the drying of uniform, nearly spherical, solid particles in a well-mixed, isothermal bed, with the drying rate controlled by moisture diffusion within the particles and the diffusion coefficient independent of concentration. A rigorous mathematical solution to this general problem is developed. The non-isochronal diffusion equation giving the drying rate is shown to be

$$\bar{M} = 1 - 1{\cdot}04\,X_\tau \exp(-0{\cdot}44\,X_\tau)$$

where $\bar{M} = (\bar{m} - m_s)/m_0 - m_s)$ is the average, reduced free moisture content of the dryer product, $X_\tau = (S/V)\sqrt{(D\theta_\tau)}$, S/V is the particle surface-to-volume ratio, D is the diffusion coefficient and θ_τ is the weight-average residence time in the drying bed. Diffusion coefficients calculated by this equation from data on drying wheat in spouted beds agree closely with the established value $D = 297 \exp(-21960/RT)$. The effective surface moisture content at relative air humidities below about 40 per cent and grain temperatures above about 100 °F is a constant $m_s = 0{\cdot}103$ lb/lb, *dry basis*. The critical grain temperature above which the baking qualities of wheat are thermally injured is given by the relation

$$t_c = 189 - 115\,(m_0 + \bar{m}), \quad (°\mathrm{F})$$

where m_0 and $\bar{m}$ are respectively the initial and final moisture contents in drying. The average heat of desorption of moisture from wheat is estimated to be 150 B.t.u/lb higher than the normal heat of vaporization from a free water surface. The correlations presented facilitate the prediction of drying rates, energy requirements and safe and economical limits of operation for spouted wheat dryers.

Résumé—Dans un lit maintenu en suspension par introduction centrale de l'air, le séchage continu du blé peut-être assimilé à celui de grains solides, uniformes, pratiquement sphériques dans un lit isotherme parfaitement agité ; la vitesse de séchage est controlée par la diffusion de l'humidité à l'intérieur des grains et du coefficient de diffusion indépendant de la concentration. Etablissement d'une solution mathématique rigoureuse pour le problème général.

Dans le cas où les grains n'ont pas un temps de résidence uniforme, l'équation de diffusion exprimant la vitesse de séchage prend la forme :

$$\bar{M} = 1 - 1{,}04\,X_\tau \exp(-0{,}44\,X_\tau)$$

avec $\bar{M} = (\bar{m} - m_s)/m_0 - m_s)$: titre moyen en humidité libre de produit du séchoir, $X_\tau = (S/V)\sqrt{(D\theta_\tau)}$, S/V représente le rapport surface volume, D est le coefficient de diffusion, θ_τ, représente la durée de séjour moyenne dans le lit. Les coefficients de diffusion calculés avec cette équation à partir des données expérimentales pour le séchage du blé dans un lit suspendu sont en étroit accord avec la valeur admise $D = 237 \exp(-21960/RT)$. Pour des humidités relatives de l'air inférieures à 40 pour cent et pour des températures du grain au-dessus de 100 °F, le degré

*Contribution from the National Research Council of Canada, Prairie Regional Laboratory, Saskatoon, Saskatchewan. Issued as N.R.C. No. 5910.

d'humidité superficielle devient constant $m_s = 0{,}103$ lb/lb, produit sec. La température critique où débute l'altération thermique des propriétés panifiables est donnée par

$$t_c = 189 - 115\,(m_0 + \overline{m}), \quad (^\circ\text{F})$$

m_0 et $\overline{m}$ étant respectivement les titres en humidité avant et après séchage. La chaleur moyenne d'élimination de l'humidité est supérieure d'environ 150 B.t.u/lb à la chaleur normale de vaporisation à partir d'une surface libre d'eau. Les corrélations établies dans le mémoire permettent la prédiction des vitesses de séchage, consommation d'énergie, les limites de sécurité et d'économie pour la conduite de séchoirs à blé, à lit suspendu.

Zusammenfassung—Die kontinuierliche Trocknung von Weizen in einem Wirbelbett kann man idealisiert auffassen als Trocknung gleichförmiger, fast kugeliger Feststoffteilchen in einem isothermen, gut durchmischten Bett, wobei die Trocknungsgeschwindigkeit bestimmt wird durch die Feuchtigkeitsdiffusion in den Teilchen und wobei der Diffusionskoeffizient unabhängig von der Konzentration ist. Eine mathematische Lösung wird für dieses allgemeine Problem entwickelt. Die nicht zeitlich konstante Diffusionsgleichung für die Trocknungsgeschwindigkeit wird angegeben als

$$\overline{M} = 1 - 1{\cdot}04\,X_s \exp(-0{\cdot}44\,X_s)$$

wobei $\overline{M} = (m - m_1)/m_0 - m_1)$ der mittlere reduzierte Teuchtigkeitsgehalt des Trockengutes ist, $X_s = (S/V)\sqrt{(D\,\theta_r)}$, S/V das Verhältnis Oberfläche zu Volumen der Teilchen, D der Diffusionskoeffizient und θ_r die auf das Gewicht bezogene mittlere Verweilzeit im Bett. Die mit Hilfe dieser Gleichung aus Werten der Weizentrocknung im Wirbelbett berechneten Diffusionskoeffizienten stimmen gut überein mit der aufgestellten Beziehung $D = 297 \exp(-21960/RT)$. Der effektive Feuchtigkeitsgehalt an der Oberfläche bei relativen Luftfeuchtigkeiten unter ca. 40 prozent und bei Korntemperaturen über ca. 100 °F ist konstant $m_s = 0{\cdot}103$ lb/lb bezogen auf Trockensubstanz. Die kritische Korntemperatur, über welcher die Backqualitäten des Weizens thermisch vermindert werden, ist gegeben durch die Beziehung

$$t_c = 189 - 115\,(m_0 + \overline{m}), \quad (^\circ\text{F})$$

wobei m_0 und $\overline{m}$ die Anfangs- und Endfeuchtigkeitsgehalte bei der Trocknung sind.

Die mittlere Desorptionswärme des Wassers im Weizen wurde mit 150 B.t.u./lb höher gegenüber der normalen Verdampfungswärme von einer freien Wasseroberfläche abgeschätzt. Die angegebenen Korrelationen erleichtern die Voraussage der Trocknungsgeschwindigkeiten, des Energiebedarfs sowie der Sicherheits- und Wirtschaftlichkeitsgrenzen in Weizen-Wirbelschichttrocknern.

INTRODUCTION

THE SPOUTED bed technique, as described by MATHUR and GISHLER [1], is a modification of conventional fluidization techniques which facilitates agitation of beds of relatively coarse particles. Instead of distributing the gas flow at inlet over a major portion of the bed, the gas is made to enter through an orifice or pipe centrally located in the bottom of the bed. The resulting pattern of agitation is a fountain-like turnover of the bed in which the jet of gas from the constricted inlet causes a stream of particles to jet upward through a well-defined core within the bed, while in the surrounding annulus there is a balancing downward movement of the bed in bulk. The advantage is gained (a characteristic of well-agitated beds) that particle temperatures are uniform throughout the bed. In the drying of wheat, grain temperature is the controlling limitation on operation [2], and this advantage is of decided importance. MATHUR and GISHLER [3] therefore made an exploratory study of the continuous drying of wheat in a spouted bed. The present investigation was undertaken to obtain a fundamental analysis of this drying process to guide the design and operation of practical dryers. The analysis demonstrates the rigorous mathematical treatment of the continuous drying of solids in a well-mixed, isothermal bed in the case where diffusion within the solid governs the drying rate and the diffusion coefficient is independent of concentration.

THE DRYER

Fig. 1 shows the salient features of the experimental spouted-bed wheat dryer. The heater, C, was an insulated column 9 in. in diameter by 6 ft. high with a 120° conical bottom and a 1¼ in. diameter standard pipe inlet. The

VOL. 13 1961

cooler, D, was a geometrically similar unit with a column diameter of 6 in.

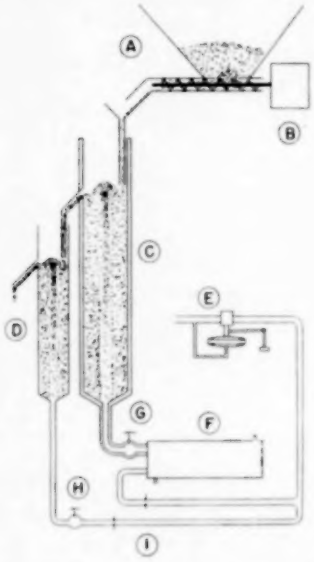

FIG. 1. Spouted bed wheat dryer. A, feeder; B, variable speed drive and motor; C, heater; D, cooler; E, pressure reducing valve; F, heat exchanger; G, H, gate valves; and I, orifice meters.

THE WHEAT

Three series of drying runs were made. Registered seed wheat (series 1, a No. 1 Rescue wheat; series 2, a No. 1 Thatcher; and series 3, a No. 2 Thatcher) was used throughout to ensure that the wheat was sound, clean, and of high and uniform baking quality. The wheat of series 3 was also used in fundamental studies of moisture movement within the wheat kernel [4], the moisture desorption isotherm of wheat [5] and the correlation of the loaf volume of thermally damaged wheat with time, temperature and moisture content [2].

The mean kernel diameter of the Thatcher wheats, expressed as the diameter of an equi-volumed sphere and measured at a moisture content of 0·10 lb/lb, dry basis, was $D_p = 0{\cdot}118$ ft. The surface sphericity (shape factor) of Thatcher wheat, based on the visibly exposed surface area, has been estimated [6] as $\Psi = 0{\cdot}91$, and may be assumed to be the same for all varieties of wheat. The kernel diameter of the Rescue wheat was 0·0110 ft. The distribution of kernel size in wheat of good grade is narrow, and is not a factor in the practical analysis of a drying operation [6].

The density of moisture-free wheat is 90·5 lb/ft^3 [6] and its heat capacity is 0·30 B.t.u./lb °F [7, 8]. Water held by wheat as moisture has practically the same density [6] and heat capacity [7] as normal liquid water.

METHODS

Tempering procedure

The moisture content of the wheat was raised to approximately 25 per cent, dry basis, by adding a measured quantity of liquid water. A conditioning period of 48 hr at 75 °F was found adequate for the absorption and uniform distribution of the added water. The wheat was thoroughly mixed at intervals during this period.

Starting procedure

The dryer was not emptied between runs. Operation was begun by introducing to the heater and cooler beds a flow of air slightly exceeding the minimum required for spouting. Feeding of wheat was commenced when the heater bed approached the expected steady state temperature. The unit was then operated for three more hours before measurements were begun.

Grain temperature measurement

A sampling cup mounted on a rod and provided with a cover removable by pulling a string was used to take wheat samples from any part of the heater bed. A fine thermocouple was immediately inserted in the sample and the temperature quickly taken. (Grain temperature must be measured immediately on removing a sample from the environment under study, before thermal effects accompanying the equilibration of moisture within and between kernels cause an appreciable rise in temperature [5].)

Air temperature measurement

Local air temperatures in the heater bed were measured with a thermocouple probe. The cylindrical probe tip housing the junction was made of wire gauze, and was loosely packed with glass wool to provide a radiation shield.

Humidity measurement

Humidities were determined gravimetrically. In determining the average humidity at the heater outlet, a stack of baffles was placed inside the column to ensure that the air sampled represented the average outlet composition.

Moisture determination

Moisture contents were determined by the one hour, 130 °C oven method [9], and are reported in lb/lb, dry basis, unless otherwise noted.

Baking test

Samples of feed and product were retained for baking tests. The feed sample was first air dried to 14 per cent moisture content, wet basis, at room temperature; both samples were then stored at 10 °C to minimize any change in baking quality between the end of a drying run and the time at which the baking tests were done. Baking tests were carried out using the standard test formula with the addition of two p.p.m. potassium bromate, since the bromate formula best reveals thermal damage to baking quality [2].

Table 1 *Operating data for series* 3

L = bed depth = 3 ft $\quad\quad$ θ_r = 0·013 hr

Run	GA (lb/hr)	W (lb/hr)	t_i (°F)	t_0 (°F)	t_e (°F)	θ_r (hr)	m_0 (lb/lb)	$\bar{m}$ (lb/lb)
1	342	87·8	207	83	114	0·639	0·2580	0·1960
2	334	90·0	249	85	127	0·591	0·2530	0·1810
3	323	94·2	331	84	153	0·571	0·2523	0·1560
4	321	61·5	223	79	124	0·884	0·2433	0·1743
5	321	68·7	289	81	145	0·784	0·2546	0·1612
6	321	76·0	247	81	128	0·703	0·2470	0·1775
7	318	77·2	325	80	153	0·705	0·2517	0·1572
8	318	71·5	327	81	161	0·698	0·2480	0·1450
9	316	62·9	330	81	167	0·767	0·2533	0·1414
10	327	49·5	243	78	141	1·100	0·2560	0·1520
11	332	58·9	269	80	145	0·923	0·2560	0·1572
12	325	77·8	304	81	149	0·697	0·2535	0·1582

It was not known at the outset that the uniformity of grain temperature in the spouted heater would permit operation at inlet air temperatures greatly exceeding the limits assigned to conventional dryers. As a result, the first two series of drying runs were largely wasted because the conditions chosen were not severe enough to damage the wheat. Attention will therefore be focused chiefly on the third series, in which significant damage occurred in five out of twelve runs. Operating data for this series are given in Table 1.

Local Conditions in the Spouted Heater Bed

A knowledge of local conditions in a dryer is a requisite for a fundamental analysis of the drying operation. Exhaustive observations of local grain and air temperatures and air humidities in the heater bed were therefore made under all operating conditions. The data were then analysed to discover their general mode and significance.

Local air temperatures

Fig. 2, which is roughly applicable to all runs, shows that the temperature of air flowing through the heater bed fell very rapidly, and in the annulus (i.e., the downward moving, quiescent bed surrounding the central, upward moving jet stream or "spout" of particles) approached thermal equilibrium with the bed at a distance of about 15 in. above the gas inlet. In the spout, the drop in temperature was stretched over a slightly greater distance, owing to the higher air velocity and sparser particle population. It is evident that, except in impractically shallow beds, air leaving a spouted wheat bed can be expected to be in thermal equilibrium with the bed at exit.

The transfer of heat in a spouted bed is not amenable to exact analysis, owing to the impossibility of accurately determining the density of

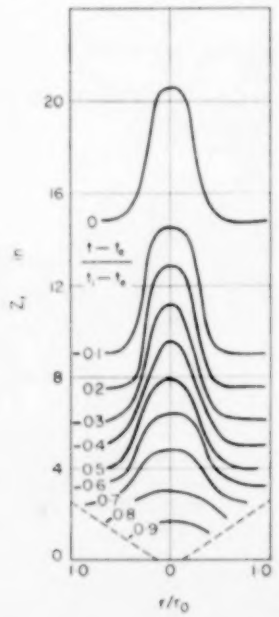

Fig. 2. Air isothermals in the heater bed.

particle population and the distribution of air flow in the zone of heat exchange. However, data can be roughly correlated as follows: the integral equation of heat transfer (with a constant transfer coefficient) for a hot stream of gas flowing uniformly through a deep, isothermal bed is easily shown to be

$$\frac{t - t_e}{t_i - t_e} = \exp\left(-\frac{h_c a z}{G c_p}\right) \qquad (1)$$

If as in the present case this equation is not strictly applicable, a correlation dependent on the gas and particle flow patterns will still exist between appropriately chosen values of the groups $(t - t_e)/(t_i - t_e)$ and az/Gc_p. Fig. 3 shows such a correlation of the air temperature in the annulus with the height above the gas inlet. The differences in this relation series between 1, 2 and 3 must be ascribed to the effects of small differences in particle size and shape on the grain and air flow patterns. The data of series 3 show a long region of linearity in which a mean heat transfer coefficient of 2·9 B.t.u/ft² hr °F can be calculated by equation (1). The expected value of the true local coefficient calculated from the correlation of Gamson *et al.* [10] for packed beds for a mean Reynolds number of 150 is 53 B.t.u/ft² hr °F. The difference between these values cannot be explained through the gas flow pattern; e.g. if it is assumed that the gas flow rate in the annulus, G_a, increased linearly with increasing height z above the gas inlet, from zero at $z = 0$ to $\frac{1}{2}G$ at $z = 1$ ft, the differential heat transfer equation for the annular bed with this gas flow pattern

$$\frac{-d\ln\left[(t - t_e)/(t_i - t_e)\right]}{d\ln z} = \frac{h_c a}{c_p\,(dG_a/dz)} + 1$$

gives heat transfer coefficients which are still an order of magnitude smaller than predicted. The only other explanation that could adequately account for the observed low rate of heat transfer is that the surface temperature of the grain in the zone of high average grain–air temperature differences was considerably above the average bed temperature. It therefore appears that in the zone of heat exchange of the heater bed sharp temperature gradients existed in wheat kernels in the immediate neighbourhood of their exposed surfaces.

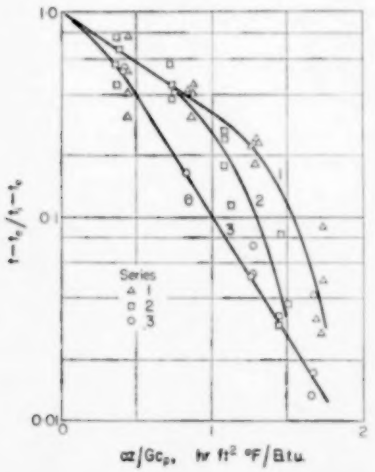

Fig. 3. Correlation of annular air temperatures in the heater bed.

	Series	G (lb/hr ft²)	$(t_i - t_e)$ (°F)	a^* (ft²/ft³)
△	1	730–800	97–135	319
□	2	850	54–75	298
○	3	730	99–246	298

*Based on an average fraction void of 0·45.

Local grain temperatures

Fig. 4 shows the longitudinal profile of measured grain temperatures in the annulus of the heater bed. As the wheat moved downwards through the zone of heat exchange (Fig. 2), it absorbed

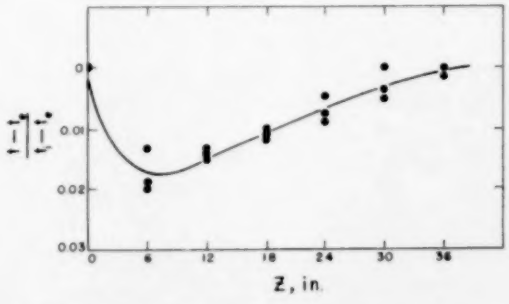

Fig. 4. Longitudinal profile of grain temperatures in the annulus of the heater bed.

heat and its temperature rose to a maximum at the base of the bed. At this point the wheat was entrained by the spout and swept to the top of the bed, its residence in the spout being so fleeting as to permit no change in its thermal condition. The grain then journeyed down the annulus back to the zone of heat exchange, the heat absorbed earlier in that zone being converted to the evaporation of moisture in the course of the journey.

Since the difference between maximum and minimum average grain temperatures in the bed represents heat absorbed for the removal of moisture, its maximum magnitude is given by the quotient of the total heat capacity of the bed into the heat used for evaporation per bed turnover cycle:

$$\Delta t_b = \frac{W\,(m_0 - \bar{m})\,(h_{fg} + \bar{h}_d)\,(\theta_c)}{B\,(c_w + mc_f)} = \frac{(m_0 - \bar{m})\,(h_g + \bar{h}_d)}{c_w + \bar{m}c_f}\,\frac{\theta_c}{\theta_r} \quad (2)$$

Observed values of Δt_b may be expected to be smaller than this by an amount roughly proportional to the fraction of the bed volume occupied by the zone of heat exchange, since the evaporation of moisture continues unabated during that part of the bed turnover cycle in which heat is being absorbed. Thus, the present experimental values of Δt_b were approximately 20 per cent lower than predicted. The observed values in all runs were in the range 2–4 °F.

It may be enquired how the measured temperature of grain taken from the zone of heat exchange was affected by gradients in the local temperature within kernels. Relevant to this question, suppose that a wheat kernel at an uniform initial temperature t_0 is suddenly put into an environment where its surface temperature assumes a constant value t_s. How long will it take until the difference between the surface and the average kernel temperatures is only 1 per cent of the initial difference, $t_0 - t_s$? The diffusion equation (3), which is also a heat conduction equation, predicts a reduced time for this event of $X^2 = 3{\cdot}75$. To translate this figure into dimensional time, consider the following data: the thermal conductivity of wheat may be conservatively assumed to be at least 0·1 B.t.u/ft hr °F, (the value for rubber, leather, celluloid and hardwood). Average values of the heat capacity and density of moist wheat are, respectively, 0·45 B.t.u/lb °F and 85 lb/ft³, giving for the thermal diffusivity of moist wheat the value 0·0026 ft²/hr. The volume-to-surface ratio of an average wheat kernel is 0·00175 ft. Thus the time in question is

$$\frac{X^2\,(V/S)^2}{D} = \frac{3{\cdot}75\,(0{\cdot}00175)^2}{0{\cdot}0026} = 0{\cdot}0044 \text{ hr or } 16 \text{ sec}$$

Since the grain temperature was experimentally recorded 20–30 sec after removing a sample from the heater bed (this being the time required for the manipulations involved in the measurement). there is no doubt that temperature gradients within kernels effectively disappeared before the grain temperature was taken. There was certainly no tendency observed for the measured temperature of a sample to *fall* with time; instead, it tended to rise, very slowly but still perceptibly, owing to the slight evolution of heat accompanying the gradual dissipation of moisture gradients [5]. The quickly measured grain temperatures are therefore correctly interpreted as weight-average values assumed upon thermal equilibration of samples.

The foregoing calculation also confirms that significant elevations of the surface temperature of wheat kernels in the heater bed were certainly likely in the presence of large grain–air temperature differences, but could not have persisted for any appreciable time outside the zone of heat exchange.

Local air humidities

The humidity of air flowing through the annulus of the heater bed increased at an accelerating rate up to about 12 in. above the gas inlet, and from there on varied linearly with distance above the inlet. Fig. 5 shows the humidity profile at bed outlet and shows that air from the spout emerged with a lower humidity than air from the annulus. This pattern is due to the fact that air in the spout moved at a higher velocity and contacted fewer particles than air in the annulus.

VOL. 13 1961

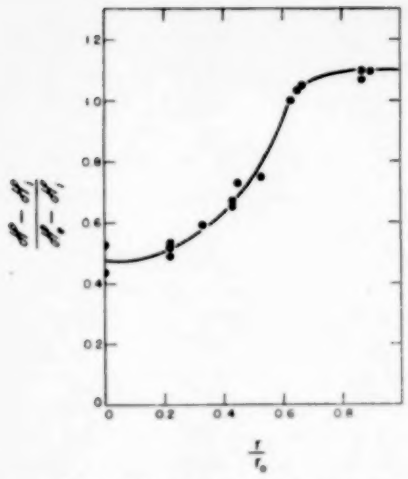

FIG. 5. Radial profile of air humidities at outlet of the heater bed.

CORRELATION OF THE DRYING RATE

The rate of drying of the wheat kernel under conditions in which the resistance to external mass transfer is small is governed by moisture diffusion within the kernel [4, 6, 11]. The external resistance in the normal atmosphere is easily reduced by circulating air past the kernel, and is negligible even at Reynolds numbers $D_v G/\mu$ as low as twenty-five [8]. The rate of isothermal drying in air of constant humidity has been described [4, 12] by the integral equation for unsteady state diffusion out of spheres subject to the conditions

$m = m_0$, $\theta = 0$
$m = m_s$ (constant) at the bounding surface, $\theta > 0$
D = constant

More recently [6], it has been shown that the non-spherical shape of the wheat kernel can be held account of if the equation is written in the general form

$$\bar{M} = \frac{6}{\pi^2} \sum_{n=1}^{\infty} \frac{1}{n^2} \exp\left(-\frac{n^2 \pi^2}{9} X^2\right) \qquad (3)$$

At reduced drying times X^2 smaller than unity, the sum on the r.h.s. closely approximates [6]

$$\bar{M} = 1 - \frac{2}{\sqrt{\pi}} . X + 0{\cdot}33\, X^2 \qquad (4)$$

while at values of X^2 larger than unity the series reduces to one significant term. The diffusion coefficient has been shown to be independent of moisture level in the range 0·13–0·25 lb/lb [4, 6] in which the data of three investigations [4, 6, 11] are represented by the Arrhenius equation

$$D = 297 \exp(-21960/RT) \qquad (5)$$

The effective value found for the surface moisture content m_s when drying wheat in a stream of dry air was 0·103 lb/lb [4], which agrees reasonably well with the values of 0·099 to 0·105 lb/lb later found for vacuum drying [6].

The diffusion equations (3) and (4) provide a rational basis for correlating drying rates in the spouted heater bed. Conditions in the heater approached the prescribed ideal reasonably closely.

(i) *Isothermicity*

It has been seen that the maximum variation in measured grain temperatures in the heater bed was only 2°–4 °F. Feed entered the bed at room temperature but was, it can be confidently assumed, very quickly heated to the temperature of the bed, (singly exposed wheat kernels placed in a hot air stream approach the air temperature within a few minutes [4] while in the spouted heater heat transfer to the feed was augmented by direct thermal contact with the surrounding hot grain). Significant elevations in the surface temperature of grain evidently occured in the zone of heat exchange, but this zone comprised only a minor fraction of the volume of the bed. Altogether, it is quite reasonable to suppose that the weight fraction of bed material with a temperature differing profoundly from the average was negligibly small insofar as diffusional analysis of the drying process is concerned. The temperature dependency of the diffusion coefficient should not be expected to be a factor in the analysis; the coefficient should exhibit the constant value corresponding to the average bed temperature.

(ii) *Boundary conditions and constancy of the effective surface moisture content*

An experiment was carried out to ascertain

the effect of the relative humidity of circulated air on the effective surface moisture content. Fully exposed wheat kernels were dried 20 min at 77 °F and constant relative humidity in an apparatus previously described [4], the humidity being regulated by carrying out the experiments in a controlled humidity chamber. The effective surface moisture content was then determined from the regression of the moisture loss on the initial moisture content [4, 6]. Fig. 6 shows the values so obtained as a function of the relative humidity. It is seen that at high relative humidities the dynamic equilibrium data merge

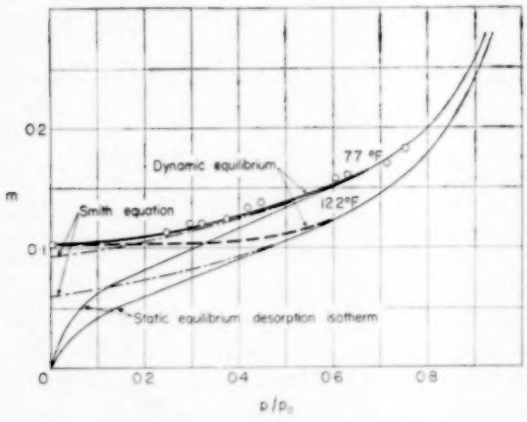

Fig. 6. Correlation of the effective surface moisture content of isothermally drying wheat with the relative water vapour pressure of the drying air.

with the static equilibrium desorption isotherm previously determined [5], while at low relative humidities they decline to a limiting minimum value of 0·103 lb/lb, which is the effective value of the surface moisture content when drying in moisture-free air [4]. The data are rather closely represented by Smith's isotherm equation [13]

$$\frac{m}{1+m} = \varpi_b - \varpi' \ln\left(1 - \frac{p}{p_0}\right)$$

which was derived for the sorption of normally condensed water on a monolayer of strongly adsorbed water molecules. This coincidence is theoretically plausible, in view of the fact that the dynamic surface moisture content at zero relative humidity is closely related to the number of primary sites available for adsorption [14], and it is quite reasonable to postulate that in general the relation between the effective surface moisture content in air drying and the relative humidity is closely approximated by merging the constant value $m_s = 0{\cdot}103$ prevailing at low relative humidities with Smith's isotherm at high relative humidities (the broken curve for 122 °F in Fig. 6 was constructed on this basis). Relative humidities at the outlet of the spouted heater were low, being in the range 7–25 per cent, and the lowest bed temperature was 100 °F. Fig. 6 indicates that one is entirely justified in assuming that in these circumstances the surface moisture content takes the constant value effective at low relative humidities, 0·103 lb/lb. Hence the boundary condition m_s = constant at $\theta > 0$ may be assumed to be generally satisfied.

(iii) *Isochronicity*

The condition of isochronal drying of wheat kernels in the spouted heater, necessary for simple application of the diffusion equations (3) and (4), was clearly not fulfilled. However, no serious difficulty is raised thereby, the mathematical form of the distribution of drying times being easily ascertainable as follows if it is assumed that mixing in a spouted bed is instantaneous and perfect. Suppose that the flow of feed is quantized in infinitely divisible slugs of dry mass δ_0, δ_0 being vanishingly small compared with the hold-up in the bed, B. If δ is the part of a slug still remaining in the bed at a time θ after injection, then the rate of erosion of the slug at that instant is $-d\delta/d\theta$. Simultaneously, the rate of efflux of the slug in the product stream is $W\delta/B = \delta/\theta_r$, where δ/B is the concentration of slug material in the product stream. Hence, by material balance,

$$\frac{-d\delta}{d\theta} = \frac{\delta}{\theta_r} \tag{7}$$

Integration of this equation subject to the condition
$\delta = \delta_0$ at $\theta = 0$ gives the residence time distribution

$$\frac{\delta}{\delta_0} = \exp\left(\frac{-\theta}{\theta_r}\right) \tag{8}$$

VOL. 13 1961

where δ/δ_0 is the fraction of material having a reduced residence time in the bed of θ/θ_r or longer.

The assumption of perfect mixing in the spouted heater bed was tested experimentally by injecting slugs of dyed wheat into the bed at the feed point and following the decrease in concentration in the bed with time. Fig. 7 indicates that in the range of weight-average residence times, θ_r, of the drying runs the assumption is fully justified. The moderate scatter of the data about the theoretical curve of equation (8) is attributable to the vagaries of the mixing process whereby a slug loses its identity in the bed, and may be assumed to have negligible significance for a diffusional analysis of the drying process.

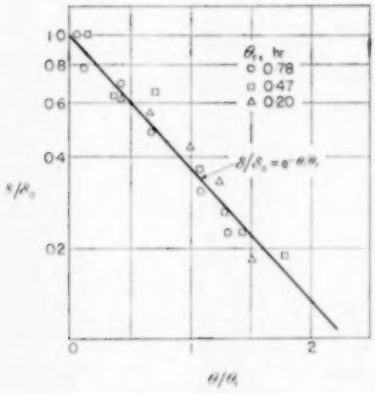

FIG. 7. Correlation of tracer data demonstrating the practical validity of the residence time distribution equation.
θ_r, hr ○ 0·78 □ 0·47 △ 0·20

To analyse the effect of the drying time distribution on the diffusional behaviour, recall the fate of a slug of feed δ_0 on entering the bed and consider the distribution of moisture content among successive fractions of the slug, $d(\delta/\delta_0)$ in size, leaving the bed at intervals of reduced time $d(\theta/\theta_r)$. If the period of consideration is extended to time infinity the reduced free moisture content of wheat leaving the heater is seen to have the average value

$$\bar{M} = \int_0^1 \bar{M}\, d\left(\frac{\delta}{\delta_0}\right) \qquad (10)$$

Substituting the diffusion equation (3) for $\bar{M}$ and the residence time distribution equation (8) for δ/δ_0, this becomes

$$\bar{M} = \int_0^\infty \frac{6}{\pi^2} \sum_{n=1}^{\infty} \frac{1}{n^2} \exp\left\{-\phi\left(\frac{n^2\pi^2}{2} X_r^2 + 1\right)\right\} d\phi \qquad (11)$$

The integral on the r.h.s. of equation (10) can be evaluated graphically, using published solutions [15, 16] of the diffusion equation (3) or solutions calculated from the limiting forms discussed in connexion with equation (4). It was thus found that in the practically important range of values X_r of 0·3 to 1·5, equation (11) is closely represented by the empirical equation

$$\bar{M} = 1 - 1{\cdot}04\, X_r \exp(-0{\cdot}44\, X_r) \qquad (12)$$

This it may be noted is a general integral diffusion equation for continuous drying in a well-mixed bed of spherical or near-spherical particles. Comparison with the equations for isochronal drying (e.g. equation 4) shows as should be expected that the distribution in residence time leads to a smaller average moisture reduction in a given weight-average residence time than if the exposure were uniform.

The validity of the non-isochronal diffusion equation (12) for the spouted heater may be verified by demonstrating the normality of diffusion coefficients calculated thereby from the drying data. Fig. 8 shows coefficients calculated from the present and from MATHUR and GISHLER's [3] data as a function of the reciprocal of the average absolute grain temperature,

$$T = 460 + t_e - \frac{\Delta t_h}{2}$$

and compares these with the very accurately determined relation for isochronal vacuum drying [6] and with the previous data on isochronal air drying [4]. The particle volume-to-surface ratio, V/S, was evaluated for these calculations at the surface moisture content (0·103 lb/lb), which has been recommended for the case in which the temporal variation in kernel volume is small [6]. It is

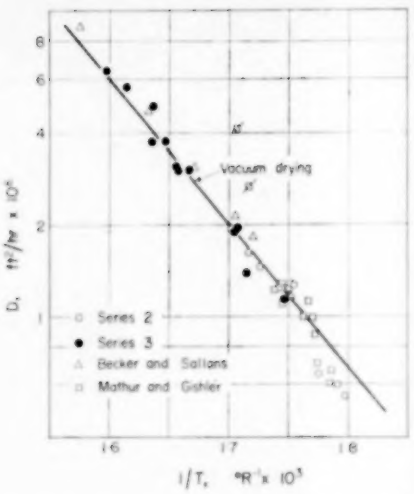

FIG. 8. Arrhenius correlation of the moisture diffusion coefficient, showing a general comparison between values calculated from data on spouted heaters and previous values for isochronal air and vacuum drying.
○ Series 2 ● Series 3
△ BECKER and SALLANS □ MATHUR and GISHLER

seen that the data of series 3 are in excellent agreement with the data on isochronal drying. So also are the data of series 2 and of MATHUR and GISHLER [3], with the exception of eight points whose irregularity is explained by abnormal conditions in the runs concerned: the large positive deviation of the two highest points (marked with slashed squares in Fig. 8) accompanies the use of shallow beds (1 and 2ft. deep) together with low weight-average residence times (0·067 and 0·140 hr), and is undoubtedly due to failure of the assumptions of isothermicity and perfect mixing under these impractical conditions. It is noteworthy that for other runs of MATHUR and GISHLER [3] with weight-average residence times as low as 0·200 hr, but with a normal bed depth of 4 ft, the diffusion coefficients are entirely normal. The consistent negative deviation of the six lowest points (those at $10^3/T > 1{\cdot}77$) is explained by the fact that the outlet relative humidities in these runs were in the high range of 50–60 per cent. Due to the combination of high average relative humidity and low bed temperature the effective surface moistures were assuredly higher than the assumed value of 0·103 lb/lb, as may be judged from Fig. 6. The standard deviation of the normal data from the relation for vacuum drying is $\pm$ 8·5 per cent. Altogether then the diffusion coefficients calculated from the data on drying in spouted heaters correlate very satisfactorily in a normal Arrhenius manner with the reciprocal of the average absolute grain temperature, the exceptions only serving to emphasize the expected conditions for deviation. Moreover, they agree closely with the Arrhenius relation $D = 297 \exp(-21960/RT)$ which has been accurately established by vacuum drying experiments [6], the application of vacuum having no demonstrable effect on the diffusion coefficient [6]. These results conclusively prove the validity of the non-isochronal diffusion equation (12) and its underlying assumptions in interpreting the present (and similar) data.

It should be noted that Fig. 8 also constitutes an ultimate correlation of drying rates. The standard deviation of the experimental drying rates from the values calculated by the conjunction of equations (5) and (12) is approximately $\pm$ 5 per cent, the drying rate being more nearly proportional to the square root of the diffusion coefficient than to its absolute value.

CORRELATION OF THE THERMAL DAMAGE RATE

The rate at which an organic solid can be dried is usually limited by the fact that its temperature must be held below certain critical levels if irreversible damage to product quality is to be avoided. Excessive thermal treatment of wheat leads to deterioration of its bread-making quality, due to thermal denaturation of the proteins. An earlier study [2] demonstrated that the extent of such damage is most clearly reflected by the decrease in volume of test loaves baked by the bromate formula. A first-order rate expression was found to apply:

$$\ln \frac{1}{V_L} = k_r \theta \qquad (13)$$

The rate constant followed the Arrhenius temperature dependency

$$k_r = A \exp\left(\frac{-116300}{RT}\right) \qquad (14)$$

The frequency factor A was found to be a function of moisture content, and is closely approximated at moistures above 0·11 lb/lb by the formula

$$\log A = 46{\cdot}59 + 8{\cdot}45 \log m \qquad (15)$$

These equations for the rate of thermal damage can be applied to the drying process in the spouted heater and, as in the case of the diffusion equations the analysis should take into account the distribution in residence time. However in this case the complexity of the situation, which also involves moisture distributions and gradients, is too great to permit of a fundamental analysis, and so equation (13) will be used directly in conjunction with the weight-average residence time, θ_r. This should not prove seriously objectionable, since the effects of temperature and moisture content ordinarily outweigh those of time [2].

Values of the rate constant were calculated for those runs (all in series 3) in which significant damage occurred, and are shown in Fig. 9 as a function of the absolute grain temperature at bed

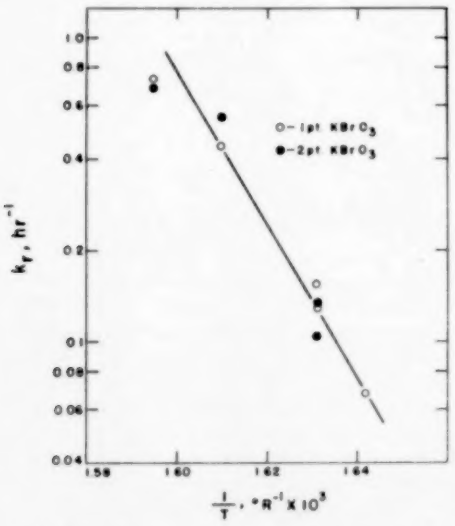

Fig. 9. Arrhenius correlation of the rate constant for thermal damage to the baking properties of wheat.
○ – 1 pt K Br 0_3 ● – 2 pt K Br 0_3

outlet, $T = 460 + t_r$. This, the maximum average grain temperature, was chosen in preference to the average bed temperature in order to assure a maximum safety factor in the correlations which follow. The curve representing the data was drawn for an energy of activation of 116,300 B.t.u./mole, the value in equation (14), and gives for the frequency factor in this equation the value $\log A = 40{\cdot}56$. This value of $\log A$ can be inserted in equation (15) to define a mean moisture content – one weighted for thermal damage to baking quality – for the runs concerned, and gives a value of 0·193 lb/lb for this parameter. This corresponds closely with the arithmetic mean moisture content in the heater, $(m_0 + \bar{m})/2$, which was in the range 0·196–0·205 lb/lb.

Fig. 10 shows an easily visualized interpretation of the data for all three series of drying runs. The group $(1 - V_L)/\theta_r$ is an approximation to the rate constant which is practically linear with grain temperature in the region of significant

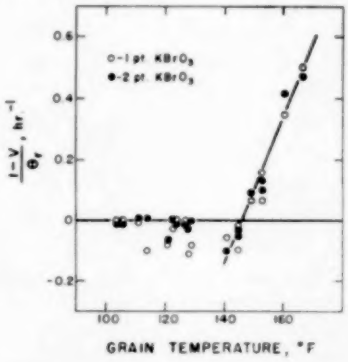

Fig. 10. Simplified correlation of damage rates in the spouted heater, showing the critical damage temperature.
○ – 1 pt K B 0_3 ● – 1 pt K Br 0_3

damage. It is clearly seen that the limiting safe grain temperature in the heater was 146 °F. At lower temperatures significant improvements in baking quality occurred in many runs. An earlier study [2] quoted critical grain temperatures for drying, calculated from equations (13), (14) and (15) for the heat treatment at constant moisture required to produce a 3 per cent decrease in loaf volume in 1 hr. (3 per cent is considered to be the minimum significant deviation in loaf volume, while at temperatures close to the critical drying times will not ordinarily exceed 1 hr).

At moisture contents above 0·11 lb/lb, these calculated critical temperatures are represented by the formula

$$t = 189 - 230\,m \qquad (16)$$

The critical temperature predicted by this formula for the arithmetic mean moisture in the heater of 0·20 lb/lb is 143 °F, in good accord with the value given by Fig. 10. One may therefore conclude that the critical bed temperature for drying wheat in a spouted heater can in general be estimated by writing equation (16) in the form

$$t_c = 189 - 115\,(m_0 + \bar{m}) \qquad (17)$$

That this equation can be safely relied on is easily seen by considering the fact that in practice moisture reductions, $m_0 - \bar{m}$, do not ordinarily exceed 0·10 lb/lb; the effect of any error in adopting the arithmetic mean moisture content in equation (17) could not therefore cause an error greater than at most 5° F in estimating t_c. To be conservative, one could in practice subtract 5° F from the critical temperature given by the equation.

The practical significance of equation (17) is that it expresses the limit on the rate at which wheat can be dried in a spouted heater if the breadmaking quality of the wheat is to be preserved unimpaired. If however the property which must be preserved during the process of drying is the viability of the wheat as seed grain, then an expression differing from equation (17), though most likely similar in form, will apply (the damage mechanism will still be thermal denaturation, but a different set of molecules with different Arrhenius constants will probably be of dominant importance). Commercial drying practice seems to indicate that critical temperatures for the preservation of viability are perhaps 20°–30 °F lower than those for the preservation of breadmaking quality.

The Energy Balance

The diffusion equation (12) in conjunction with the Arrhenius equation (5) gives the drying rate of wheat in a spouted heater at any selected bed temperature. The energy requirements at a given drying rate are then determined by the energy balance. The total energy balance for the heater in steady operation is (omitting insignificant terms)

$$Q_L = \left\{W(c_w + \bar{m}c_f) + GA\,(c_p + \mathscr{H}_e c_g)\right\}(t_e - t_r) + E\,(h_{fg} + \bar{h}_d)_{t_r} - GA\,(c_p + \mathscr{H}_i c_g)\,(t_i - t_r) - W\,(c_w + m_0 c_f)\,(t_0 - t_r) \qquad (18)$$

where, by material balance,

$$E = W\,(m_0 - \bar{m}) = GA\,(\mathscr{H}_e - \mathscr{H}_i) \qquad (19)$$

The energy balance was used in the present analysis to calculate experimental values of the average net heat of desorption, $\bar{h}_d$. The calculated net heats ranged in value from zero to 300 B.t.u/lb, with an average value over all runs of 150 B.t.u per pound of moisture removed. Since the contribution of the net heat toward the total energy requirement in drying was small, and since all errors in the energy balance were accumulated in its computation, these results cannot be said to be very accurate. However the average value (150 B.t.u/lb) is of the right magnitude (see [5]), gives satisfactory closure of the energy balance and is therefore recommended for all calculations on drying wheat in spouted beds.

Cooling of the Heater Produce

Wheat should be stored at a temperature within 10 °F of the prevailing ambient temperature [17], and it is the object of the cooling operation to reduce the temperature of the heater product to this level. It is desirable that the cooling effect be derived as far as possible from the evaporation of moisture from the grain. To encourage this, the cooler should provide a long residence time (for the slow diffusion of moisture at low temperature levels) and should be operated at low air velocities (to depress heat transfer to the air). The air should emerge with a relative humidity of 50–60 per cent, judging from Fig. 6. These conditions are probably best met by a cooler employing crossflow of a shallow bed of wheat and a gentle stream of air. Mathur and Gishlers' data [3] on a counterflow cooler indicate that 50–80 per cent of the reduction in sensible heat of wheat in an efficient cooler may be utilized for the evaporation of moisture. There is no justification for spouting the cooler bed: uniformity of bed temperature, a virtue in a heater, is a defect in a cooler, for, since the air may be expected to leave at the temperature of the bed, it is evident that an exorbitant

flow of air will be required if the cooled grain is to be no more than 10 °F above the ambient temperature. Moreover, the air would have to be supplied at a needlessly high pressure. The spouted cooler used in the present study was very inefficient in all respects and will not, therefore, be reported on.

Conclusion

It is outside the present scope, which has been limited to a fundamental analysis of the drying process, to discuss the prediction of air flow rates, pressure drops and other factors connected with the physical operation of spouted beds. These have been partially investigated by Mathur and Gishler [1], and will be treated in sufficient detail in a forthcoming paper to permit the design of smoothly functioning, optimumly sized spouted heaters.

Owing to its own fundamentality of approach and to the fact that the drying rate is moisture diffusion controlled, the analysis which has been presented of the drying process is a generally valid one, and is wholly independent of such scale-up problems as may present themselves in the physical operation of spouted beds, provided only that assumptions of isothermicity, perfect mixing, etc. are satisfied. It may be noted that there are many other polymeric materials besides wheat, both of natural and synthetic origin, whose moisture diffusion coefficients are independent of concentration, and to whose continuous drying in a well-mixed, isothermal bed the present analysis is therefore applicable.

Appendices

Appendix A illustrates the practical use of the present correlations by the solution of an example problem. Appendix B gives a brief comparison between the merits of spouted and standard commercial wheat dryers.

Acknowledgements—The present investigation was initiated at the request of Dr. P. E. Gishler then of the National Research Council of Canada, Ottawa, Canada. We are indebted to Dr. Gishler and to Mr. K. B. Mathur for communicating the full results of their work, and to Dr. I. Hlynka for a report on work done at the Grain Research Laboratory, Board of Grain Commissioners of Canada, Winnipeg, Man. The baking tests were done by Mr. Allen Rose, and were carried out in the Cereals Laboratory of the University of Saskatchewan.

Notation

a	= area of heat transfer surface in unit volume of a bed	ft^2/ft^3
A	= cross-sectional area of a column	ft^2
A	= frequency factor	hr^{-1}
B	= hold-up in a bed, dry basis	lb
c_f	= heat capacity of water (liquid)	B.t.u/lb °F
c_g	= heat capacity of water (vapour)	B.t.u/lb °F
c_p	= heat capacity of dry air	B.t.u/lb °F
c_w	= heat capacity of dry wheat	B.t.u/lb °F
D	= diffusion coefficient	ft^2/hr
D_v	= particle diameter measured as the diameter of an equi-volumed sphere	ft
E	= rate of moisture removal in the heater	lb/hr
G	= mass dry air velocity	lb/hr ft^2
G_a	= average mass air velocity in the annulus of a spouting bed	lb/hr ft^2
h_c	= heat transfer coefficient	B.t.u/hr ft^2 °F
h_{fg}	= latent heat of vaporization	B.t.u./lb
$\bar{h}_d$	= average net heat of desorption	B.t.u/lb
k_r	= rate constant	hr^{-1}
m	= moisture content, dry basis	lb/lb
$\bar{m}$	= average moisture content of a drying particle	lb/lb
$\bar{\bar{m}}$	= average moisture content of a statistical population of drying particles	lb/lb
m_0	= uniform moisture content prior to drying	lb/lb
m_s	= effective moisture content at the surface of a drying particle	lb/lb
p/p_0	= relative vapour pressure	
Q_L	= heat loss from heater to surroundings	B.t.u/hr
r	= radial co-ordinate originating at the column axis	ft
r_0	= radius of column	ft
R	= gas constant (1·987 B.t.u/mole °R)	
S	= particle surface area	ft^2
t	= local average temperature of air or particles	°F
t_e	= equilibrium temperature of air and particles leaving the heater	°F
t_i	= temperature of air entering the heater	°F
t_0	= initial temperature of particles ; temperature of particles entering the heater	°F
t_r	= reference temperature	°F
t_s	= surface temperature of particles	°F
Δt_b	= difference between the maximum and minimum average particle temperatures in the heater	°F
T	= absolute temperature	°R
V	= particle volume	ft^3
W	= feed rate of particles to heater, dry basis	lb/hr
w_b, w'	= dimensionless constants in Smith's isotherm equation	
z	= height above the gas inlet ; the axial co-ordinate in the heater column	ft
δ_0	= mass of a slug of feed, dry basis	lb
δ	= part of δ_0 still remaining in the heater bed θ hrs after injection	lb
$\mathscr{H}$	= local humid moisture content of air, dry basis	lb/lb

$\mathscr{H}_e$ = average humid moisture content of air leaving the heater lb/lb
$\mathscr{H}_i$ = humid moisture content of air entering the heater lb/lb
θ = time hr
θ_c = duration of the heater bed turnover cycle hr
$\theta_\tau = B/W$ = weight-average residence time hr
ρ = air density lb/ft^3
μ = air viscosity lb/ft hr

Reduced variables in the rate equations

$\overline{M} = (\overline{m} - m_s)/(m_0 - m_s)$ = reduced free moisture content of a drying particle
$\overline{\overline{M}} = (\overline{\overline{m}} - m_s)/(m_0 - m_s)$ = reduced free moisture content of a statistical population of drying particles
V_L = ratio between the volumes of test loaves baked from the heater product and the feed wheat
$X = (S/V)\sqrt{(D\theta)}$ = square root of the reduced isochronal drying time
$X_\tau = (S/V)\sqrt{(D\theta_\tau)}$ = square root of the reduced weight-average residence time
$\phi = \theta/\theta_\tau$ = reduced residence time
$\Psi = 6V/SD_v$ = particle surface sphericity (shape factor)

Appendix A

A problem illustrating the practical use of the correlations for drying wheat in a spouted heater.

A feasible heater for practical drying consists of a column 2 ft in diameter with a 90° conical bottom and a 4 in. diameter air inlet. A dryer has been built which consists of this heater and a cross-flow cooler. The heater is to be operated at a bed depth of 4 ft. Wheat at 70 °F with a moisture content of 0·230 lb/lb is to be dried to the maximum safe storage moisture of 0·163 lb/lb (14 per cent wet basis) and cooled to the maximum safe storage temperature of 10 °F above the atmospheric temperature. The kernel diameter of the wheat at a moisture of 0·10 lb/lb is 0·0115 ft. The atmospheric temperature, pressure and relative humidity are respectively 64 °F, 29 in. Hg and 10 per cent. The crossflow cooler may be assumed to be 50 per cent efficient in converting the sensible heat of the heater product to the evaporation of moisture.

Problem. Find the critical safe grain temperature in the heater, the maximum safe drying rate, the inlet air temperature and the thermal energy requirements of the heater. Check the validity of the assumptions concerning boundary conditions and local conditions in the heater bed.

Solution. (i) Assume that the moisture content of the wheat is reduced 0·010 lb/lb in the cooler.

$\therefore \overline{\overline{m}} = 0{\cdot}163 + 0{\cdot}010 = 0{\cdot}173$ lb/lb

$\therefore$ by equation (17)

$$t_e = 189 - 115\,(m_0 + \overline{\overline{m}}) = 189 - 115\,(0{\cdot}230 + 0{\cdot}173) = 143\ ^\circ\text{F}$$

Check: for the maximum safe storage temperature of 74 °F, the sensible heat removed in the cooler is approximately

$$(c_w + c_f m)\,(t_e - 74) = (0{\cdot}30 + 0{\cdot}17)\,(143 - 74) = 42\ \text{B.t.u.}$$

per pound of wheat, dry basis.

$\therefore$ the quantity of moisture removed in the cooler is, at 50 per cent efficiency,

$$\frac{\frac{1}{2}\,(32)}{h_{fg} + \overline{h}_d} = \frac{16}{1030 + 150} = 0{\cdot}013\ \text{lb/lb}$$

$\therefore$ the corrected heater product moisture content is

$$\overline{\overline{m}} = 0{\cdot}163 + 0{\cdot}013 = 0{\cdot}176\ \text{lb/lb}$$

$\therefore$ the corrected maximum safe grain temperature in the heater is, by equation (17),

$$t_e = 189 - 115\,(0{\cdot}230 + 0{\cdot}176) = 142\ ^\circ\text{F}$$

(ii) Assume that the effective surface moisture content is 0·103 lb/lb (the value obtaining at low relative humidities). The reduced free moisture content of the heater product is then

$$\overline{M} = \frac{\overline{\overline{m}} - m_s}{m_0 - m_s} = \frac{0{\cdot}176 - 0{\cdot}103}{0{\cdot}230 - 0{\cdot}103} = 0{\cdot}575$$

$\therefore$ by equation (12), the square root of the reduced weight-average residence time is $X_\tau = 0{\cdot}506$.

Assume that the difference between maximum and minimum average grain temperatures in the heater is 8 °F. The arithematic average absolute grain temperature in the heater is then

$$T = t_e - \frac{\Delta t_b}{2} + 460 = 142 - 4 + 460 = 598\ ^\circ\text{R}$$

$\therefore$ by equation (5), the diffusion coefficient is

$$D = 297 \exp - \frac{21960}{RT} = 297 \exp\left(-\frac{21960}{1{\cdot}987 \times 598}\right) = 2{\cdot}8 \times 10^{-6}\ \text{ft}^2/\text{hr}$$

The volume to surface ratio of the wheat is (the surface sphericity being $\Psi = 0{\cdot}91$)

$$\frac{V}{S} = \frac{D_v\,\Psi}{6} = \frac{0{\cdot}0115 \times 0{\cdot}91}{6} = 0{\cdot}00174\ \text{ft}$$

$\therefore$ the weight-average residence time in the heater is

$$\theta_\tau = \frac{(X_\tau\,V/S)^2}{D} = \frac{(0{\cdot}506)^2 \times (0{\cdot}00174)^2}{2{\cdot}8 \times 10^{-6}} = 0{\cdot}278\ \text{hr}$$

(iii) The volume of the heater bed is

$$A\,(L - \tfrac{2}{3}\,r_0) = \pi\,(4 - \tfrac{2}{3}) = 10{\cdot}44\ \text{ft}^3$$

The fraction void of a spouting bed is approximately 0·45.

∴ the volume of wheat in the heater is

$$10{\cdot}44\,(1 - 0{\cdot}45) = 5{\cdot}75\ \text{ft}^3$$

The absolute density of the heater product is

$$\frac{90{\cdot}5\,(1 + \bar{m})}{(1 + 453\,\bar{m}} = \frac{90{\cdot}5\,(1 + 0{\cdot}176)}{(1 + (1{\cdot}453 \times 0{\cdot}176)} = 85\ \text{lb/ft}^3$$

∴ the hold-up in the heater is $5{\cdot}75 \times 85 = 489$ lb, wet basis, or

$$B = \frac{489}{(1 + \bar{m})} = \frac{489}{(1 + 0{\cdot}176)} = 416\ \text{lb (dry basis)}$$

∴ the feed rate is

$$W = B/\theta_r = \frac{416}{0{\cdot}278} = 1500\ \text{lb/hr (dry basis)}$$

(iv) The thermal energy requirements of the heater are

(a) To heat the feed to heater outlet temperature

$$W\,(c_w + m_0\,c_f)\,(t_e - t_0) = 1500\,(0{\cdot}30 + 0{\cdot}23)\,(142 - 70) = 54000\ \text{B.t.u./hr}$$

(b) To evaporate moisture in the heater

$$W\,(m_0 - \bar{m})\,(h_{fg} + \bar{h}_d) = 1500\,(0{\cdot}230 - 0{\cdot}176)\,(1013 + 150) = 94000\ \text{B.t.u/hr}$$

Total = 148000 B.t.u/hr

(v) A correlation on the physical operation of spouted beds (to be published) gives as the duration of the bed turnover cycle in the heater $\theta_c = 0{\cdot}020$ hr.

∴ by equation (2) the maximum difference in grain temperatures in the heater bed is

$$\Delta t_b = \frac{W\,(m_0 - \bar{m})\,(h_{fg} + \bar{h}_d)\,(\theta_c)}{B\,(c_w + \bar{m}c_f)} = \frac{94000 \times 0{\cdot}020}{416 \times 0{\cdot}476} = 9{\cdot}5\ ^\circ\text{F}$$

This agrees satisfactorily with the assumed value of 8 °F; hence the preceding calculations need not be repeated.

(vi) A correlation on the physical operation of spouted beds (to be published) gives for the minimum mass air velocity required to spout the heater bed $G = 580$ lb/hr ft². Allowing a mass air flow 10 per cent in excess of this minimum (to ensure stability of the spout) the total air flow to the heater is

$$GA = 1{\cdot}1 \times 580\ \pi = 2000\ \text{lb/hr}$$

∴ the heater inlet air temperature is

$$t_i = \frac{t_e + (\text{total heat from item iv})}{GAc_p} = \frac{142 + 148000}{2000 \times 0{\cdot}24} = 447\ ^\circ\text{F}$$

(vii) The relative humidity at heater outlet is

$$\frac{W\,(m_0 - \bar{m})}{GA\,\mathscr{H}_s} = \frac{1500\,(0{\cdot}230 - 0{\cdot}176)}{2000 \times 0{\cdot}164} = 0{\cdot}25$$

∴ by Fig. 6, the assumption of an effective surface moisture content of 0·103 lb/lb is well justified.

(viii) At a fraction void of 0·45, the specified heat transfer surface in the heater bed is

$$\frac{6\,(1 - \epsilon)}{D_v\,\Psi} = \frac{6\,(1 - 0{\cdot}45)}{0{\cdot}0115 \times 0{\cdot}91} = 290\ \text{ft}^2/\text{ft}^3$$

By Fig. 2, the mean heat transfer coefficient is of the order of 3 B.t.u/hr ft² °F. Equation (1) then gives a reduced air temperature of $(t - t_e)/t_i - t_e) = 0{\cdot}002$ at a height above the gas inlet of

$$z = \frac{Gc_p}{h_c a}\left(\ln\frac{t_i - t_e}{t - t_e}\right) = \frac{(1{\cdot}1 \times 580 \times 0{\cdot}24 \times 2{\cdot}3 \times 2{\cdot}7)}{(3 \times 290)} = 1{\cdot}1\ \text{ft}$$

At this point $t - t_e = 0{\cdot}6$ °F. Hence it is certain that air and grain left the heater at the same temperature t_e.

Appendix B

A comparison of the performance of the spouted heater described in Appendix A with that of a standard, commercial-type pilot model

The performance of the spouted dryer described in Appendix A may be compared with that of an experimental dryer described by Stansfield and Cook*. This dryer was designed to simulate the performance of commercial wheat dryers of the kind still in general use in North America, (the Ellis, Hess, Morris and Randolph dryers). The purpose of their study was to define safe operating limits for commercial drying, and as a result of their and other investigations the maximum inlet air temperature in commercial drying is officially limited to 180 °F.

We choose from Stansfield and Cooks' Table 5, subseries A–19, a run in which the dryer was operated to maximum capacity at the prescribed inlet air temperature of 180 °F without damage to the wheat, the initial and final moisture contents being the same as in the problem in Appendix A. The feed grain was at approximately 70°F. However, the cooling air was at the low winter level of 9° F. It may be assumed that with air at this low temperature the amount of drying done in the cooler was negligible. Hence the moisture content was reduced from 0·230 to 0·163 lb/lb in the heater alone. Recalculation of the quantities involved in the operation of the spouted heater in Appendix A for this moisture reduction gives $t_e = 147$ °F, $\theta_r = 0{\cdot}416$ hr, $W = 1000$ lb/hr

*Stansfield E. and Cook W. B. *The Drying of Wheat.* Report No. 25. National Research Council of Canada 1932.

and $t_i = 395$ °F. The following is a comparison of the performance of the heaters:

		Spouted	*Standard*
1	Air flow to heater (lb/hr per lb) wheat charged, dry basis	2·0	6·9
2	Nominal length of path followed by air through heater bed (ft)	4	0·8
3	Air pressure drop through heater (in H_2O)	42	5
4	Product of air pressure drop times air flow (proportional to blower power)	84	34
5	Air inlet temperature (°F)	395	180
6	Air outlet temperature (°F)	147	84
7	Air outlet humidity (lb/lb)	0·034	0·010
8	Air outlet relative humidity (%)	18	40
9	Maximum grain temperature (°F)	147	133
10	Minimum grain temperature (°F)	139	70
11	Heater outlet grain temperature (°F)	147	99
12	Weight-average residence time (hr)	0·42	0·73
13	Enthalpy of inlet air above 70°F (B.t.u. per pound moisture evaporated)	2340	2730

This table permits a fair comparison of the merits of standard and spouted heaters.

Although the air flow required to operate a spouted heater (item 1) is less than one third that for a standard dryer, it is not low enough to offset the difference in delivery pressures (item 3) and so the spouted heater requires more than twice as much blower power as the standard model (item 4).

On the other points the spouted heater compares more favourably. Due to the uniformity of grain temperature, (items 9, 10 and 11) it can be operated at a very much higher average bed temperature. This increases the drying rate to such an extent that the weight-average residence time is little more than half that in the standard model. Due to the high inlet temperature of the air (item 5), the heat requirements are slightly lower (item 13) despite the higher outlet temperature (item 6).

It may be noted, concerning Stansfield and Cooks' work, that the official prescription of a maximum inlet air temperature rather than a maximum grain temperature is due to the fact that, because of the absence of efficient mixing, the maximum grain temperature in commercial heaters is rather closely associated with the maximum air temperature. This association does not hold in spouted heaters, and hence the official limit on air temperature should not be applied to restrict their operation.

The foregoing comparisons underline the salient features of spouted wheat dryers, and give direction for further evaluation of their potentialities.

VOL. 13 1961

References

[1] Mathur K. B. and Gishler P. E. *A.I.Ch.E. Journal* 1955 **1** 157.

[2] Becker H. A. and Sallans H. R. *Cereal Chem.* 1956 **33**, 254.

[3] Mathur K. B. and Gishler P. E. *J. Appl. Chem.* 1955 **5** 624.

[4] Becker H. A. and Sallans H. R. *Cereal Chem.* 1955 **32** 212.

[5] Becker H. A. and Sallans H. R. *Cereal Chem.* 1956 **33** 79.

[6] Becker H. A. *J. Appl. Polymer Sci.* 1959 **1** 212.

[7] Phalzner P. M. *Can. J. Technology* 1951 **29** 261.

[8] Simmonds W. H. C., Ward G. T. and McEwen E. *Trans. Instn. Chem. Engrs.* 1953 **31** 265.

[9] *Cereal Laboratory Methods* (5th ed.). American Association of Cereal Chemists. St. Paul, Minnesota 1947.

[10] Gamson B. W., Thodos G. and Hougen O. A. *Trans. Amer. Inst. Chem. Engrs.* 1943 **39** 1.

[11] Jones C. R. *J. Sci. Food Agric.* 1951 **2** 565.

[12] Babbit J. D. *Canad. J. Res.* 1949 **27F** 55.

[13] Smith S. E. *J. Amer. Chem. Soc.* 1947 **69** 646.

[14] Becker H. A. *Canad. J. Chem.* 1958 **36** 1416.

[15] Ingersoll L. R., Zobel O. J. and Ingersoll A. C. *Heat Conduction* (1st ed.) Appendix H. McGraw-Hill, New York 1948.

[16] Newman A. B. *Trans. Amer. Inst. Chem. Engrs.* 1931 **27** 310.

[17] Oxley T. A. *The Scientific Principles of Grain Storage.* Northern Publishing Company, Liverpool 1948.

Chemical Engineering Science, 1961, Vol. 13, pp. 113 to 119. Pergamon Press Ltd., London. Printed in Great Britain

Simultaneous heat and mass transfer in free convection

W. R. WILCOX*

University of California, Lawrence Radiation Laboratory
and
Department of Chemical Engineering, Berkeley, California

(*Received* 6 *April* 1960)

Abstract—The problem of simultaneous heat and mass transfer in *laminar* free convection from a vertical flat plate is investigated theoretically. An integral method is used to find solutions for zero wall velocity and for a mass-transfer velocity at the wall, with the wall either insulated or held at a constant temperature. The zero-wall-velocity solution is compared with existing solutions and data for simultaneous heat and mass transfer, heat transfer alone and mass transfer alone.

Résumé—L'auteur fait une étude théorique du problème du transfert simultané de chaleur et de masse dans une convection libre laminaire à partir d'une surface plane verticale. Une méthode intégrale est utilisée pour trouver des solutions dans le cas d'une vitesse nulle, et dans le cas d'une vitesse finie de transfert de masse sur la paroi, celle-ci étant isolée ou maintenue à température constante. La solution du premier cas est comparée aux solutions existantes et aux données relatives au transfert de masse et de chaleur, simultanées, de chaleur seule, et de masse seule.

Zusammenfassung—Das Problem des simultanen Wärme- und Stoffübergangs von einer senkrechten flachen Platte bei laminarer freier Konvektion wird theoretisch untersucht. Es wurde eine Integralmethode benutzt, um Lösungen zu finden für den Fall einer Wandgeschwindigkeit gleich Null und für eine Stofftransportgeschwindigkeit and der Wand, welche isoliert ist oder konstante Temperatur besitzt. Die Lösung für den Fall der Wandgeschwindigkeit gleich Null wird verglichen mit den bestehenden Lösungen und Daten für simultanen Wärme- und Stoffübergang sowie für alleinigen Wärmetransport und für alleinigen Stofftransport.

INTRODUCTION

IN MANY processes mass transfer and heat transfer occur simultaneously. In free convection these may either hinder or aid one another. For example mass-transfer rates that are 100 per cent greater than those predicted by considering only the effects of mass transfer were obtained by MATHERS *et al.* [1] for sublimation of spheres with simultaneous heat transfer. Seemingly anomalous mass-transfer results have also been observed in zone melting work performed by this author [2].

Two theoretical solutions have been carried out for this situation. SOMERS used an integral method for the problem of evaporation and condensation, taking into account the non-zero wall velocity arising from the mass transfer [3]. His solution, although perfectly correct, is complex and difficult to apply to specific problems. MATHERS *et al.* used an analogue computer to solve the problem for zero wall velocity [1]. However in the process they dropped the inertia terms in the momentum equation. Thus their solution strictly holds only for high Prandtl and Schmidt numbers. They also obtained data which shows that the general form of the solution is valid for constant Prandtl and Schmidt numbers.

It is the purpose of this paper to derive simple results which will be expected to apply for all Prandtl and Schmidt numbers and for various situations. In part it is intended to bridge the gap between the work of SOMERS and that of MATHERS *et al.*

INTEGRAL EQUATIONS

The basic equations for the approximate integral solution can be shown to be [3, 4, 5]:

*Present address: Pacific Semiconductors, Inc., Los Angeles, California.

$$\text{Mass} \quad \frac{d}{dx}\int_0^{\delta''} u\,\psi\,dy = v_0 - D\left(\frac{\partial \psi}{\partial y}\right)_0 \tag{1}$$

$$\text{Energy} \quad \frac{d}{dx}\int_0^{\delta'} u\,\phi\,dy = v_0 - a\left(\frac{\partial \phi}{\partial y}\right)_0 \tag{2}$$

$$\text{Momentum} \quad \frac{d}{dx}\int_0^{\delta} u^2\,dy = -\nu\left(\frac{\partial u}{\partial y}\right)_0 + \beta g\,(T_0 - T_\infty)\int_0^{\delta'} \phi\,dy + \alpha\, g\,(C_0 - C_\infty)\int_0^{\delta''} \psi\,dy \tag{3}$$

where the various symbols are defined in the tabulation of nomenclature at the end of this paper.

Equation (3) includes the assumption that density is a linear function of both concentration and temperature. This will be examined in detail later for perfect gases. Note also that in the momentum equation the limits of the last two integrals are δ' and δ'', not δ. This is justified by the following argument. The concentration and temperature profiles provide the driving force for the velocity profile. Thus we have $\delta \geqslant \delta'$, $\delta \geqslant \delta''$. Since $\phi = 0$ for $y \geqslant \delta'$, and $\psi = 0$ for $y \geqslant \delta''$ the limits on the integrals are correct as shown. The only way this would not be true is if either α or β were zero. If this were true, however, the integral concerned would drop out of the momentum equation and so the limit there is not important.

So that these equations may be solved it is necessary to assume a form for the velocity, concentration and temperature profiles. It is tacitly assumed that the shape of the velocity profile is independent of the ratio of the mass and heat transfer, while actually, of course, it is not. However if the Schmidt and Prandtl numbers are not too different the result should be quite good anyway because the equations will still be satisfied on the average.

Solution for zero velocity at the wall

Strictly speaking the condition of zero wall velocity is true only for equal-molal counter-diffusion. However for low rates of mass transfer the wall velocity is small enough to be safely neglected.

Accordingly we assume the following profiles:

$$\left.\begin{aligned} \frac{u}{u_x} &= \left(\frac{y}{\delta}\right) - 2\left(\frac{y}{\delta}\right)^2 + \left(\frac{y}{\delta}\right)^3 \\ \phi &= 1 - \frac{3}{2}\left(\frac{y}{\delta'}\right) + \frac{1}{2}\left(\frac{y}{\delta'}\right)^2 \\ \psi &= 1 - \frac{3}{2}\left(\frac{y}{\delta''}\right) + \frac{1}{2}\left(\frac{y}{\delta''}\right)^2 \end{aligned}\right\} \tag{4}$$

If these profiles are substituted into equations (1), (2) and (3), the following equations result:

Momentum

$$\frac{1}{105}\frac{d}{dx}(\delta\, u_x^2) = -\frac{\nu\, u_x}{\delta} + \beta\, g\,(T_0 - T_\infty)\,\tfrac{3}{8}\,\delta' + \alpha\, g\,(C_0 - C_\infty)\,\tfrac{3}{8}\,\delta'' \tag{5}$$

Energy

$$\frac{4}{105}\kappa'\left[\frac{21}{8} - \frac{105}{48}\kappa' + \frac{63}{112}\kappa'^2\right]\frac{d}{dx}(u_x\,\delta') = \left(\frac{3a}{2\,\delta'}\right) \tag{6}$$

Mass

$$\frac{4}{105}\kappa''\left[\frac{21}{8} - \frac{105}{48}\kappa'' + \frac{63}{112}\kappa''^2\right]\frac{d}{dx}(u_x\,\delta'') = \left(\frac{3D}{2\,\delta''}\right) \tag{7}$$

where

$$\kappa' = \frac{\delta'}{\delta},$$

$$\kappa'' = \frac{\delta''}{\delta}.$$

To solve these equations we must assume a relationship between δ, δ' and δ''. For $Sc > Pr$ the temperature profile must extend farther into the fluid than the concentration profile, i.e. $\delta' > \delta''$. Furthermore the velocity must extend out to the end of the temperature profile, i.e. $\delta = \delta'$. This situation is here called "heat-transfer controlling," and is now solved in detail as an example.

VOL. 13 1961

If u_x, δ and δ'' are each assumed to be proportional to various powers of x and it is further required that the terms in x drop out when these are substituted into equations (5), (6) and (7) then we have

$$u_x = \alpha_1 x^{1/2}, \quad \delta = \delta' = \alpha_2 x^{1/4}, \quad \delta'' = \alpha_3 x^{1/4},$$

where α_1, α_2, α_3 are constants to be determined by substitution into equations (5), (6) and (7). This substitution yields

Momentum

$$\frac{5}{420}\alpha_1^2\alpha_2 = -\nu\frac{\alpha_1}{\alpha_2} + \beta g (T_0 - T_\infty)\tfrac{1}{8}\alpha_2 + \alpha g (C_0 - C_\infty)\tfrac{1}{8}\alpha_3 \quad (8)$$

Energy

$$\frac{3}{105}\alpha_1\alpha_2 = \left(\frac{3a}{2\alpha_2}\right) \quad (9)$$

Mass

$$\frac{3}{105}\alpha_1\alpha_3 r\left[\frac{21}{8} - \frac{105}{48}r + \frac{63}{112}r^2\right] = \left(\frac{3D}{2\alpha_3}\right) \quad (10)$$

where $r = \alpha_3/\alpha_2 = \delta''/\delta'$.

From equations (9) and (10) we obtain

$$\left(\frac{D}{a}\right) = \left(\frac{\mathrm{Pr}}{\mathrm{Sc}}\right) = r^3\left[\frac{21}{8} - \frac{105}{48}r + \frac{63}{112}r^2\right) \quad (11)$$

which defines r vs. Pr/Sc. This relationship will be calcuated in detail later.

From equations (8) and (9) and the definition of r the value of α_2 is obtained. However what is usually desired is the Nusselt numbers, $h_x x/k$ and $K_x x/D$. It can be shown that these definitions yield [3]

$$\left.\begin{aligned}\mathrm{Nu}_x &= -x\left(\frac{\partial\phi}{\partial y}\right)_0 \\ *\,\mathrm{Nu}_x' &= -x\left(\frac{\partial\psi}{\partial y}\right)_0\end{aligned}\right\}, \quad (12)$$

From the assumed velocity profiles and the form assumed for δ' and δ'' we obtain

$$\left.\begin{aligned}\mathrm{Nu}_x &= \frac{3}{2}\frac{x^{3/4}}{\alpha_2} \\ \mathrm{Nu}_x' &= \frac{3}{2}\frac{x^{3/4}}{\alpha_3} = \frac{1}{r}\mathrm{Nu}_x\end{aligned}\right\}. \quad (13)$$

Thus for heat-transfer controlling we have

$$\mathrm{Nu}_x = 0{\cdot}435\,(\mathrm{Pr})^{1/4}\left(1 + \frac{0{\cdot}625}{\mathrm{Pr}}\right)^{-1/4}(\mathrm{Gr}_x + r\,\mathrm{Gr}_x')^{1/4} \quad (14)$$

where

Gr_x = local Grashof number for heat transfer $(= g x^3 \beta (T_0 - T_\infty)/\nu^2)$,

Gr_x' = local Grashof number for mass transfer $[= g x^3 \alpha (C_0 - C_\infty)/\nu^2]$.

Somers [3] and Mathers *et al.* [1] have found that $r \simeq (\mathrm{Pr}/\mathrm{Sc})^{1/2}$, which will also be demonstrated later. With this fact and by summation over the height of the plate we obtain the over-all Nusselt numbers, hL/k and KL/D, for heat-transfer controlling

$$\mathrm{Nu} = 0{\cdot}58\,\frac{(\mathrm{Pr})^{1/4}[\mathrm{Gr} + (\mathrm{Pr}/\mathrm{Sc})^{1/2}\mathrm{Gr}']^{1/4}}{[1 + (0{\cdot}625/\mathrm{Pr})]^{1/4}} \quad (15)$$

$$\mathrm{Nu}' = \left(\frac{\mathrm{Sc}}{\mathrm{Pr}}\right)^{1/2}\mathrm{Nu}$$

where

Gr = over-all Grashof number for heat transfer $[= gL^3 \beta (T_0 - T_\infty)/\nu^2]$,

Gr′ = over-all Grashof number for mass transfer $[= gL^3 \alpha (C_0 - C_\infty)/\nu^2]$.

In a like manner for mass-transfer controlling (Pr > Sc), we get

$$\mathrm{Nu} = \left(\frac{\mathrm{Pr}}{\mathrm{Sc}}\right)^{1/2}\mathrm{Nu}'$$

$$\mathrm{Nu}' = 0{\cdot}58\,\frac{(\mathrm{Sc})^{1/4}[\mathrm{Gr}' + (\mathrm{Sc}/\mathrm{Pr})^{1/2}\mathrm{Gr}]^{1/4}}{[1 + (0{\cdot}625/\mathrm{Sc})]^{1/4}} \quad (16)$$

These results can also be reduced from Somers' solution by making the same simplifying assumptions and the same definitions as made here [6].

A. Parabolic temperature and concentration profiles

The constants in the equations just obtained are slightly different than those usually obtained

*Primed dimensionless parameters are for mass transfer, unprimed for heat transfer.

by the integral method [4]. Therefore a solution will now be obtained using the usual parabolic temperature and concentration profiles; i.e. let

$$\phi = \left(1 - \frac{y}{\delta'}\right)^2, \quad \psi = \left(1 - \frac{y}{\delta''}\right)^2 \qquad (17)$$

Proceeding as before, we obtain a new defining relation for r:

$$\frac{\mathrm{Pr}}{\mathrm{Sc}} = r^3\left[\tfrac{8}{2} - 2r + \tfrac{1}{2}r^2\right] \qquad (18)$$

Likewise there is obtained for heat-transfer controlling:

$$\mathrm{Nu} = 0{\cdot}667\,\frac{(\mathrm{Pr})^{1/4}\,[\mathrm{Gr} + (\mathrm{Pr}/\mathrm{Sc})^{1/2}\,\mathrm{Gr}']^{1/4}}{[1 + (0{\cdot}952/\mathrm{Pr})]^{1/4}}$$

$$\mathrm{Nu}' = (\mathrm{Sc}/\mathrm{Pr})^{1/2}\,\mathrm{Nu} \qquad (19)$$

and for mass-transfer controlling:

$$\mathrm{Nu} = \left(\frac{\mathrm{Pr}}{\mathrm{Sc}}\right)^{1/2}\mathrm{Nu}'$$

$$\mathrm{Nu}' = 0{\cdot}667\,\frac{(\mathrm{Sc})^{1/4}\,[\mathrm{Gr}' + (\mathrm{Sc}/\mathrm{Pr})^{1/2}\,\mathrm{Gr}]^{1/4}}{[1 + (0{\cdot}952/\mathrm{Sc})]^{1/4}} \qquad (20)$$

B. Comparison of results

In form, these results approach those of MATHERS *et al.* [1] as the Schmidt and Prandtl numbers grow large and as they approach one another in value. For these conditions equations (19) and (20) reduce to

$$\left.\begin{aligned}\mathrm{Nu} &= 0{\cdot}677\,(\mathrm{Pr})^{1/4}\,[\mathrm{Gr} + (\mathrm{Pr}/\mathrm{Sc})^{1/2}\,\mathrm{Gr}']^{1/4}\\ \mathrm{Nu}' &= 0{\cdot}677\,(\mathrm{Sc})^{1/4}\,[\mathrm{Gr} + (\mathrm{Sc}/\mathrm{Pr})^{1/2}\,\mathrm{Gr}]^{1/4}\end{aligned}\right\} \qquad (21)$$

At this point it is interesting to compare these various results reduced to the case of heat transfer alone ($\mathrm{Gr}' = 0$) with Ostrach's exact numerical solution for free convection heat transfer [7]. This is done in Table 1.

Inspection of Table 1 shows that equation (15) is best for low Prandtl numbers, while equation (19) is best for high Prandtl numbers. Equation (21) and therefore MATHERS' analogue solution is suitable only for relatively high Prandtl numbers. It is expected that the same statements will hold true for simultaneous heat and mass transfer with "Prandtl numbers" replaced in the foregoing by "Prandtl and Schmidt numbers."

Table 1. Comparison of theoretical results for heat transfer by free convection

	Calculated values of $\mathrm{Nu}/\mathrm{Gr}^{1/4}$			
Prandtl number	OSTRACH [7] (*numerical*)	*Equation* (15) ($\mathrm{Gr}' = 0$)	*Equation* (19) ($\mathrm{Gr}' = 0$)	*Equation* (21) ($\mathrm{Gr}' = 0$)
0·01	0·0766	0·0650	0·0648	0·212
0·733	0·479	0·460	0·509	0·627
1	0·535	0·514	0·573	0·677
2	0·676	0·644	0·730	0·806
10	1·103	1·016	1·177	1·204
100	2·07	1·83	2·09	2·14
1000	3·74	3·26	3·81	3·81

C. Relationship between r and Pr/Sc

Previously it was stated that $r \simeq (\mathrm{Pr}/\mathrm{Sc})^{1/2}$. Table 2 shows the exact relation between r and Pr/Sc as given by equations (11) and (18).

Table 2. Relation between r and Pr/Sc *as given by equations* (27)*and* (35)

	(Pr/Sc)		$(\mathrm{Pr}/\mathrm{Sc})^{1/2}$	
r	*Equation* (11)	*Equation* (18)	*Equation* (11)	*Equation* (18)
1·0	1·0	1·0	1·0	1·0
0·8	0·623	0·632	0·790	0·795
0·6	0·320	0·327	0·566	0·572
0·4	0·114	0·118	0·337	0·343
0·2	0·0170	0·0196	0·130	0·140
0·0	0·0	0·0	0·0	0·0

This table shows that $r = (\mathrm{Pr}/\mathrm{Sc})^{1/2}$ is a reasonable approximation to the relation between r and Pr/Sc as given by the integral method. This approximation improves as Pr/Sc approaches 1.

D. Expansion coefficients for a perfect gas

As stated previously, it has been assumed that density is a linear function of concentration and temperature. Over a limited range this is often true for liquids. For a perfect gas the exact relationship may be derived as follows.

Let C, M_1 = concentration and molecular weight of the concerned component

C_2, M_2 = concentration and average molecular weight of the rest of the mixture

C_T = total molecular concentration, $C + C_2$

Then we have $\rho = (CM_1 + C_2M_2)$ (22)

but $(C + C_2) = C_T = \frac{n}{V} = \frac{P}{RT}$ (23)

where

n = number of moles

V = volume

P = total pressure

R = ideal gas constant

T = absolute temperature

Therefore we have

$$\rho = C(M_1 - M_2) + \frac{PM_2}{RT} \tag{24}$$

and so

$$\left(\frac{\rho_\infty - \rho}{\rho}\right) = \frac{(C_\infty - C)(M_1 - M_2) + [(1/RT_\infty) - (1/RT)]\,PM_2}{C(M_1 - M_2) + (P/RT)M_2}. \tag{25}$$

To get this into a form linear in C and T we must assume that the density varies only slightly so that in the denominator an average temperature $\bar{T}$ and an average concentration $\bar{C}$ can be used to the first approximation. With this assumption we obtain

$$\left(\frac{\rho_\infty - \rho}{\rho}\right) = \frac{(C_\infty - C)}{\bar{C} - (P/RT)\,[1 - (M_1/M_2)]} + \frac{(T - T_\infty)}{T_\infty\{1 - (\bar{C}TR/P)\,[1 - (M_1/M_2)]\}} \tag{26}$$

From this we find by definition of α and β that

$$\alpha = -\frac{1}{\bar{C} - (P/RT)\,[1 - (M_1/M_2)]} \tag{27}$$

and

$$\beta = \frac{1}{T_\infty\{1 - (\bar{C}TR/P)\,[1 - (M_1/M_2)]\}} \tag{28}$$

In general therefore for gases or liquids α and β must be evaluated at constant temperature and and at constant concentration. Both must be the value at some average value of both concentration and temperature.

Finite wall-velocity solutions

In many practical cases there is a bulk flow of material to or from the interface. This flow is caused by such processes as crystallization, dissolution, evaporation and condensation. The problem for an arbitrary flow through the boundary is extremely difficult however and has not been solved. As mentioned before however this flow may often be ignored to the first approximation. In fact this author has used the form of equation (20) for correlating mass transfer results in zone melting [2]. Velocities through the boundary layer of several cm/hr were used.

Simpler is the situation when only the component of interest partakes in these processes, i.e. it is dissolved in an inert solvent. In this case the bulk flow is caused by diffusion. A material balance at the wall yields [3]:

$$v_0 = -\frac{D}{C_T - C_0}\left(\frac{\partial C}{\partial y}\right)_0, \tag{29}$$

where C_T is the total molar concentration at the wall. In such processes the wall can either be held at some constant temperature or it can be insulated.

A. Specified wall temperature

This is the same problem as previously solved except that v_0 in equations (1) and (2) is given by equation (29), and is not zero. It is the situation examined by Somers, although in a slightly different form [3]. Assuming the parabolic profile, equation (17), and proceeding as before we obtain for heat transfer controlling

$$\frac{ra}{D} = -\frac{C_0 - C_\infty}{C_T - C_0} + \frac{(C_T - C_\infty)/(C_T - C_0)}{r^2\left[\frac{1}{2} - 2r + \frac{1}{2}r^2\right]}. \tag{30}$$

$$\mathrm{Nu} = \frac{0{\cdot}677\,(\mathrm{Pr})^{1/2}\,(\mathrm{Gr} + r\,\mathrm{Gr}')^{1/4}}{\{0{\cdot}952\,\{1 + (\mathrm{Pr}/80\,r\,\mathrm{Sc})\,[(C_0 - C_\infty)/(C_T - C_0)]\}^2 + \mathrm{Pr} + (\mathrm{Pr}^2/80\,r\,\mathrm{Sc})\,[(C_0 - C_\infty/C_T - C_0)]\}^{1/4}} \qquad (31)$$

and $\mathrm{Nu}' = \mathrm{Nu}/r$

Actually, the parabolic profile is not entirely satisfactory in this case, because the profiles cannot be corrected for the effect of velocity at the wall. This effect could conceivably be quite large. It would be better to use a fourth order polynomial for the velocity profile and third-order polynomials for concentration and temperature.

B. Adiabatic wall

Occasionally convective mass-transfer processes may take place at an insulated wall [8]. In these cases the heat necessary for the phase transition is supplied or removed by the bulk fluid. A heat balance at the wall, expressing the fact that the heat conducted to the wall is used up as latent heat, is given by

$$k\left(\frac{\partial T}{\partial y}\right)_0 = v_0\,\rho_0\,\lambda \qquad (32)$$

where λ is the latent heat (taken as positive for melting, evaporation, etc.). Substitution for v_0 from equation (29) and assuming the parabolic concentration and temperature profiles we obtain

$$r = \left(\frac{D}{a}\right)\left(\frac{C_0 - C_\infty}{C_T - C_0}\right)\frac{\lambda}{c_p\,(T_\infty - T_0} \qquad (33)$$

This together with equations (30) and (31) and the equilibrium relation between C_0 and T_0 is the solution to the adiabatic wall problem.

C. Example calculation

The following example calculation illustrates the adiabatic wall solution.

Assume: Water evaporating into air.
No water vapour in bulk air.
Bulk temperature of 120 °F.
One atmospheric pressure.

Problem: What is the wall temperature?

Solution: Note that in this case we have:

$$\left.\begin{aligned}(C_0 - C_\infty)/(C_T - C_0) &= p_s/(P - p_s)\\ (C'_T - C_\infty)/(C_T - C_0) &= P/(P - p_s)\end{aligned}\right\} \qquad (34)$$

where p_s = vapour pressure of water at T_0.

When the following physical properties are used:

$c_p = 0{\cdot}25$ B.t.u/lb °F (Perry [9])
$\lambda = 1060$ B.t.u/lb (Keenan and Keyes [10])
$a/D = 0{\cdot}81$ (Sherwood and Pigford [8])

Equations (32) and (35) become:

$$r = 5220\left(\frac{p_s}{P - p_s}\right)\left(\frac{1}{T_\infty - T_0}\right) \qquad (35)$$

$$f = \frac{p_s}{P - p_s} + 0{\cdot}81\,r - \left[\frac{P/(P - p_s)}{r^2(\tfrac{5}{2} - 2r + \tfrac{1}{2}r^2)}\right] = 0 \qquad (36)$$

The method of solution is trial and error. The temperature T_0 is assumed, and p_s is obtained from reference 10. With these values r is calculated from equation (29). The correct result is recognized when f as defined by equation (36) is zero. Table 3 summarises the calculations for this problem. The result is that the calculated wall temperature is about 54 °F, which is about 10 °F lower than the temperature of adiabatic saturation given by Perry [9].

Table 3. Sample calculation for adiabatic wall

T_0 (°F)	p_s (p.s.i.a.)	$P - p_s$ (p.s.i.a.)	$T - T_0$ (°F)	r	f
64	0·295	14·4	56	1·91	1.009
50	0·178	14·5	70	0·915	−0·358
55	0·214	14·5	65	1·186	0·107
54	0·206	14·5	66	1·122	0·038

Conclusion

The problem of simultaneous heat and mass transfer in laminar free convection has been solved approximately by the integral method. The cases of equal-molal counterdiffusion, isothermal wall and adiabatic wall have been investigated in detail. The expected validity of the results improves as Pr/Sc approached 1. The form of the final results are already proving useful in the correlation of data for situations in which

VOL. 13 1961

heat and mass transfer are both important in free convection [1, 2].

Acknowledgments—The author wishes to thank R. A. SEBAN and E. V. SOMERS for their helpful discussions and suggestions. This work was supported financially by the National Science Foundation and by the U.S. Atomic Energy Commission.

NOMENCLATURE

a = Thermal diffusivity of liquid $(k/c_p\rho)$.

$C, C_\infty, C_0, \bar{C}$ = Concentration of the concerned component at a point, in the bulk fluid, at the wall and and the average in the boundary layer, respectively.

C_2 = Concentration of the remainder of the fluid at a point.

C_T = Total molar concentration of solution at a point or at the wall

c_p = Heat capacity of the fluid

D = Molecular diffusivity of the concerned component

g = Acceleration due to gravity (taken as positive for flow up the plate and negative for flow down)

h_x, h = Local and over-all heat-transfer coefficient respectively

K_x, K = Local and over-all mass-transfer coefficients, respectively

k = Thermal conductivity of the fluid

L = Height of the plate

M_1, M_2 = Molecular weight of the concerned component and average molecular weight of the rest of the fluid, respectively.

n = Number of moles in a given volume

P, p_s = Total pressure and partial pressure at the wall, respectively

R = Ideal gas content

r = Ratio of concentration to temperature boundary-layer thicknesses

$T, T_0, T_\infty, \bar{T}$ = Temperature at a point, at the wall, in the bulk fluid and the average temperature in the boundary-layer, respectively

u = Velocity of the fluid parallel to the plate in a positive x direction

u_x = A reference velocity

V = Volume

v, v_0 = Velocity out from the wall, at a point and at the wall, respectively

x = Distance along the plate, from the bottom edge up for flow up, and from the top edge down for flow down

y = Distance from the plate

α = Concentration densification coefficient $(1/\rho)(\partial\rho/\partial C)_T$.

β = Temperature densification coefficient, $(1/\rho)(\partial\rho/\partial T)_C$.

$\delta, \delta', \delta''$ = Velocity, temperature and concentration boundary-layer thicknesses, respectively

κ', κ'' = Ratios of thermal and of concentration boundary-layer thicknesses to the velocity boundary-layer thickness, respectively

λ = Latent heat (taken as positive for melting, evaporation, etc.)

ν = Kinematic viscosity

ρ, ρ_∞ = Density of the fluid at a point and in the bulk fluid, respectively

$\phi = (T - T_\infty)/(T_0 - T_\infty)$

$\psi = (C - C_\infty)/(C_0 - C_\infty)$

$\mathrm{Gr}_x, \mathrm{Gr}$ = Local and over-all Grashof numbers for heat transfer, respectively. Defined by $g x^3 \beta (T_0 - T_\infty)/\nu^2, g L^3 \beta (T_0 - T_\infty)/\nu^2$

$\mathrm{Gr}_x', \mathrm{Gr}'$ = Local and over-all Grashof numbers for mass transfer, respectively. Defined by $g x^3 \alpha (C_0 - C_\infty), /\nu^2, g L^3 \alpha (C_0 - C_\infty)/\nu^2$.

$\mathrm{Nu}_x, \mathrm{Nu}$ = Local and over-all Nusselt numbers for heat transfer, respectively. Defined by $h_x x/k$ and hL/k

$\mathrm{Nu}_x', \mathrm{Nu}'$ = Local and over-all Nusselt numbers for mass transfer, respectively. Defined by $K_x x/D$ and KL/D

Pr = Prandtl number (ν/a)

Sc = Schmidt number (ν/D)

REFERENCES

[1] MATHERS W. G., MADDEN A. J. Jr. and PIRET E. L., *Industr. Engng. Chem.* 1957 **49** 961.

[2] WILCOX W. R., Ph.D. Dissertation, University of California, June, 1960.

[3] SOMERS E. V., *J. Appl. Mech.* 1956 **23** 295.

[4] WILKE C. R., TOBIAS C. W. and EISENBERG M., *Chem. Engng. Progr.* 1953 **49** 663.

[5] SCHLICHTING H., *Boundary Layer Theory* p. 256 McGraw-Hill, New York 1955.

[6] SOMERS E. V., private communication. Westinghouse Electric Corporation, Research Laboratories, Pittsburgh 35, Pa., May, 1959.

[7] OSTRACH S., National Advisory Committee Aeronautical Technical Note 2645, Lewis Flight Propulsion Laboratory, Cleveland, Ohio, February, 1952.

[8] SHERWOOD T. K. and PIGFORD R. L., *Absorption and Extraction*, pp. 94–101, McGraw-Hill, New York 1952.

[9] PERRY J. H., *Chemical Engineers' Handbook*, pp. 228 and 765, McGraw-Hill, New York 1950.

[10] KEENAN J. H. and KEYES F. G., *Thermodynamic Properties of Steam* p. 28, John Wiley, New York 1936.

Chemical Engineering Science, 1960, Vol. 13, pp. 120 to 129. Pergamon Press Ltd., London. Printed in Great Britain

Ion exchange kinetics : the removal of oxalic acid from glycol solutions

CHI TIEN* and GEORGE THODOS

The Technological Institute, Northwestern University, Evanston, Illinois, U.S.A.

(*First received* 17 *July* 1959 ; *in revised form* 18 *May* 1960)

Abstract—The kinetics for the removal of oxalic acid from glycol solutions through the use of the ion exchange resin, Permutit SKB, has been studied. The mechanism was found to be controlled by the combined resistances of both the liquid and resin phases. The equilibrium relationship of the system was determined experimentally and the results were found to fit a Freundlich type of equation. Liquid film mass transfer coefficients were established and correlated with the variables of this system. Simple experimental procedures together with the diffusion equation enabled the determination of the diffusion coefficient for the resin phase. This information in conjunction with the proper mathematical developments has made possible the prediction of the break-through curve which has been found to be in agreement with experimental results.

Résumé—L'étude cinétique de l'élimination de l'acide oxalique des solutions de glycol par la résine échangeur d'ions, la permutite SKB, montre que le phénomène est contrôlé par les résistances combinées des deux phases liquide et résine. La relation d'équilibre du système est déterminée expérimentalement et les résultats s'accordent avec l'équation du type Freundlich. Les coefficients d'échange massique de film liquide ont été établis et exprimés en fonction des paramètres du système. Des procédés éxperimentaux simples ainsi que l'équation de diffusion permettent la détermination du coefficient de diffusion pour la phase résine. Ces résultats permettent de prévoir au moyen de développements mathématiques la cassure de la courbe en accord avec les résultats expérimentaux.

Zusammenfassung—Die Kinetik der Abtrennung von Oxalsäure aus Glycollösungen bei Benutzung eines Ionenaustauscherharzes, Permutit SKB, ist untersucht worden. Es wurde gefunden, dass der Mechanismus durch die kombinierten Widerstände von Flüssigkeits- und Harzphase bestimmt wird. Die Gleichgewichtsbeziehungen des Systems wurden experimentell bestimmt, und die Ergebnisse erfüllten eine Gleichung vom Typ der Freundlich'schen Beziehung.

Es wurden Stofftransportkoeffizienten für den Flüssigkeitsfilm aufgestellt und mit den Variablen des Systems korreliert. Einfache Experimente erlaubten zusammen mit der Diffusionsgleichung die Bestimmung des Diffusionskoeffizienten für die Harzphase. In Verbindung mit entsprechenden mathematischen Ableitungen war es möglich, aus diesen Werten die Durchbruchskurven vorauszuberechnen, die gut mit den experimentellen Ergebnissen übereinstimmten.

THE removal of the acidic constituents formed in antifreeze solutions has been a subject of considerable recent interest. GLASER and THODOS (1) considered the process involving the recovery of ethylene glycol by means of vacuum distillation after pretreating the feed stock with excess sodium hydroxide. Although this procedure has proved successful the current market price of ethylene glycol does not make such a process profitable. A direct approach without the stringent requirements associated with vacuum distillation suggests the use of ion exchange resins for the removal of these acids formed in glycol solutions.

The object of this investigation concerns the kinetic study of the removal of acid components from glycol solutions with the use of ion exchange resins. In this connexion the physical properties of the system pertinent to this study have been established and involve the determination of equilibrium relationships, liquid film mass transfer coefficients and the diffusion coefficient for the resin phase. The various phases of this work are presented in the sections that follow.

*Present Address : Essex College, Assumption University of Windsor, Windsor, Ontario, Canada.

VOL. 13 1961

Material for study

For this study Permutit SKB was used. This ion exchange resin, furnished by the Permutit Company, is a strong basic resin and has been used primarily for the concentration of uranium. The resin is supplied in the chloride form and ranges, on an air dry basis from 14 to 25 mesh in size. Before use it is converted to the hydroxyl form according to the instructions furnished by the manufacturer. The resin particles were found to swell when saturated with the glycol solution.

The ethylene glycol used was of chemical grade and was supplied by the Dow Chemical Company. Aqueous solutions containing 30 per cent glycol were prepared, to which various quantities of oxalic acid were added to approximate a composition similar to that of antifreeze solutions.

Equilibrium Relationship

Measured volumes of glycol solutions of known acid concentrations were added to bottles containing a weighed amount of Permutit SKB resin. The volumes of solutions used varied from 500 to 1000 cm³. The bottles were sealed and occasionally agitated. Small quantities of the solution were removed at convenient time intervals and titrated with a standard sodium hydroxide solution. This procedure was repeated until the acid concentration no longer changed. To reach equilibrium one to several days were required. The equilibrium relationship obtained at room temperature (75°F) expressed as acid concentration in the solution, C^*, vs. the acid concentration in the resin phase, q^*, is presented in Fig. 1.

The results presented in Fig. 1 indicate that at the beginning q^* increases rapidly with C^* and asymptotically approaches a constant value. Different empirical equations can be used to fit the experimental results for different ranges of concentration. For concentrations up to $C^* = 0{\cdot}10$, the following expressions give the equilibrium relationship:

$$q^* = 3{\cdot}05 + 40{\cdot}6\,C^* \quad 0{\cdot}01 < C^* < 0{\cdot}05 \qquad (1)$$

$$q^* = 10{\cdot}83\,C^{*1/4} \quad 0{\cdot}05 < C^* < 0{\cdot}10 \qquad (2)$$

It may be argued that a better representation for these equations is possible. Nevertheless, a straight line has been selected in order to simplify the subsequent developments. This assumption seems to be justified by the close agreement found between predicted and experimental values as presented later.

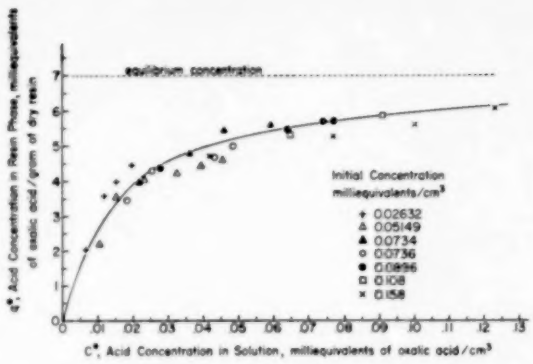

Fig. 1. Equilibrium relationship of oxalic acid in ethylene glycol solutions and Permutit SKB resin.

Mass transfer coefficient for liquid film

A schematic diagram of the equipment used for the determination of mass transfer coefficients is shown in Fig. 2. The main part of this unit consists of the differential reactor presented in Fig. 3. The reactor is made up of two sections; the lower-half being permanently fixed to a base while the upper-half is capable of sliding into position and thus permitting the flow of liquid through the reactor. The two parts are forced

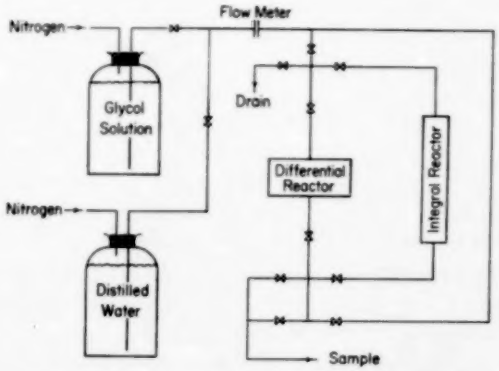

Fig. 2. Schematic diagram of experimental equipment.

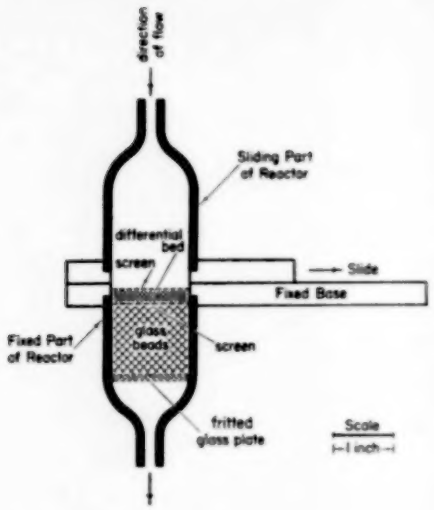

FIG. 3. Essential features of differential reactor,

together with light springs to prevent leakage between the contacting surfaces. The sliding movement of the upper half of the unit is guided by two grooves located on either side of the reactor and running parallel to the motion of the slide. The differential reactor has an inside diameter of $1\frac{5}{16}$ in. The bed height confined between the two screens can be varied by changing the amount of glass beads placed immediately above the fritted glass plate.

The experimental procedure consisted of placing between the two screens approximately 1 g of resin in the differential reactor. This quantity of resin corresponds to a bed height of less than 1 cm and, therefore, could be treated as a differential reactor. With the two parts of the reactor disengaged, the resin was first saturated with acid-free glycol solution, while the upper half of the reactor was filled with the acid-containing glycol solution. By sliding the upper half of the reactor in line with the lower half, the reactor became functional and permitted the flow of the acid solution through the differential bed. Periodic samples of the effluent liquid were analysed by titrating with standard sodium hydroxide solution. The total effluent was collected and used to establish the average flow rate.

To utilize the information obtained from these experiments the following mathematical approach has been developed. The rate of transfer considered from the liquid side can be expressed as

$$\frac{\partial q}{\partial t} = k_l (C - C_s) \tag{3}$$

The continuity equation is given by the expression

$$\frac{u}{\phi}\frac{\partial C}{\partial z} + \frac{\partial C}{\partial t} = -\frac{\rho}{\phi}\frac{\partial q}{\partial t} \tag{4}$$

Combining equations (3) and (4) and neglecting the second term of equation (4) produces the following

$$\frac{u}{\rho}\frac{\partial C}{\partial z} = -k_l (C - C_s) \tag{5}$$

The total cumulative liquid volume, $V = ust$, and the amount of resin, $m = sz\rho$, when substituted in equation (5), produce,

$$us\frac{\partial C}{\partial m} = -k_l (C - C_s) \tag{6}$$

Since the bed is considered to be differential

$$\frac{\partial C}{\partial m} = -\frac{C_{in} - C_{out}}{M} \tag{7}$$

where M is the total amount of resin in the differential bed. Combining equations (6) and (7) results in

$$k_l = \frac{us\,C_{in} - C_{out}}{M\,(C - C_s)_{av.}} \tag{8}$$

where $(C - C_s)_{av.}$ represents the arithmetic average of the top and bottom conditions of the differential bed. Of the quantities appearing in equation (8) C_s is unknown for the general case. However, for the case where the diffusion through the resin phase is exteemely rapid as compared with that taking place through the liquid film, the concentration gradient across the particle becomes insignificant and C_s can be obtained from the equilibrium relationship, or,

$$C^* = f(q^*)$$

where q^* can be established from the material balance. Letting k_l' be defined as

$$k_l' = \frac{us\,C_{in} - C_{out}}{M\,(C - C^*)_{av.}} \tag{9}$$

An essentially constant value of k_l' over the entire period of a run is an indication of the absence of internal diffusion resistance. A decreasing k_l' with time gives evidence that the resistance due to internal diffusion cannot be overlooked. However, at the beginning of a run, since the particle is free of solute, k_l' becomes the same as k_l and, therefore, provides a means for computing the true mass transfer coefficient from the experimental data.

A total of 47 runs were made for the determination of mass transfer coefficients for the liquid film. The flow rate as expressed in g/sec cm² varied from 0·02 to 0·31 while the concentration of the glycol solution expressed as milliequivalents of oxalic acid/cm³ ranged from 0·03 to 0·09. Four different particle sizes varying from 0·0338 to 0·0578 in. have been used.

The values of k_l' as defined by equation (9) were computed and found to be decreasing with time. The results of Run T–1 are presented in Fig. 4. This is an indication that internal diffusion is significant. The values of k_l' thus obtained were plotted vs. q, and the limiting value at

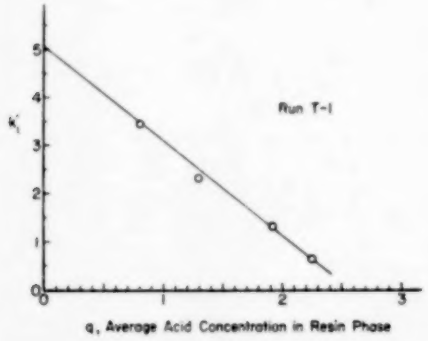

Fig. 4. Determination of liquid film coefficient.

$q = 0$ corresponding to $t = 0$ was taken as the value of the true mass transfer coefficient for the liquid film. The results of the experimental runs are summarized in Table 1. The numerical values of k_l ranged from 0·012 to 0·249. When the quantity d_pG is plotted vs. k_l/G on log–log co-ordinates a linear relationship results as shown in Fig. 5. The equation for this correlation is

$$\frac{k_l}{G} = \frac{0{\cdot}0708}{(d_pG)^{0{\cdot}595}} \qquad (10)$$

where d_p = particle size, cm
G = mass velocity, g/sec cm²
k_l = mass transfer coefficient, milliequivalents/sec g of dry resin milliequivalents/cm³

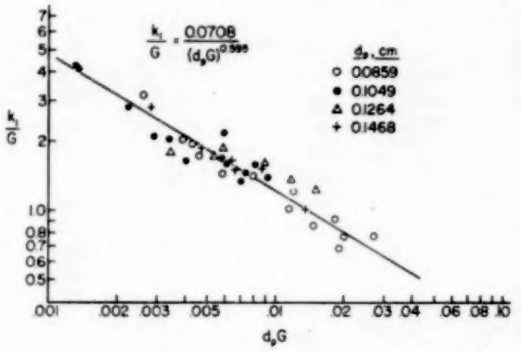

Fig. 5. Correlation of liquid film mass transfer coefficients.

In order to show that k_l is a true liquid film coefficient values of $1/k_l$ were plotted against $1/G^{0{\cdot}405}$. Since the resistance of the liquid film decreases with flow rate it is expected that such a plot should go through the origin, if the resistance due to surface reaction is insignificant. This fact is substantiated from the results appearing in Fig. 6. In the light of this evidence together with the results presented in Fig. 4 a strong

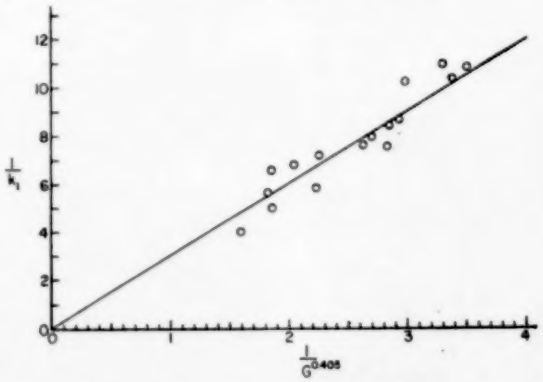

Fig. 6. Correlation of liquid film coefficients for establishment of absence of resistance due to surface reaction.

Table 1. *Experimental results for determination of mass transfer coefficients of liquid film*

Run no.	d_p	*su*	G	C_0	k_l	d_pG	k_l/G
f–3	0·0859	0·239	0·0304	0·0698	0·0453	$2{\cdot}61 \times 10^{-3}$	1·491
f–4	0·0859	0·601	0·0704	0·0698	0·113	6·05	1·609
f–5	0·0859	0·39	0·0496	0·07	0·0967	4·26	1·950
f–6	0·0859	1·755	0·2205	0·07	0·15	18·94	0·680
g–2	0·0859	0·416	0·0528	0·0302	0·0915	4·54	1·733
g–3	0·0859	0·238	0·0303	0·0302	0·0671	2·60	2·214
g–4	0·0859	0·593	0·0754	0·0300	0·119	6·48	1·580
g–5	0·0859	1·793	0·2279	0·0300	0·177	19·58	0·775
g–6	0·0859	1·346	0·1711	0·0300	0·147	14·70	0·861
g–7	0·0859	1·052	0·1337	0·0300	0·140	11·50	1·015
g–12	0·1468	0·72	0·0915	0·0282	0·0933	13·43	1·020
g–14	0·1468	0·587	0·0587	0·0587	0·0900	8·62	1·533
g–15	0·1468	0·45	0·0435	0·0278	0·012	6·39	1·655
g–16	0·1468	0·318	0·0318	0·0278	0·06	4·67	1·887
g–18	0·1468	0·446	0·0446	0·0278	0·0671	6·55	1·504
h–1	0·1264	0·653	0·083	0·0397	0·104	10·49	1.254
h–2	0·1264	0·322	0·0422	0·0397	0·0733	5·33	1·737
h–4	0·1264	0·248	0·0315	0·0397	0·0401	3·98	1·273
h–5	0·1264	0·555	0·0706	0·0397	0·116	8·92	1·644
h–7	0·1264	0·363	0·0462	0·0397	0·0883	5·84	1·911
h–8	0·1264	0·723	0·0919	0·0397	0·128	11·62	1·387
h–9	0·1264	0·213	0·027	0·0397	0·0491	3·41	1·818
s–14	0·1049	0·603	0·0766	0·0963	0·121	8·04	1·584
s–15	0·1049	0·523	0·0665	0·0963	0·090	6·98	1·353
s–16	0·1049	0·690	0·0877	0·0963	0·123	9·18	1·406
s–17	0·1049	0·215	0·0284	0·0963	0·0577	2·87	2·106
s–18	0·1049	0·429	0·0545	0·0963	0·0933	5·72	1·712
s–19	0·1049	0·348	0·0442	0·0963	0·087	4·64	1·968
s–20	0·1049	0·251	0·0319	0·0963	0·0658	3·35	2·063
s–22	0·1049	0·101	0·0128	0·0963	0·0537	1·34	4·195
s–23	0·1049	0·442	0·0562	0·0963	0·123	5·90	2·194
s–24	0·1049	0·322	0·0409	0·0963	0·166	4·29	4·061
s–25	0·1049	0·166	0·0212	0·0963	0·0607	2·22	2·863
s–27	0·1049	0·666	0·0846	0·0963	0·139	8·88	1·643
s–28	0·1049	0·298	0·0379	0·0963	0·100	3·98	2·641
s–30	0·1049	0·097	0·0124	0·0963	0·0503	1·30	4·298
t–1	0·0859	0·416	0·0529	0·0573	0·0851	4·54	1·609
t–4	0·0859	0·53	0·0674	0·0573	0·098	5·79	1·454
t–5	0·0859	0·675	0·0858	0·0573	0·126	7·37	1·472
t–7	0·0859	0·604	0·0768	0·0573	0·133	6·60	1·732
t–8	0·0859	0·722	0·0918	0·0573	0·130	7·89	1·422
t–9	0·0859	1·09	0·1385	0·0573	0·171	11·90	1·235
t–10	0·0859	2·02	0·2163	0·0573	0·202	18·58	0·932
t–12	0·0859	0·354	0·0451	0·0573	0·0923	3·87	2·047
t–14	0·0859	2·5	0·3178	0·0573	0·249	27·30	0·786

VOL. 13 1961

inference exists that the rate-controlling step for this ion exchange operation is represented by a combination of resistances due to the liquid and resin phases.

Diffusion coefficients of the resin phase

To obtain the necessary experimental data that would permit the evaluation of the diffusion coefficient for the resin phase the following procedure was adopted. To a designated amount of glycol solution containing oxalic acid, a specified amount of resin was introduced and rigorous agitation was provided with a mechanical stirrer. This mechanical agitation was introduced in order to eliminate the liquid film resistance surrounding the particles. For this particular arrangement it was found that a stirring corresponding to 1300 r.p.m. completely eliminated such a resistance and therefore this work was conducted with agitation speeds above this value.

Periodic samples were withdrawn and analysed for acid content. Since the liquid film resistance for these runs has been eliminated the concentration of the solute on the surface of the resin is in equilibrium with that in the liquid phase. Therefore, once the concentration of the solute in the liquid phase in known it becomes possible to account for the concentration of the solute on the surface of the particles with the use of the equilibrium relationship. This information, together with the subsequent mathematical developments enables the calculation of the diffusion coefficient.

The diffusion equation expressed in spherical co-ordinates can be used to describe the physical problem

$$\frac{\partial q_i}{\partial t} = D\left[\frac{\partial^2 q_i}{\partial r^2} + \frac{2}{r}\frac{\partial q_i}{\partial r}\right] \qquad (11)$$

with the initial condition

$$q_i = 0 \qquad \text{for } t < 0 \qquad 0 < r < b$$

and the boundary condition

$$q_i = q_s \quad \text{at} \quad r = b \quad \text{and} \quad t > 0$$

Equation (11) can be solved provided q_s is a known function of time. From the experimental data values of q_s are determined at different times and it is possible to approximate this relationship with a polynomial equation of the form

$$q_s = A + Bt + Ct^2 \qquad (12)$$

where A, B and C are constants determined from the experimental results.

The solution of equation (11) satisfying the boundary condition expressed by equation (12) is found to be

$$\begin{aligned} q_i = {} & A + \frac{2Ab}{\pi r}\sum_{n=1}^{\infty}\frac{(-1)^n}{n} \\ & \exp\left[-D\left(\frac{n\pi}{b}\right)^2 t\right]\sin\frac{n\pi}{b}r + \\ & + B\left[t - \frac{b^2 - r^2}{6D}\right] - \\ & - \frac{2Bb^3}{\pi^3 Dr}\sum_{n=1}^{\infty}\frac{(-1)^n}{n^3} \\ & \exp\left[-D\left(\frac{n\pi}{b}\right)^2 t\right]\sin\frac{n\pi}{b}r + \\ & + C\left[t^2 - \frac{b^2 - r^2}{D}\left(\frac{t}{3} + \frac{3r^2 - 7b^2}{180\,D}\right)\right] + \\ & + \frac{4Cb^5}{\pi^5 D^2 r}\sum_{n=1}^{\infty}\frac{(-1)^n}{n} \\ & \exp\left[-D\left(\frac{n\pi}{b}\right)^2 t\right]\sin\frac{n\pi}{b}r \qquad (13) \end{aligned}$$

Letting w represent the total amount of acid adsorbed per particle up to time t and recognizing the fact that the concentration in the resin phase is expressed on a mass basis, we have

$$w = \int_0^t D\rho\left(\frac{\partial q_i}{\partial r}\right)(4\pi b^2)\,dt \qquad (14)$$

Differentiating equation (13) with respect to r and letting $r = b$, substituting in equation (14) and carrying out the integration, the following expression results

$$\frac{w/\frac{4}{3}\pi b^3 \rho}{A + Bt + Ct^2} = \frac{q}{q_s} =$$

$$= 1 - \left\{ \frac{6}{\pi^2} \phi_1 \sum_{n=1}^{\infty} \frac{1}{n^2} \exp\left(-\frac{n^2 \pi^2}{\psi}\right) + \right.$$

$$+ \phi_2 \left[\frac{\psi}{15} - \frac{6\psi}{\pi^4} \sum_{n=1}^{\infty} \frac{1}{n^4} \exp\left(-\frac{n^2 \pi^2}{\psi}\right) \right] +$$

$$+ \phi_3 \left[\frac{2\psi}{15} - \frac{12\psi^2}{945} \right.$$

$$\left. \left. + \frac{12\psi^2}{\pi^6} \sum_{n=1}^{\infty} \frac{1}{n^6} \exp\left(-\frac{n^2 \pi^2}{\psi}\right) \right] \right\} \quad (15)$$

where

$$\phi_1 = \frac{A}{A + Bt + Ct^2}$$

$$\phi_2 = \frac{Bt}{A + Bt + Ct^2}$$

$$\phi_3 = \frac{Ct^2}{A + Bt + Ct^2}$$

and $$\psi = \frac{b^2}{Dt}$$

It can be seen that equation (15) is a function of ϕ_1, ϕ_2 and ϕ_3 for a specified value of ψ. The ϕ's are functions of time and, therefore, it is possible to plot t vs. q/q_s with ψ as a parameter. On the the other hand values of q/q_s obtained from the experimental results when plotted against time produce a relationship which intersects the calculated curves corresponding to different values of ψ. From the values of time and the parameter ψ corresponding to each intersection point values of the diffusion coefficient, D, are computed with the definition of $\psi = b^2/Dt$. These results are presented in Figure 7.

To illustrate the procedure used to calculate the diffusion coefficient, the experimental data of Run M–13 are analysed.

To 500 cc of glycol solution with $C_0 = 0{\cdot}0512$ milliequivalents of oxalic acid/cm^3, 2·7 g (dry basis) of Permutit SKB were added and vigorously agitated to eliminate the resistance of the liquid film. The resin when fully wet was 0·049 in. in diameter. The time–concentration history as obtained from the titration of periodic samples was as follows:

Time (sec)	C/C_0	q_s	q	q/q_s
300	0·811	4·89	1·8	0·368
600	0·74	4·76	2·46	0·517
1000	0·665	4·64	3·25	0·700
1800	0·579	4·46	4·04	0·906
3000	0·536	4·36	4·39	1·000
4500	0·524	4·34	4·54	—

The values of q_s are obtained from the equilibrium relationship corresponding to the concentration of the liquid solution, while q, the amount of acid

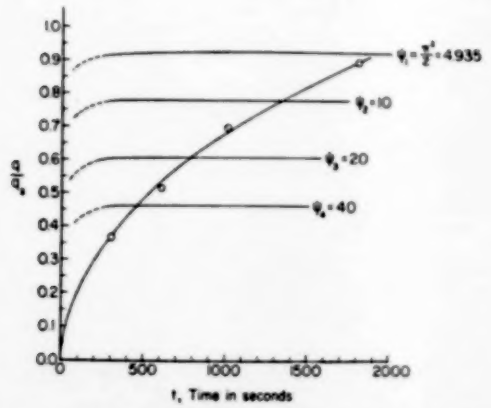

FIG. 7. Analysis of experimental data for determination of diffusional coefficients.

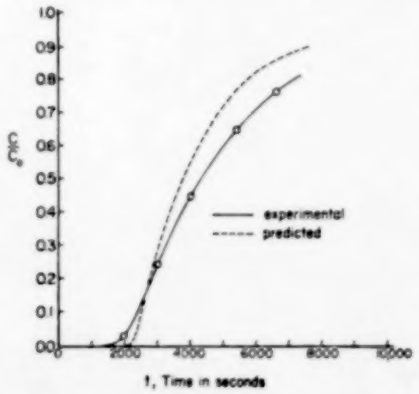

FIG. 8. Comparison of experimental and predicted break-through curve.

Table 2. Diffusion coefficients for the adsorption of oxalic acid on Permutit SKB resin

Run no.	d_p (*cm*)	C_0	D (cm²/sec)	*% deviation*
M-3	0·1264	0·0376	$2{\cdot}12 \times 10^{-7}$	16·48
M-4	0·1049	0·361	1·77	2·75
M-5	0·0859	0·0178	1·56	14·29
M-6	0·1264	0·0329	1·90	4·40
M-7	0·1264	0·0332	1·77	2·75
M-8	0·1264	0·0328	1·53	15·93
M-9	0·1264	0·0323	1·42	21·98
M-10	0·1264	0·0324	1·65	9·34
M-13	0·1264	0·0515	2·26	24·18
M-19	0·1264	0·108	2·23	22·53
			$·8321 \times 10^{-7}$	13·46

adsorbed per gram of dry resin, is calculated from a material balance.

With this information q_s can be approximated with equation (12) to be

$$q_s = 4{\cdot}83 - 2{\cdot}06 \times 100^{-4}t + 2{\cdot}12 \times 100^{-5}t^2$$

Values of q/q_s are calculated from equation (15) for different times, t, and parameters, ψ. The results of these calculations are presented in Fig. 8. In this Fig. the values of q/q_s obtained from the experimental data are also plotted to produce the single curve which intersects the calculated values of q/q_s at the following points:

t (sec)	$\psi = b^2/Dt$	D
482	40	$5{\cdot}25 \times 10^{-5}b^2$
802	20	$5{\cdot}24 \times 10^{-5}b^2$
1340	10	$6{\cdot}67 \times 10^{-5}b^2$
		$5{\cdot}83 \times 10^{-5}b^2$

Since $b = \dfrac{d}{2} = 0{\cdot}0245$ in.

$$D = 2{\cdot}256 \times 10^{-7}\ \text{cm}^2/\text{sec}$$

In this particular case D was found to be increasing with t; however, in other cases, the opposite trend was observed. Since no definite trend exists a simple arithmetic average was taken as the true value for the diffusion coefficient. A total of ten runs was made and the results are summarized in Table 2. For these runs, an average value for the diffusion coefficient was found to be $1{\cdot}82 \times 10^{-7}$ cm²/sec. This value agrees in order of magnitude with other systems reported by other investigators [2, 4].

Prediction of break-through curve

The experimental information obtained for this system is used in conjunction with the mathematical developments presented elsewhere [3] to predict the break-through curve for the removal of oxalic acid from glycol solutions with Permutit SKB resin. Experimental run P-1 has been carried out in the integral reactor shown in Fig. 2 and the break-through curve resulting for it has been compared with the predicted curve. The pertinent experimental data are as follows:

Column diameter	1·625 in.
Bed height	5·0 in.
Amount of resin	68·9 g (dry basis)
Particle size	0·0413 in. (fully wet)
Flow rate	0·976 cm³/sec

Concentration of influent solution: $C_0 = 0{\cdot}0461$ milliequivalents/cm³. The concentration history of the effluent stream was found to be:

Time (sec)	C/C_0
1000	—
2000	0·0289
3000	0·245
4000	0·45
5400	0·65
6600	0·762

Since the initial concentration $C_1 = 0.0461$ equation (1) applies under which conditions the equilibrium relationship is

$$q^* = 3.05 + 40.625\,C^* \qquad (1)$$

It has been pointed out elsewhere [3] that the explicit expression for the concentration ratio depends on the form of the equilibrium relationship. For this particular system, the results of the general linear case [3] can be applied. This expression has been found to be

$$\frac{C(\xi, \tau)}{C_0} = -\frac{K_1}{K_2 C_0} + \left[1 + \frac{K_1}{K_2 C_0}\right] \Phi(\xi, \tau) \qquad (16)$$

Numerical values for $\Phi(\xi, \tau)$ are available in the literature [3]. Using equation (16) concentration ratios have been calculated. The procedure involved is given as follows:

From the equilibrium relationship $K_1 = 3.05$ and $K_2 = 40.625$. Therefore, the parameter

$$\frac{K_1}{K_2 C_0} = \frac{3.05}{40.625 \times 0.0461} = 1.632$$

For this run k_l is calculated to be 0.0982 milliequivalents of oxalic acid transferred/sec gram of dry resin milliequivalent/cm³.

It has already been pointed out [4] that $\Phi(\xi, \tau)$ is related to the parameters

$$N = \frac{3\,D\,K_2}{b^2 k_l}, \quad \gamma\xi = \frac{3\,D\,K_2}{b^2}\,\frac{\rho}{u}\,z$$

$$\text{and} \quad \sigma\tau = \frac{2D}{b^2}\left(t - \frac{\phi}{u}\,z\right).$$

Substituting the appropriate values:

$$N = \frac{3\,(1.82 \times 10^{-7})\,(40.625)}{(0.05245)^2\,(0.0982)} = 0.082$$

$$\gamma = \frac{3\,(1.82 \times 10^{-7})\,(40.625)}{(0.05245)^2} = 8.063 \times 10^3$$

$$\xi = \frac{\rho}{u}\,z = \frac{s\rho z}{su} = \frac{68.9}{0.976} = 70.59$$

$$\gamma\xi = (8.063 \times 10^{-3})\,(70.59) = 0.5692$$

$$\sigma = \frac{2D}{b^2} = \frac{2\,(1.82 \times 10^{-7})}{(0.05245)^2} = 1.3231 \times 10^{-4}$$

$$\tau = t - \frac{\phi}{u}\,z = t - \frac{A\,\phi\,z}{Au}$$

The quantity $A\,\phi\,z$ represents the void volume of the bed which is found to be 44 cm³. Therefore

$$\tau = t - \frac{44}{0.976} = t - 45.1$$

Therefore $\tau = 1.3231 \times 10^{-4}\,(t - 45.1)$

$$\text{or} \quad t = \frac{\sigma\tau}{1.3231 \times 10^{-4}} + 45.1 \qquad (17)$$

Equation (17) relates the parameter $\sigma\tau$ with the time, t. Using the solutions of $\Phi(\xi, \tau)$, together with equation (16), the following concentration ratios have been calculated for different times:

t (sec)	C/C_0
2310	0.0000
2648	0.1578
3046	0.3052
3444	0.4262
3822	0.521
4578	0.6631
5334	0.7658
6089	0.8289
6845	0.8710
7601	0.9000

The predicted values of C/C_0 are compared with the experimental results in Fig. 8. The experimental break-through curve made its appearance earlier than predicted, but its slope increased at a slower rate. This agreement is quite favourable and particularly since the correlations used to obtain the mass transfer coefficient and the equilibrium relationship as well as the average value of the diffusion coefficient can vary as much as 10 per cent.

NOTATION

A, B, C	constants for equation (12)	
b	radius of particle	cm
C	concentration of solution	milliequivalents/cm³
C_0	concentration of influent solution	milliequivalents/cm³
C_s	concentration of solution at surface	milliequivalents/cm³
C^*	equilibrium concentration in liquid phase	milliequivalents of oxalic acid/cm³ of solution
d_p	particle diameter	cm

VOL. 13 1961

D	diffusion coefficient in resin phase	cm^2/sec
G	mass velocity	$g/sec\ cm^2$
k_l	mass transfer coefficient for liquid film milliequivalents/sec gram of dry resin	milliequivalent/cm^3
k_l'	pseudo-mass transfer coefficient for liquid film, milliequivalents/sec gram of dry resin	milliequivalent/cm^3
N	$3DK_2/b^2k_l$	
m	amount of resin in bed	g
M	amount of resin present in differential bed	g
q	average concentration in resin	milliequivalents/g dry resin
q^*	equilibrium concentration in resin phase	milliequivalents/g dry resin
q_i	point concentration in resin	millequivalents/g dry resin
q_s	concentration on resin surface	milliequivalents/g dry resin
s	cross-sectional area of reactor	cm^2
t	time	sec
u	superficial velocity	cm/sec
W	amount of acid adsorbed in resin	milliequivalents/particle
z	bed height	cm
γ	$3DK_2/b^2$	
ξ	$\rho z/u$	
ρ	bulk density or resin	g dry resin/cm^3
σ	$2D/b^2$	
τ	$t - \phi z/u$	
ϕ	porosity	
ϕ_1	$A/(A + Bt + Ct^2)$	
ϕ_2	$Bt/(A + Bt + Ct^2)$	
ϕ_3	$Ct^2/(A + Bt + Ct^2)$	
ψ	b^2/Dt	

References

[1] Glaser M. B. and Thodos G. *Chem. Engng. Progr.* 1956 **62** 94.

[2] Iwasyk J. M. and Thodos G. *Chem. Engng. Progr.* 1958 **54** 69.

[3] Tien Chi and Thodos G. *A. I. Ch. E. Journal* 1959 **5** 373.

[4] Wilson S. and Lapidus L. *Industr. Engng. Chem.* 1956 **48** 972.

Chemical Engineering Science, 1961, Vol. 13, pp. 130 to 142. Pergamon Press Ltd., London. Printed in Great Britain

Heat transfer in reacting Systems

Heat transfer to N_2O_4 gas flowing normal to a heated cylinder*

J. L. Richardson, F. P. Boynton†, K. Y. Eng and D. M. Mason
Division of Chemical Engineering, Stanford University, Stanford, California, U.S.A.

(*Received* 3 *June* 1960)

Abstract—The $N_2O_4 - NO_2$ gas system is convenient for experimental studies at relatively low temperatures of heat transfer processes in equilibrium-type reacting systems. The thermal conductivity and specific heat of these systems are unusually large and are non-uniform functions of temperature making difficult the assignment in heat transfer correlations of effective film values of these thermal properties. Rates of forced-convective heat transfer from a cylinder to N_2O_4–NO_2 gas at 1 atm were experimentally determined at free stream velocities up to about 40 ft/sec. If specific enthalpy instead of temperature is used as the driving force for heat transport a consistent correlation of the over-all heat-transfer rate data can be obtained by dimensional analysis, employing equilibrium properties in the conventional relationship,

$$N_{Nu} = \phi (N_{Pr}, N_{Re})$$

The advantages of using specific enthalpy as a driving force are justified from theoretical considerations. Due primarily to the high thermal conductivity of this system, values of conventional heat transfer coefficients based on a temperature driving force may be as high as eight times those for a similar non-reacting system.

Résumé—Le mélange gazeux NO_2–N_2O_4, est utilisable pour des études d'échanges de chaleur des réactions d'équilibre à des températures relativement basses. Comme la conductivité thermique et la chaleur spécifique de ces systèmes sont anormalement élevées, et ont une variation non uniforme en fonction de la température, il est difficile de relier la valeur effective du film à ses propriétés thermiques. Les vitesses d'échange de chaleur en convection forcée d'un cylindre de NO_2 gazeux sons une atmosphère ont été déterminées expérimentalement pour des vitesses de la veine gazeuse atteignant près de 40 ft/sec.

Si le potentiel pour l'échange de chaleur est l'enthalpie spécifique au lieu de la température, on obtient une relation pour la vitesse de l'échange de chaleur global en se servant de l'analyse dimensionnelle, les propriétés d'équilibre étant sous la forme conventionnelle :

$$N_{Nu} = \phi (N_{Pr}, N_{Re})$$

L'emploi de l'enthalpie spécifique comme potentiel se justifie d'un point de vue théorique. A cause de la valeur élevée de la conductivité thermique de ce système, les valeurs habituelles des coefficients d'échange basés sur la température sont jusqu'à huit fois plus grands que ceux des systèmes stables analogues.

Zusammenfassung—Das gasförmige System $N_2O_4 - NO_2$ ist für experimentelle Studien bei relativ tiefen Temperaturen von Wärmeübergangsvorgängen bei Gleichgewichsreaktionen gut geeignet.

Die Wärmeleitfähigkeit und die spezifische Wärme dieses Systems sind ungewöhnlich gross und sind uneinheitliche Funktionen der Temperatur, wodurch die Zuordnung der effektiven Filmwerte dieser thermischen Eigenschaften bei der Korrelation des Wärmeübergangs schwierig wird.

Die Geschwindigkeit des Wärmeübergangs bei erzwungener Konvektion von einem Zylinder in ein $N_2O_4 - NO_2$ – Gas bei 1 atm wurden experimentell bestimmt bei freien Damfgeschwindigkeiten bis zu ca. 40 ft/sec. Wenn man an Stelle der Temperatur die spezifische Enthalpie als treibende Kraft für den Wärmetransport benutzt, erhält man mit Hilfe der Dimensionsanlayse eine Korrelation der Gesamt-Wärmeübergangsgeschwindigkeitsdaten, wobei in der konventionellen Beziehung

$$N_{Nu} = \phi (N_{Pr}, N_{Re})$$

*Presented at the American Institute of Chemical Engineers Annual Meeting, San Francisco, December 1959.
†Present address: Convair Astronautics, San Diego, California, U.S.A.

Gleichgewichtseigenschaften benutzt wurden.

Die Vorteile bei der Benutzung der spezifischen Enthaplie als treibende Kraft ergeben sich aus theoretischen Betrachtungen.

Besonders wegen der hohen Wärmeleitfähigkeit des Systems können die Werte für die konventionellen Wärmeübergangskoeffizienten bezogen auf die Temperatur als treibende Kraft bis acht mal so hoch sein als bei ähnlichen nichtreagierenden Systemen.

Introduction

The detailed and theoretical experimental study of heat transfer in reacting systems has been of great interest to investigators in many different fields in recent years. A large part of the impetus for this study has arisen from the modern development of high-speed missiles, where heat transfer processes in rocket engines and re-entry aerodynamic heating involve chemical dissociation. The problem is also of interest in the field of combustion and industrial chemical processes. In 1904, Nernst [1] derived a theoretical expression for the thermal conductivity of a dissociating gas. Recently more exact expressions have been obtained by Hirschfelder [2], Franck [3], Frank and Spalthoff [4], Haase [5] and Butler and Brokaw [6]. Studies of the internal problem of heat transfer to N_2O_4 gas flowing at subsonic velocities in a tube have been made by Beal and Lyerly [7], Schotte [8] and Krieve and Mason [9]. Brokaw [10] has analysed the data of Beal and Lyerly and recommended several correlations. Rose and Stark [11] have measured stagnation point heat transfer in dissociated air at velocities above sonic using a shock tube, and their results appear to support the theoretical analysis of Fay and Riddell [12]. Rosner [13] has summarized much of the available theoretical and experimental work applied to the problem of dissociation accompanying aerodynamic heating.

Sensitivity of equilibrium thermal properties to temperature

Equilibrium thermal properties are not only unusually large but are non-uniform functions of temperature making difficult the assignment of effective values to properties of a fluid surrounding a heated body. Experimental values of isobaric heat capacity and thermal conductivity of the N_2O_4 system are shown in Fig. 1 from which this temperature dependence is evident. In subsequent discussion properties are assumed to be equilibrium properties unless otherwise specified, and the term N_2O_4 will refer to an equilibrium mixture of N_2O_4 and NO_2 in accordance with

$$N_2O_4 \rightleftharpoons 2NO_2$$
$$\Delta H_r = 2{\cdot}47 \times 10^4 \text{ B. Th. U. at } 77^\circ \text{F} \quad (1a)$$

All properties used in this paper are those compiled by Brokaw [10] for a total pressure of 1 atm. A system is designated as an equilibrium-type where chemical equilibrium is established so rapidly that reaction kinetics do not affect processes occuring in the system. The reaction of equation (1a) is in this category for subsonic flow processes as supported by the data of Bauer and Gustafson [14] and Carrington and Davidson [15] which indicate that equilibrium near room temperature is established in the order of a μ sec. If heat is added isobarically and with no heat loss to a closed endothermic system, the temperature rise is smaller than would be predicted from a weighted average of the heat capacities of the individual species of the mixture since a portion of the heat is absorbed as enthalpy of reaction. Thus the measured equilibrium isobaric heat capacity C_p is larger than the sum of the weighted heat capacities of the individual species, C_{p_f}, the so-called frozen heat capacity. Similarly, the equilibrium thermal conductivity k, of an endothermically reacting system is greater than that of the same system frozen, k_f, due to the added contribution of the diffusion of enthalpy of reaction. Thus a reacting mixture, flowing past a heat source, absorbs more energy per unit time than does a frozen system under otherwise similar conditions.

For a general endothermic equilibrium dissociation of the type:

$$X_2 \rightleftharpoons 2X \quad (1b)$$

the isobaric heat capacity C_p may be expressed as the sum of a frozen and reaction component as shown by Prigogine [16]:

$$C_p = \left(\frac{\partial H}{\partial T}\right)_p = C_{p_f} + C_{p_d} \tag{2a}$$

where

$$C_{p_d} = \frac{\Delta H_r}{M_{X_3}} \left(\frac{\partial \xi}{\partial T}\right)_p \tag{2b}$$

For systems in chemical equilibrium, the term $(\partial\xi/\partial T)_p$ may be evaluated by utilizing the van't Hoff relationship [17] giving:

$$C_p = C_{p_f} + \frac{\xi(1-\xi^2)}{2RM_{X_3}} \left(\frac{\Delta H_r}{T}\right)^2 \tag{2c}$$

Depending on the magnitude of ΔH_r the reaction component, C_{p_d}, may be much greater than the frozen component, C_{p_f}, resulting in large values of equilibrium specific heats.

Similarly the thermal conductivity, k, on the assumption of additivity of a frozen and reaction contribution and neglecting thermal and pressure diffusion may be expressed as described in Refs. [4] and [5]:

$$k = k_f + k_d \tag{3a}$$

where for the equilibrium-type system of equation (1b) k_d is shown in Ref. [5] to be equivalent to $D_{12}\rho C_{p_d}$, and thus

$$k = k_f + D_{12}\rho C_{p_d} \tag{3b}$$

Within the precision of the existing experimental thermal conductivity data of Franck and Spalthoff [4] and Coffin and O'Neal [18] this assumption of addivity appears to be valid.

Insensivity of k/C_p to temperature

It will be shown that the ratio k/C_p is relatively insensitive to temperature compared to either of these individual properties. This fact will prove to be of convenience in correlating cylinder heat transfer data where by using specific enthalpy instead of temperature as a driving force the ratio k/C_p instead of k alone appears in the Nusselt number, making the corresponding heat transfer film coefficient much less sensitive to temperature than the coefficient based on a temperature driving force. By dividing equation (3b) by equation (2a), an expression for k/C_p results:

$$\frac{k}{C_p} = \frac{k_f + D_{12}\rho C_{p_d}}{C_{p_f} + C_{p_d}} = \frac{(k/C_p)_f\left[(C_{p_f}/C_{p_d}) + (D_{12}\rho C_{p_f}/k_f)\right]}{\left[(C_{p_f}/C_{p_d}) + 1\right]} \tag{4a}$$

$$\frac{D_{12}\rho C_{p_f}}{k_f} = N_{Le_f} \tag{4b}$$

Hirschfelder *et al.* [19] and Butler and Brokaw [6] show that for gaseous systems of the type of equation (1b) N_{Le_f} is approximately unity and thus from equation (4a) and (4b)

$$\frac{k}{C_p} \simeq \left(\frac{k}{C_p}\right)_f = \frac{\mu}{N_{Pr_f}} \tag{4c}$$

Since calculations based on the kinetic theory [19] show that for gases N_{Pr_f} is not a marked function of temperature and μ varies approximately as $T^{1/2}$, equation (4c) indicates that k/C_p might be relatively insensitive to temperature. This conclusion is substantiated by data for the N_2O_4 system shown in Fig. 2.

Constant specific enthalpy gradient

Another result of the relative insensitivity of the ratio k/C_p to temperature is that the specific enthalpy gradient in a thin laminar boundary layer surrounding a cylinder will be shown to be approximately constant at a given position along the leading portion of the cylinder. This fact further enables one to assign appropriate effective film properties of the fluid by basing them on a state corresponding to a linear average of the free-stream and surface specific enthalpy. One may write for steady-state two-dimensional heat flux in the laminar boundary layer on a cylinder:

$$-\frac{Q}{A} = k\frac{dt}{dr} \tag{5a}$$

or for an isobaric, equilibrium process where $dH = C_p dt$

$$-\frac{Q}{A} = \left(\frac{k}{C_p}\right)\frac{dH}{dr} \tag{5b}$$

Substituting k from equation (3b) into equation (5b) and eliminating C_{p_d} by equation (2a)

$$-\frac{Q}{A} = \frac{1}{C_p}\left[k_f + \rho D_{12}(C_p - C_{p_f})\right]\frac{dH}{dr} \tag{5c}$$

VOL. 13 1961

Substituting equation (4b) in (5c) and rearranging

$$-\frac{Q}{A} = \left[\left(\frac{k}{C_p}\right)_\xi N_{Le_\xi} + \frac{k_\xi}{C_p}(1 - N_{Le_\xi})\right]\frac{dH}{dr} \quad (6a)$$

Since for gaseous systems of the type of equation (1b), $N_{Le_\xi} \sim 1$, equation (6a) becomes

$$-\frac{Q}{A} \sim \left(\frac{k}{C_p}\right)_\xi \frac{dH}{dr} \quad (6b)$$

It has been noted in the previous Section $(k/C_p)_\xi$ for gases is not markedly a function of temperature, and thus for the case of steady-state heat transfer through a cylindrical laminar film so thin that A in equation (6b) is effectively constant, the specific enthalpy profile would be expected to be approximately linear throughout the film. That the laminar momentum boundary layer on a cylinder is relatively thin is verified from SCHLICTING [20] where for $N_{Re_f} > 1500$ the boundary layer thickness is less than 9 per cent of the radius of the cylinder. Shown in Fig. 3, assuming that the thicknesses of the thermal and momentum boundary layers are the same, are three temperature and corresponding specific enthalpy profiles for the N_2O_4 system calculated from equations (5a) and (5b) respectively for average thermal boundary layer thicknesses of 0·0094 in. ($N_{Re_f} = 3220$), 0·012 in. ($N_{Re_f} = 1980$) and 0·014 in. ($N_{Re_f} = 1470$). It is evident from Fig. 3, as expected from equation (6b), that the specific enthalpy profile is quite linear, whereas, as might qualitatively be predicted from equation (5a) used in conjunction with the conductivity data in Fig. 1, the temperature profile is curved. Thus both thermal and non-thermal properties based on linearly averaged specific enthalpy

$$H_f = \frac{H_S + H_\infty}{2} \quad (7a)$$

should approximate the effective film state and lead to consistent heat transfer correlations, whereas properties based on linearly averaged temperature:

$$t_f = \frac{t_S + t_\infty}{2} \quad (7b)$$

would be less accurate.

Heat flux through laminar boundary layer

For separated flow such as occurs around a cylinder for Reynolds numbers greater than the order of unity and less than 10^5 where the boundary layer becomes turbulent, it is necessary to consider the relative magnitudes of heat transfer through the laminar boundary layer and through the separated region. DOUGLAS and CHURCHILL [21] have proposed a method of correlating heat transfer to cylinders for non-reacting systems by considering the heat transfer coefficient to consist of two thermal resistances in parallel: a laminar boundary layer in the front of the cylinder and a flow region beyond the point of separation. Even at the maximum Reynolds number of approximately 18,000 which was encountered in the present set of measurements, the laminar film portion contributes 73 per cent to the film coefficient calculated from equation (4) of Ref. [21]. Thus in the present investigation the heat flux through the laminar boundary layer predominates. At higher Reynolds number the separated region contributes more to the relative heat flux from the cylinder, with turbulent transport becoming more predominant; thus the sensitivity of correlations to the film properties might be expected to diminish.

Heat transfer correlation using specific enthalpy as driving force

Cylinder heat transfer coefficients may be defined either in terms of temperature or specific enthalpy as a driving force in accordance with

$$\frac{Q}{A} = h(t_s - t_\infty) = h\,\Delta t = h'(H_s - H_\infty) = h'\,\Delta H \quad (8)$$

Using temperature or specific enthalpy as driving forces together with average film properties based on an average between the surface and free stream temperature, or an average between the surface and free stream specific enthalpy respectively, and applying the techniques of dimensional analysis as described by MCADAMS [22], one obtains respectively, the following relationships:

$$N_{Nu_f} = \frac{hD_0}{k_f} = \phi\left[\left(\frac{D_0 U \rho}{\mu}\right)_f, \left(\frac{C_p \mu}{k}\right)_f\right]$$
$$= \phi\,(N_{Re_f}, \quad N_{Pr_f}) \qquad (9a)$$

$$N_{Nu_{f'}} = \frac{h' D_0}{(k/C_p)_{f'}} = \phi'\left[\left(\frac{D_0 U \rho}{\mu}\right)_{f'}, \quad \left(\frac{C_p \mu}{k}\right)_{f'}\right]$$
$$= \phi'(N_{Re_{f'}}, \quad N_{Pr_{f'}}) \qquad (9b)$$

For given values of N_{Re} and N_{Pr} the value of N_{Nu} is established. With temperature as a driving force the heat transfer coefficient, h, is directly proportional to k_f (equation 9a), which has been seen to be temperature sensitive making the assignment of the effective state of the film quite critical, and particularly since the inherent curvature of the temperature profiles (Fig. 3) precludes a simple linear average for effective film temperature (equation 7b). On the other hand with specific enthalpy as a driving force the heat transfer coefficient, h', is proportional to $(k/C_p)_{f'}$ equation (9b) which has been seen to be not very temperature sensitive, making the assignment of the effective state of the film much less critical. Also, because of the greater constancy in the film of specific enthalpy gradients as compared to temperature gradients, properties such as μ and ρ and also N_{Re} and N_{Pr} can be assigned precise values based on an average film specific enthalpy (equation 7a) since these properties are more nearly linear with specific enthalpy than with temperature.

EQUIPMENT AND METHODS

These experiments were performed in a closed-cycle flow system shown schematically in Fig. 4. The working section consisted of a two-dimensional flow channel, formed by two parallel aluminum plates 24 in. wide, 7 ft. long and separated by a distance of 2 in. The maximum velocity encountered in this set of measurements in the channel was 37·8 ft/sec. The intensity of turbulence measured with a hot wire anemometer set described by FUQUA [23] was less than 0·52 per cent in air flowing at 33 ft/sec. just upstream of the cylinder. Bulk velocity was measured by means of a calibrated Venturi meter, the velocity being adjusted to the desired value by control of the blower speed.

The cylinder used in these studies was a modified General Electric Calrod Tubular Heater with an internal heater insulated with ceramic material from an Inconel sheath, 0·315 in. in outside diameter, 0·255 in. in inner diameter and 18 in. in length. A pair of 36 B. and S. gauge, Teflon-insulated iron–constantan thermocouple wires were placed in each of two longitudinal grooves, approximately $\frac{1}{32}$ in. deep, machined on diametrically opposite sides of the sheath. Each of the two grooves extended from the opposite ends of the sheath to about 1 in. from the midpoint where the thermocouple junctions were spot-welded directly to the surface of the Inconel sheath. The wires were cemented in the grooves with Sauereisen low expansion cement which was polished flush with the cylinder surface in order to eliminate protuberances. The heated cylinder was inserted near the top of the channel normal to the flow of gas and midway between the channel walls as depicted in Fig. 4. At this position the maximum boundary layer thickness on the channel walls encountered in these experiments was less than 10 per cent of the distance between the walls. Thus the effect of the channel walls boundary layers on the cylinder was negligible. The cylinder could be rotated through 180° permitting complete circumferential temperatures to be obtained from the two thermocouples positioned 180° from one another. For each free stream gas velocity and heat input, the average cylinder surface temperature was determined by averaging, arithmetically, the temperatures measured at 30° intervals around the circumference of the cylinder. An accurate measurement of the d.c. power delivered to the cylinder was obtained by means of a simple voltage divider network.

Radiation losses from the polished Inconel cylinder surface to the polished aluminum walls of the channel section were calculated and found to be less than one per cent of the total heat flux and were therefore neglected. As has been mentioned previously in the literature [8], natural convection effects can be appreciable in reacting systems due to abnormally large coefficients of thermal expansion. The natural convection loss in the N_2O_4 system will be

VOL. 13 1961

relatively large at low Reynolds numbers due to its large Grashof number. Crude calculations for test no. 3, using N_2O_4 equilibrium properties (based on T_f) in the usual natural convection correlations for non-reacting systems, indicated that natural convection may account for as much as 10 per cent of the cylinder heat flux at this low Reynolds number, but because of the uncertainty in these calculations for reacting systems, no corrections were made. The effect on U of the cylinder blockage of flow in the two-dimensional channel was in all cases less than 2·6 per cent and was therefore neglected.

Nitrogen tetroxide supplied by the Matheson Company was used in these studies. The purity of the gas was checked by noting that a frozen sample was straw-white indicating a lack of impurities such as N_2O_3, which imparts a bluish color to the solid. Before introduction to the tunnel the nitrogen tetroxide was passed through a tank containing solid drying agents. Gas density measurements performed between runs indicated that as much as 15 vol. % of air may have been present in the system. Weighted on a molal basis, properties of the system were insignificantly affected by this quantity of air.

Results and discussion of data

As shown in Tables 1–3, sixteen tests were made, covering a range of free stream gas velocities from 8·86 to 37·8 ft/sec. Corresponding average cylinder film Reynolds numbers ranged from about 1,300 to 19,000 and over all average Nusselt numbers from about 30 to 80, exact values depending upon whether temperature driving force and properties based on the average temperature (equation 7b) or specific enthalpy driving force and properties based on the average specific enthalpy were used. As shown in Table 1, heat flux densities (equation 7a) ranged from 2,203 to 23,050 B.Th.u./hr ft², producing temperature differences from 12·6 °F to 553 °F between the cylinder surface and the free stream. It should be noted that these large temperature differences resulted in large, non-uniform variation of thermal conductivity in the film (Fig. 1). Free stream temperatures were maintained constant during each test at about 75 °F. That the cylinder surface temperature approached isothermal conditions is indicated in Table 1 where the maximum difference in circumferential temperature, $\Delta t_{c_{max}}$ is presented. The largest value of $\Delta t_{c_{max}}/t_s$, 0·25, occurred in Test no. 8.

Table 1. *Summary of experimental heat transfer data*

Test no.	U $\left(\frac{ft}{sec}\right)$	$\frac{\mathring{Q}}{A}$ $\left(\frac{\text{B.Th.U.}}{\text{hr ft}^2}\right)$	t_∞ (°F)	t_S (°F)	$\Delta t_{c_{max}}$ (°F)	H_∞ $\left(\frac{\text{B.Th.U.}}{\text{lb}}\right)$	H_S $\left(\frac{\text{B.Th.U.}}{\text{lb}}\right)$	$H_{f'}$ $\left(\frac{\text{B.Th.U.}}{\text{lb}}\right)$
1	8·86	14·950	74·8	438	77	47·5	350	199
2	9·11	2·208	78·8	102	7·2	52·5	86·0	69·3
3	9·28	18·580	77·1	630	72	50·3	399	225
4	17·7	2·208	81·1	96·0	2·6	55·3	76·5	65·9
5	18·7	15·080	75·2	178	30	48·1	228	138
6	19·9	18·810	77·9	207	40	51·2	265	158
7	20·0	8·769	78·4	135	17	52·0	149	100
8	20·6	22·910	78·2	272	68	51·8	306	179
9	25·3	2·203	81·7	94·3	3·6	56·1	74·5	65·3
10	28·4	14·900	75·2	150	12	48·1	179	114
11	29·5	18·830	78·0	168	20	51·4	213	132
12	29·7	23·050	78·2	198	31	51·8	255	153
13	31·8	8·593	83·3	123	10	58·1	125	91·6
14	37·2	14·780	75·2	138	12	48·1	155	101
15	37·6	22·950	78·1	179	18	51·6	230	141
16	37·8	19·040	76·9	155	15	50·0	189	120

Table 2. Value of properties at 1 atm employed

Test no.	t_f (°F)	$k_f \times 10^6$ $\left(\frac{\text{B.Th.U.}}{\text{sec ft °F}}\right)$	C_{pf} $\left(\frac{\text{B.Th.U.}}{\text{lb °F}}\right)$	$(\mu/\rho)_f \times 10^4$ $\left(\frac{\text{ft}^2}{\text{sec}}\right)$	$t_{f'}$ (°F)	$k_{f'} \times 10^6$ $\left(\frac{\text{B.Th.U.}}{\text{sec ft °F}}\right)$	$C_{pf'}$ $\left(\frac{\text{B.Th.U.}}{\text{lb °F}}\right)$	$(\mu/\rho)_{f'} \times 10^4$ $\left(\frac{\text{ft}^2}{\text{sec}}\right)$
1	256	6·50	0·460	1·43	161	21·5	1·85	0·867
2	90·4	19·5	1·47	0·448	91·2	19·6	1·48	0·453
3	354	4·80	0·249	1·86	176	18·5	1·60	0·972
4	88·6	19·0	1·45	0·443	88·9	19·2	1·45	0·445
5	127	24·5	1·96	0·630	130	24·5	1·98	0·659
6	143	24·0	2·00	0·740	140	24·2	2·00	0·720
7	107	22·3	1·74	0·523	110	22·9	1·79	0·541
8	175	18·5	1·60	0·965	150	23·1	1·96	0·793
9	88·0	18·9	1·44	0·440	88·5	19·0	1·44	0·442
10	113	23·2	1·81	0·557	117	23·8	1·88	0·575
11	123	24·3	1·92	0·610	127	24·5	1·96	0·635
12	138	24·3	2·00	0·710	137	24·3	2·00	0·708
13	103	21·9	1·68	0·506	105	22·1	1·71	0·516
14	107	22·3	1·63	0·520	111	22·9	1·79	0·544
15	129	24·5	1·97	0·645	135	24·5	2.00	0·686
16	116	23·6	1·86	0·575	120	24·0	1·91	0·595

Some heat transfer measnrements were made with air in the apparatus for comparison with N_2O_4. The resulting experimental heat transfer coefficients, h, for air and N_2O_4 are presented as functions of gas velocity in Fig. 5 where it may be seen that values of h for N_2O_4 are much higher and more scattered than for air. For comparison, heat transfer coefficients for the frozen N_2O_4 system are included. These values were obtained using experimental values of U and t_f from Tables 1 and 2 and calculating frozen properties therefrom. Values of $N_{Nu_{f_\xi}}$ were calculated from data in the literature, Ref. [21], using a value of 0·7 for N_{Pr_ξ} since, for the frozen N_2O_4 system, the

Table 3. Values of dimensionless groups

Test no.	N_{Re_f}	N_{Pr_f}	N_{Nu_f}	$\frac{N_{Nu_f}}{N_{Pr_f}^{1/3}}$	$N_{Re_{f'}}$	$N_{Pr_{f'}}$	$N_{Nu_{f'}}$	$\frac{N_{Nu_{f'}}}{N_{Pr_{f'}}^{1/3}}$
1	1·630	0·902	46·2	47·8	2·680	0·906	31·1	32·1
2	5·340	0·631	35·6	41·5	5·280	0·632	36·3	42·3
3	1·310	0·737	51·0	56·4	2·510	0·951	33·5	34·0
4	10·500	0·625	56·8	66·4	10·400	0·627	57·4	67·1
5	7·810	0·765	43·6	47·7	7·460	0·778	49·3	53·6
6	7·070	0·834	44·2	46·9	7·770	0·821	53·1	56·7
7	10·000	0·681	51·0	58·0	9·700	0·695	51·8	58·5
8	5·610	0·950	46·4	47·2	6·820	0·865	55·7	58·4
9	15·100	0·624	67·5	79·0	15·000	0·625	66·1	77·3
10	13·400	0·704	62·8	70·6	13·000	0·723	65·6	72·9
11	12·700	0·746	62·8	69·2	12·200	0·766	68·1	74·4
12	11·000	0·814	57·9	62·0	11·000	0·810	68·1	73·1
13	16·500	0·670	71·7	81·9	16·200	0·676	72·5	82·3
14	18·800	0·682	77·2	87·5	18·000	0·697	79·2	89·3
15	15·300	0·772	67·7	73·7	14·400	0·800	76·4	82·2
16	17·300	0·720	75·3	84·0	16·700	0·736	79·2	87·7

VOL. 13 1961

Prandtl number varied between 0·71 and 0·73 over the range of values of t_f in Table 2.

Values of dimensionless groups are shown in Table 3. A log–log plot of $N_{Nu}/(N_{Pr})^{1/3}$ vs. N_{Re} was made employing both temperature and specific enthalpy as the driving force in accordance with equation (9a) and (9b) respectively. In Fig. 6 is shown the correlation with temperature as a driving force and with film properties based on a linear average of the free-stream and surface temperature. For comparison data from Ref. [21] for air and nitrogen with N_{Pr_f} taken as 0·70 are shown as a solid line. It is noteworthy that there is considerable scatter in this correlation particularly in the tests (1 and 3) with the highest values of t_S. An average deviation of 38 per cent from the line of Ref. [21] and a definite non-linear trend in the data are observed. Using specific enthalpy as a driving force and film properties based on a linear average specific enthalpy a similar plot is shown in Fig. 7. This correlation is seen to be much more consistent, with an average deviation from the line for air and nitrogen of 5·8 per cent. A least-squares analysis of the data in the form of this latter correlation gives

$$\frac{N_{Nu_{f'}}}{(N_{Pr})_{f'}^{1/3}} = 0{\cdot}559\,(N_{Re})_{f'}^{0{\cdot}519} \qquad (10)$$

It is noteworthy from Table 3 that where t_S is high, as in tests 1 and 3, there is a great variation in properties through the film due to the large difference between $t_{f'}$ and t_f shown in Table 2, and thus there is a large difference between $N_{Re_{f'}}$ and N_{Re_f}. Corresponding values of N_{Pr} are less sensitive to a choice of film properties as suggested by Hansen [24].

The data were also plotted in a form suggested by Douglas and Churchill [21] which is based on the concept of two parallel thermal resistances consisting of a laminar film resistance and a separated zone resistance. A better correlation results when specific enthalpy is employed as a driving force (with film state based on equation 7a) than when the temperature is employed as driving force (with film state based on equation 7b). In the former case the data deviated on the average 5·3 per cent from the curve recommended in [21], equation (4) ($N_{Pr_f} = 0{\cdot}7$).

Conclusions

The experimental results are in accord with the theory for the mechanism of heat transfer in a dissociating gas. Heat transfer rates are encountered which are several times greater than for non-reacting or frozen gases under similar conditions. The results indicate that heat transfer data from a heated cylinder in an equilibrium reacting system can be correlated in a simple manner using forms of correlation similar to those used for non-reacting systems. A successful correlation results when specific enthalpy is used as the driving force and the film properties are evaluated at the average specific enthalpy. Since the present study was restricted to low Reynolds numbers where the heat transfer through the laminar boundary layer accounts for the major contribution to heat transfer, further studies at higher Reynolds numbers up through the region of transition to a turbulent boundary layer should be made. Also a study at Reynolds numbers less than unity, where laminar flow around the cylinder without separation occurs, would be of interest, where the assumption of a thin film used in the present investigation would be invalid.

It would be of interest to study local behaviour by measuring local heat transfer coefficients around the cylinder circumference. Also, temperatures and velocities near the cylinder and in the wake should be measured and checked with theoretical predictions. Comparison of the width of temperature and velocity wakes should give relative magnitudes of the eddy conductivity and eddy viscosity and provide a test of the Reynolds Analogy (Ref. [22]), for reacting systems.

A theoretical and experimental investigation of heat transfer in non-equilibrium reacting systems should be made, and thus the role of reaction kinetics on the heat transfer processes determined. At the present time, there are no detailed data with regard to this problem.

Acknowledgment—The support of the National Science Foundation under Contracts No. G-2425 and G-7327 is gratefully acknowledged. This paper is an abridgment of theses for the Master of Science degree in Chemical Engineering written by Frederick P. Boynton (December 1958) and Ken Y. Eng (October 1959).

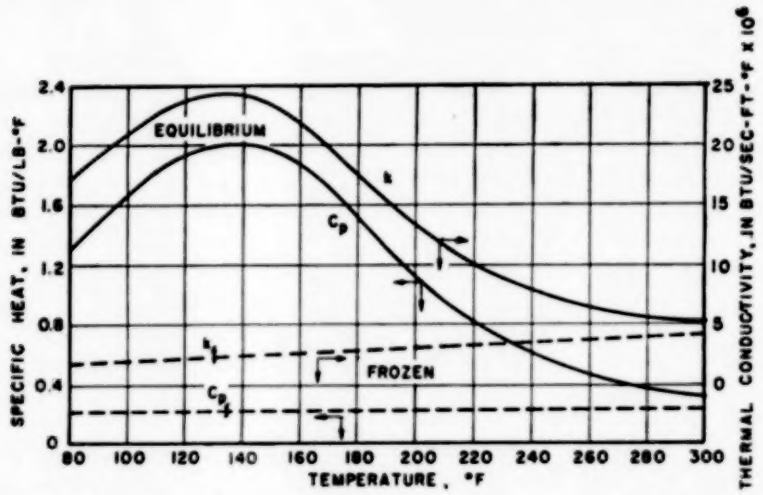

Fig. 1. Thermal conductivity and isobaric heat of N_2O_4 system at 1 atm.

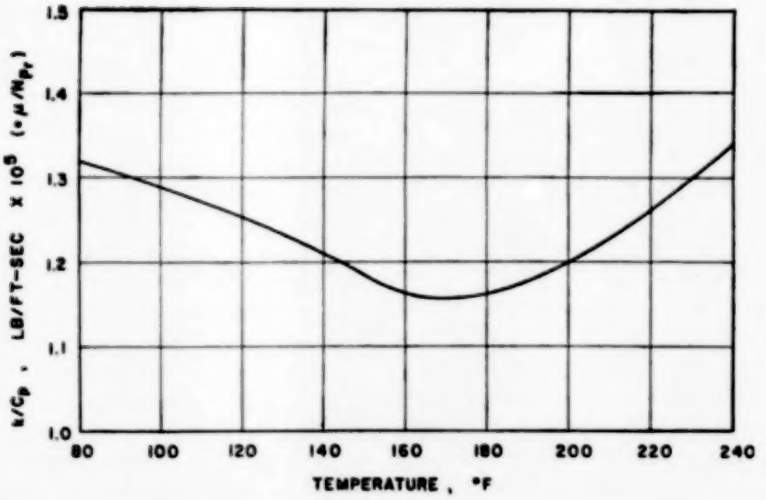

Fig. 2. Ratio of thermal conductivity to isobaric specific heat of N_2O_4 system.

VOL. 13 1961

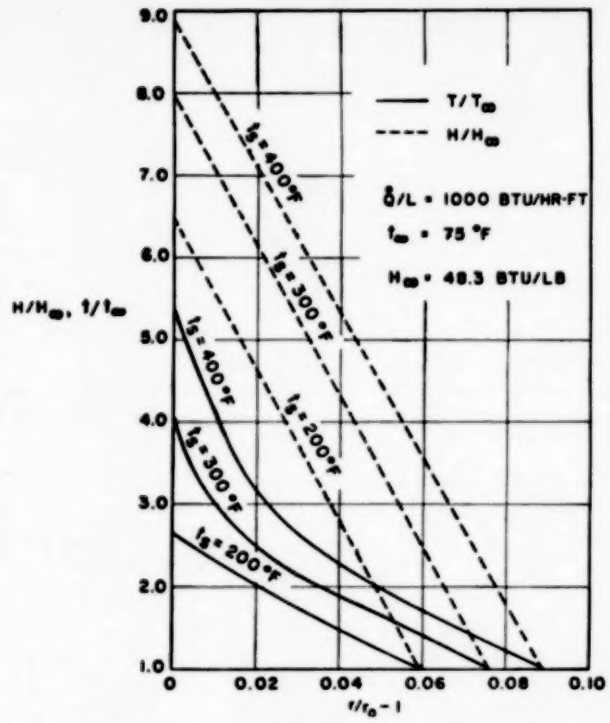

FIG. 3. Temperature and enthalpy profiles in a thin reacting film of N_2O_4.

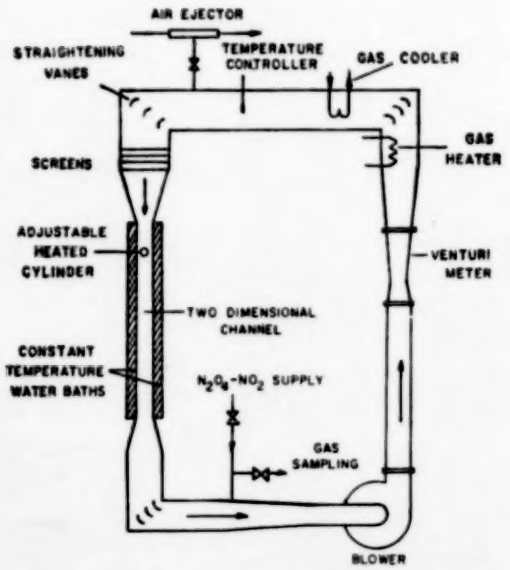

FIG. 4. Schematic diagram of the experimental flow system.

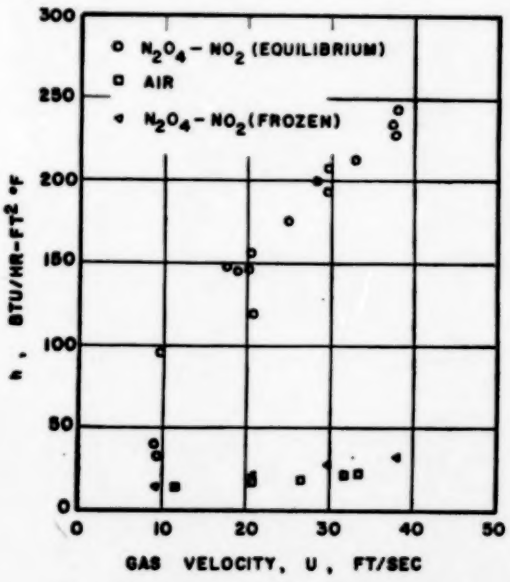

FIG. 5. Summary of heat transfer data.
○ N_2O_4–NO_2 system, equilibrium (experimental)
△ N_2O_4–NO_2 system, frozen (calculated)
□ Air (experimental).

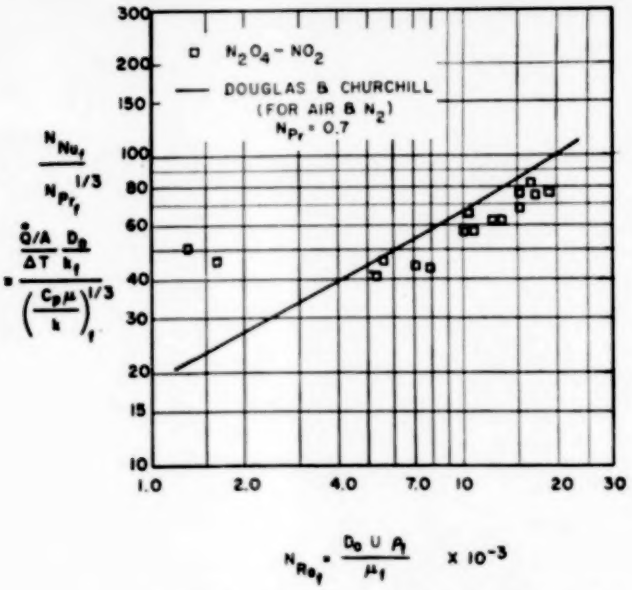
$N_2O_4 - NO_2$
DOUGLAS & CHURCHILL
(FOR AIR & N_2)
$N_{Pr} = 0.7$
$\frac{N_{Nu_f}}{N_{Pr_f}^{1/3}} = \frac{\frac{Q/A}{\Delta T}\frac{D_0}{k_f}}{\left(\frac{C_p\mu}{k}\right)_f^{1/3}}$
$N_{Re_f} = \frac{D_0 U \rho_f}{\mu_f} \times 10^{-3}$

Fig. 6. Correlation of heat transfer data for N_2O_4 system employing temperature as a driving force and properties at average film temperature.

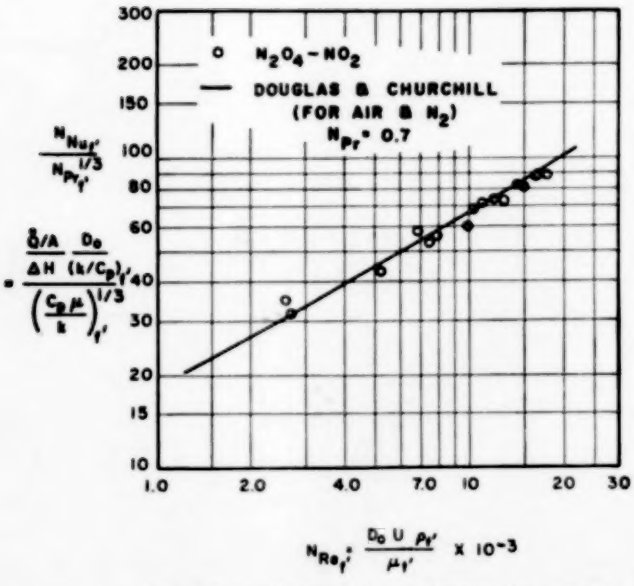
$N_2O_4 - NO_2$
DOUGLAS & CHURCHILL
(FOR AIR & N_2)
$N_{Pr} = 0.7$
$\frac{N_{Nu_{f'}}}{N_{Pr_{f'}}^{1/3}} = \frac{\frac{Q/A}{\Delta H}\frac{D_0}{(k/C_p)_{f'}}}{\left(\frac{C_p\mu}{k}\right)_{f'}^{1/3}}$
$N_{Re_{f'}} = \frac{D_0 U \rho_{f'}}{\mu_{f'}} \times 10^{-3}$

Fig. 7. Correlation of heat transfer data for N_2O_4 system employing specific enthalpy as driving force and properties at average film specific enthalpy.

Notation

A	area normal to heat flux	ft^2
C_p	isobaric specific heat	B.Th.U/lb °F
D_{12}	binary diffusion coefficient	(ft^2/sec)
D_0	outside diameter of cylinder	(ft)
H	specific enthalpy of equilibrium mixture including enthalpy of dissociation and relative to $H_{N_2O_4} = 0$ at 77 °F (B.Th.U./lb.)	
ΔH_r	enthalpy of reaction per lb. mol. of reactant equation (1a or 1b)	(B.Th.U./lb mole)
h	heat transfer coefficient (temperature driving force)	B.Th.U./sec ft^2 °F or B.Th.U./hr ft^2 °F
h'	heat transfer coefficient (enthalpy driving force)	lb/ft^2 sec
k	thermal conductivity	B.Th.U./ft °F sec
L	length along cylinder	ft
M_{X_2}	molecular weight of associated species N_2O_4	lb/lb mole
P	total pressure	lb$_{force}$/ft^2
Q	heat flux	B.Th.U./sec or B.Th.U./hr
r	radial distance	ft
r_0	outside radius of cylinder	ft
R	universal gas constant	1·987 B.Th.U./lb mole °R
T	absolute temperature	°R
t	temperature	°F
U	free-stream velocity	ft/sec
X or X_2	designation for lb mole of dissociated or associated species respectively as defined by equation (1b)	

Greek letters

μ	absolute viscosity	lb/ft sec
ρ	mass density lb/ft^3	$M_{X_2}P/(1+\xi)RT$
ϕ or ϕ'	function of	
ξ	degree of advancement, cf. Ref. [17], of reaction of type $X_2 \rightleftarrows 2X$ for a system of mass, M_{X_2}; in which case $1 \geqslant \xi \geqslant 0$	

Subscripts

c	refers to circumferential point on cylinder
d	component of property attributable to dissociation
f	refers to film property based on arithmetic average temperature
f'	refers to film property based on arithmetic average specific enthalpy
∞	property at state of free-stream
S	property at average state around cylinder surface
ξ	thermal property frozen at constant degree of advancement of reaction

Dimensionless parameters

$N_{Nu_{f \text{ or } f'}}$	Nusselt number	hD_0/k_f or $h'D_0/(k/C_p)_{f'}$
N_{Le_ξ}	Frozen Lewis number	$D_{12}\rho C_{p\xi}/k_\xi$
$N_{Pr_{f \text{ or } g'}}$	Prandtl number	$(C_p\mu/k)_{f \text{ or } f'}$
$N_{Re_{f \text{ or } f'}}$	Reynolds number	$(D_0U\rho/\mu)_{f \text{ or } f'}$

References

[1] Nernst W. *Ann. Phy. Lpz.* 1904 904.

[2] Hirschfelder J. O. *J. Chem. Phys*, 1957 **26** 274.

[3] Frank E. U. *Z. Phys. Chem.* 1952 **201** 16.

[4] Franck E. U. and Spalthoff W. *Z. Electrochem.* 1954 **58** 374.

[5] Haase R. *Z. Naturf.* 1953 8a 729.

[6] Butler J. N. and Brokaw R. S. *J. Chem. Phys.* 1957 **26** 1636.

[7] Beal J. L. and Lyerly R. L. *Influence of gas dissociation on Heat Transfer.* WADC Technical Report 56–494 ASTIA Doc. No. AD 118074 September 1956.

[8] Schotte W. *Industr. Engng. Chem.* 1958 **50** 683.

[9] Krieve Walter F. and Mason David M. *Heat Transfer in Reacting Systems*: I. *Heat Transfer to* N_2O_4 *under Turbulent Pipe Flow Conditions.* Progress Report No. 20-366, Jet Propulsion Laboratory, November 3 1958.

[10] Brokaw R. S. *Correlation of Turbulent Heat Transfer in a Tube for the Dissociating System* $N_2O_4 \rightleftarrows 2NO_2$. NACA RM E57K19a, March 1958.

[11] Rose P. H. and Stark W. I. *J. Aero. Sci.* 1958 **25** 86.

[12] Fay J. A. and Riddell F. R. *J. Aero Sci.* 1958 **25** 73.

[13] Rosner D. E. *Jet Propulsion* 1958 **28** 445

[14] Bauer S. H. and Gustafson M. R. *Disc. Faraday Soc.* 1954 **17** 69.

[15] Carrington T. and Davidson N. *J. Phys. Chem.* 1953 **57** 418.

[16] Prigogine I. *Introduction to Thermodynamics of Irreversible Processes* p. 10. Thomas, Springfield, Illinois 1955.

[17] Prigogine I. and Defay R. *Chemical Thermodynamics* pp. 10–13, 128. Longmans Green, London 1954.

[18] Coffin K. P. and O'Neal C. Jr. *Experimental Thermal Conductivities of the* $N_2O_4 \rightleftharpoons 2NO_2$ *System*. NACA TN 4209 (1958).

[19] Hirschfelder J. O., Curtiss C. F. and Bird R. B. *Molecular Theory of Gases and Liquids*. pp. 14 and 16 John Wiley, New York, 1954.

[20] Schlicting H. *Boundary Layer Theory*. pp. 206–216, 24. Pergamon Press, London 1955.

[21] Douglas W. J. M. and Churchill S. W. *Chem. Engng. Progr.* 1956 52 Symposium Series No. 18 p. 23.

[22] McAdams W. H. *Heat Transmission* (3rd Ed.) Chap. 5, p. 209. McGraw-Hill, New York 1954.

[23] Fuqua D. G. M.S. Thesis pp. 9–14 (Division of Chemical Engineering) Stanford University 1959.

[24] Hansen C. F. *J. Aero. Sci.* 1953 20 789.

VOL.
13
1961

Chemical Engineering Science, 1961, Vol. 13, pp. 143 to 154. Pergamon Press Ltd., London. Printed in Great Britain

Mixing and contacting in gas–solid fluidized beds

J. J. VAN DEEMTER*

Shell Oil Company, Houston Research Laboratory, P.O. Box 2527, Houston 1, Texas

(*Received* 27 *October* 1959)

Abstract—The two-phase model of a gas–solid fluidized bed is applied to steady-state and transient gas mixing tests. The two phases are: a dense phase consisting of particle aggregates and a dispersed phase of high vertical gas velocity. Gas and solids are exchanged continuously between the two phases by disintegration of particle aggregates and coalescence of dispersed phase solids.

Expressions for gas back-mixing and for the standard deviation of the gas residence time distribution are derived and it is shown that the gas eddy diffusivity of the dense phase and the rate of mass-transfer between the two phases may be determined with the aid of suitable mixing tests.

Zusammenfassung—Das Zweiphasenmodell eines Gas-Feststoff-Fliessbetts wird auf Versuche über stationäre und nicht-stationäre Gasmischung angewandt. Die zwei Phasen sind: eine dichte Phase von Feststoffaggregaten und eine dispergierte Phas emit grosser Gasgeschwindigkeit. Zwischen beiden Phasen findet Austausch von Gas und Feststoff statt, zufolge Desintegration der Aggregaten und Bildung neuer Aggregaten von dispergierten Feststoffteilchen.

Ausdrücke für Gasrückvermischung und für die Streuung in der Gasverweilzeit werden abgeleitet. Ferner wird gezeigt, dass sich die effektive Gasläng sdiffusion in der dichten Phase und der Gasstoffaustausch zwischen den beiden Phasen mit Hilfe geeigneter Mischversuche bestimmen lassen.

Résumé—Le modèle en deux phases pour des lits fluidisés à l'aide de gaz est appliqué sur des essais pour déterminer le mélange de gaz dans ces lits. Les deux phases sont: une phase dense se composant d'agrégats de particules solides et une phase dispersée de grande vitesse de gaz. Le gaz et les solides sont échangés continuellement par suite de la désintégration des agrégats et de la coalescence des solides dispersés.

L'auteur déduit des équations pour le mélange vertical de gaz et pour la dispersion du temps de séjour de gaz. Il démontre que la diffusion verticale de gaz dans la phase dense et le transfert de matière dans le gaz entre les deux phases peuvent être déterminés à l'aide d'essais de mélange appropriés.

Introduction

The behaviour of gas–solid fluidized reactors has been the subject of many studies and discussions in the past decade. Although fluidization research has made considerable progress, the fluid mechanical aspects are still not completely understood. This situation makes it difficult to explain in some detail what is going on in a fluidized bed when heterogeneous reactions take place.

Earlier studies [1] on gas back-mixing in fluidized catalyst beds have shown that the down-mixing increases as the bed diameter is increased. Extrapolation to commercial scale leads to the conclusion that a large-diameter fluidized reactor may, as a first approximation, be considered as one well-mixed stage.

Later information from tests on commercial units, as well as from experiments on a smaller scale, has indicated that the actual situation is much more complicated than was suggested by the earlier work. During sampling in the regenerator of a commercial catalytic cracking unit [1], it was observed that oxygen concentrations in the bed were appreciably lower than the

*Present address: Koninklijke/Shell-Laboratorium, Amsterdam, Netherlands. (Shell Internationale Research Maatschappij).

oxygen concentration in the stack gas. In order to explain this phenomenon a two-phase fluidization mechanism was postulated, according to which the major portion of the gas passes through the bed in the form of " bubbles " or " cavities." In these discontinuities the oxygen concentration is considerably higher than the dense continuous phase, where most of the oxygen is rapidly consumed by burning. The low oxygen concentrations which were observed are then the result of preferential sampling from the dense phase. It was concluded that a fluidized reactor might be inefficient in establishing gas–solid contact.

The theory of two-phase fluidization was developed more explicitly by TOOMEY and JOHNSTONE [2], SHEN and JOHNSTONE [3], PANSING [4] and LEWIS *et al.* [5]. In the mathematical model a transfer coefficient is introduced which describes the interchange of gas between bubble phase and dense phase. Gas back-mixing in the bubble phase is neglected. For the dense-phase gas only the two extremes of zero back-mixing or complete vertical mixing were considered. The latter is evidently a serious restriction since it excludes the use of an eddy diffusivity as a separate parameter. MAY [6, 7] was the first to introduce a vertical diffusion coefficient for the dense-phase gas in the two-phase model. In the evaluation of this model with the aid of gas and solids mixing tests it was assumed that the vertical solids diffusivity was equal to the dense-phase vertical gas diffusivity. Although this assumption would seem to be reasonable it need not necessarily be true.

In the present paper the model of MAY is applied to gas mixing experiments to determine both dense-phase gas vertical diffusivity and gas interchange between the two phases without using the assumption of equal diffusivity of solids and dense-phase gas.

THE PHYSICAL PICTURE

The main feature of gas–solid aggregative fluidization is the formation and disintegration of aggregates of particles in a sort of dynamic equilibrium. Large aggregates fall down through the bed, carrying with them entrained gas until they are broken up into smaller fragments; small aggregates or single particles are carried upward by the gas stream until they coalesce with other aggregates. The continuous disintegration and coalescence of aggregates imposes a random motion on the vertical gas flow.

As the gas velocity is increased, the aggregates are more easily disintegrated. They have a shorter lifetime and become smaller. The result is that the average bed density decreases. With further increase in velocity, finally all the aggregates and single particles are carried upward and dispersed-phase pneumatic transport becomes possible.

When the gas velocity decreases, the aggregates become larger until they eventually form a continuous phase through which the gas, together with a small fraction of the particles, flows up in " cavities." With still smaller gas velocities the bed becomes quiescent and the " cavities " disappear.

In the region of the wall and other solid boundaries, the formation of larger aggregates with longer lifetime is promoted. Downflow of gas and particles will, therefore, often take place along the wall, although for large-diameter vessels it is just as possible that local downflow occurs in the centre.

In general it will not be appropriate to speak of the dense phase as the continuous phase, because there is no sharply defined phase reversal. In the region of the wall, for instance, the dense phase might be continuous in character whereas, more centrally, dense aggregates are present in a continuous dilute phase.

In order to define more clearly two phases in a fluidized bed, it is convenient to consider an instantaneous situation. Part of the gas will have high vertical velocities and will carry only very small aggregates and single particles. This will be called the dispersed-phase gas. The dense-phase gas consists then of the gas in the interstices of the large aggregates.

In the dynamic situation the continuous disintegration and formation of aggregates effects an exchange of gas (and particles) between the dense and the dispersed phase. This mass-transfer mechanism is of importance for heterogeneous reactions because it brings unreacted gas into

VOL. 13 1961

contact with the bulk of the solids and it removes products from the dense phase back into the dispersed phase.

The density of the aggregates is usually assumed to be equal to the density of the fluidized bed at incipient fluidization. The volumes of dense and dispersed phase may then be easily calculated from the overall bed density at any higher gas velocity. It should be realized that the bed expansion, and therefore the volumes of the phases is dependent not only on gas velocity, but also on vessel diameter, gas and solid properties, etc.

Now what will happen when a gas-mixing test is carried out or a heterogeneous reaction is taking place?

When a pulse of tracer gas is injected at the bottom of the bed, initially most of the tracer molecules will travel up in the dispersed phase at a rather high speed. Gradually part of them will be transferred to the dense phase, where down-mixing takes place, until they are removed (stripped) back into the dispersed phase. Depending on the height of the bed, or more accurately, on the number of transfers between dense and dispersed phase and on the degree of random motion, the output signal will exhibit more or less spread in residence times. A considerable spread in residence times, for instance, may be the result of either considerable down-mixing in the dense phase combined with rapid transfer between the phases or little down-mixing combined with a slow rate of transfer or any other situation in between. In other words, a pulse test alone is insufficient to evaluate the parameters of the model.

In a steady-state gas-mixing test a tracer gas is injected at a steady rate higher up in the bed and the tracer concentration distribution is determined by sampling at various locations in the bed. There will be no appreciable concentration of tracer gas below the injection point when the down-mixing is slow and, in addition to that, the rate of transfer between dense and dispersed phase is rapid. Otherwise the concentration gradients in the bed may become small.

For the case of a heterogeneous reaction, a fluidized bed may be considered as two parallel reactors with exchange of both gas and solids. Without any exchange the reactor corresponding to the dense phase would operate at extremely small throughput and almost zero space velocity and, therefore, yield practically 100 per cent conversion. The reactor corresponding to the dispersed phase would be a high throughput, very-low-conversion reactor. The total conversion would, therefore, also be very low. As the rate of transfer between the two reactors increases, the total conversion will increase until it levels off when complete participation of all the solids is approached. It is evident that, for incomplete participation of the solids, possible secondary reactions are enhanced.

True bypassing will only occur when the rate of transfer between the dense and the dispersed phase is very small and the dispersed phase contains very little solids.

Mathematical formulation

Let the gas in the dispersed phase occupy a volume fraction, F, and let the average vertical velocity be V. When f and v represent the same quantities for the gas in the dense phase, then the superficial gas velocity u, is equal to

$$u = F\,V + f\,v \qquad (1)$$

The rate of mass transfer between the phases is assumed to be proportional to the difference in the average concentrations C and c: rate of transfer per unit height $= k\,(C - c)$.

The random motions in the gas will be described with the aid of an eddy diffusivity, E. Although the vertical gas mixing has only partly to do with the behaviour of the dense phase it will nevertheless be assumed in the following that the eddy motions take place in the dense phase only.

The eddy diffusivity concept imposes certain restrictions on the applicability of the model. If, for instance, there should be a continuous fall of aggregates from top to bottom along the wall, the eddy currents would lose their random character and the eddy diffusivity would afford at the most a rather qualititive picture*. On the

*Another possible model circumventing this difficulty is perhaps: countercurrent flow of gas in the phases combined with mass transfer. The rate of gas down-flow in the dense phase (caused by the falling large aggregates) would then be the important factor for the degree of down-mixing in the bed.

other hand it should be realized that the model should describe in the first instance the ideal fluidized bed. Deviations such as extreme wall effects or uneven gas distribution will then be characterized by unusual behaviour of the parameters of the model.

The material balances for a differential height, dx, in the fluidized bed lead to the following differential equations

$$F\frac{\partial C}{\partial t} + V F\frac{\partial C}{\partial x} + k(C - c) = 0 \qquad (2)$$

$$f\frac{\partial c}{\partial t} + v f\frac{\partial c}{\partial x} + k(c - C) - f E\frac{\partial^2 c}{\partial x^2} = 0 \qquad (3)$$

For a steady-state gas-mixing test $\partial c/\partial t$ and $\partial C/\partial t$ are equal to zero. For the case of a chemical reaction $\partial c/\partial t$ and $\partial C/\partial t$ may be expressed in terms of rate constants and concentrations of the two phases.

The limiting cases of incipient fluidization ($F = 0$) and infinitely high rate of mass transfer ($k = \infty$) lead to the same simplification of (2) and (3).

$$(f + F)\frac{\partial c}{\partial t} + u\frac{\partial c}{\partial x} - f E\frac{\partial^2 c}{\partial x^2} = 0 \qquad (4)$$

Steady-state gas back-mixing tests

In a gas back-mixing test a tracer gas is injected at a steady rate higher up in the bed and the concentration gradient below the point of injection is observed. Fig. 1 shows the result of a typical small-scale back-mixing test. What happens apparently is that tracer is transferred from the centre to the wall from where it is carried down below the injection point until it is stripped from the dense phase by the upflowing gas in the centre. This behaviour bears a close analogy to the theoretical model. The downstream concentration profiles indicate that it takes about 1 ft. for the tracer to become transferred to the dense region at the wall; in other words, the height of a transfer unit is roughly equal to 1 ft. It may, therefore, be expected that when the bed level above the injection point becomes smaller than 1 ft., the back-mixing decreases.

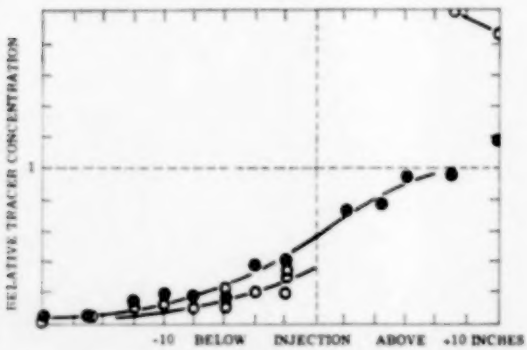

Fig. 1. Back-mixing in a 3 in. diameter fluidized bed according to Mason [8]. Tracer injection int he centre. 155 μ glass beads 1·2 ft/sec superficial gas velocity
○ Centre ● Wall

It should also be expected that tracer injection at the wall will give more back-mixing than tracer injection in the centre since in the first case no additional transfer step is required. This has been confirmed by Mason [8, 9] who compared single-point injection at the centre with multiple-point injection over the cross-section.

In large commercial vessels the analysis of a steady-state mixing test is complicated by radial mixing effects. The mathematical treatment will, therefore, be confined to small-scale experiments which, except for the transfer between dense and dispersed phase, are essentially one-dimensional.

Under steady-state conditions, equations (2) and (3) reduce to:

$$V F\frac{dC}{dx} + k(C - c) = 0 \qquad (5)$$

$$f E\frac{d^2 c}{dx^2} - v f\frac{dc}{dx} + k(C - c) = 0 \qquad (6)$$

Subtracting (5) from (6) gives

$$f E\frac{d^2 c}{dx^2} - v f\frac{dc}{dx} - V F\frac{dC}{dx} = 0$$

or, integrated,

$$f E\frac{dc}{dx} - v f c - V F C = \text{constant} \qquad (7)$$

Applying equation (7) to a level in the bed far enough above the tracer injection point, $x = 0$, where dc/dx may be considered as being substantially equal to zero and where C and c will have the same value C_0, it is seen that

$$f E \frac{dc}{dx} - v f c - V F C = - (v f + V F) C_0 = - u C_0 \text{ for } x > 0. \quad (8)$$

Below the injection point

$$f E \frac{dc}{dx} - v f c - V F C = 0 \text{ for } x < 0 \quad (9)$$

Across the boundary, $x = 0$, between the two regions the concentration c is continuous, but by (8) and (9)

$$V F \Delta C = u C_0 + f E \Delta \left(\frac{dc}{dx}\right) \text{ across } x = 0 \quad (10)$$

The fraction of tracer injected into the dense phase is equal to

$$\alpha = - \frac{Ef}{uC_0} \Delta \left(\frac{dc}{dx}\right)_{x=0} \quad (11)$$

When all the tracer is injected into the dense phase:

$$\alpha = 1, \Delta C = 0, \text{ and } \Delta \left(\frac{dc}{dx}\right) = - \frac{uC_0}{fE}$$

When all the tracer is injected into the dispersed phase:

$$\alpha = 0, V F \Delta C = u C_0, \text{ and } \Delta \left(\frac{dc}{dx}\right) = 0$$

The boundary conditions at the bottom of the bed are

$$C = 0 \text{ and } E \frac{dc}{dx} = v c \text{ for } x = - L \quad (12)$$

The solution of the differential equations (8) and (9) subject to the boundary conditions (10), (11) and (12) may be obtained by standard methods.

The concentration in the dense phase is found to be

$$\frac{c}{C_0} = A \exp\left(\frac{\lambda x}{L}\right) + B \exp\left(\frac{\mu x}{L}\right) \text{ for } x < 0 \quad (13)$$

$$\frac{c}{C_0} = 1 + D \exp\left(\frac{\mu x}{L}\right) \text{ for } x > 0 \quad (14)$$

where λ is the positive and μ is the negative root of the equation

$$y^2 + \left(\frac{kL}{FV} - \frac{Lv}{E}\right) y - \frac{kL^2}{fE}\left(1 + \frac{fv}{PV}\right) = 0 \quad (15)$$

The constants A, B, and D are

$$A = \frac{\alpha (L/E)(u/f) - \mu}{\lambda - \mu} \quad (16)$$

$$B = - A \frac{\lambda - (Lv/E)}{\mu - (Lv/E)} \exp(\mu - \lambda) \quad (17)$$

$$D = A \left[1 - \frac{\lambda - (Lv/E)}{\mu - (Lv/E)} \exp(\mu - \lambda)\right] - 1 \quad (18)$$

The concentration in the dispersed phase may be derived from (13) and (14) with the aid of equations (8) and (9).

Under many conditions a considerable simplification is feasible. When the superficial gas velocity is not too small (say $> 0{\cdot}5$ ft./sec.) most of the gass passes through the bed in the dispersed phase; i.e. fv may be neglected compared with FV. Finally, often the tracer concentration at the bottom of the bed is negligibly small. Then L is infinite for practical purposes. Under these conditions the solutions become for the dense phase

$$\frac{c}{C_0} = \left(\alpha \frac{\beta^2 - 1}{4\beta} + \frac{\beta + 1}{2\beta}\right) \exp\left(\frac{\beta - 1}{2} \frac{kx}{u}\right) \text{ for } x < 0 \quad (19)$$

$$\frac{c}{C_0} = 1 + \left(\alpha \frac{\beta^2 - 1}{4\beta} - \frac{\beta - 1}{2\beta}\right) \exp\left(\frac{\beta + 1}{2} \frac{kx}{u}\right) \text{ for } x > 0 \quad (20)$$

and for the dispersed phase

$$\frac{C}{C_0} = \left(\alpha \frac{\beta - 1}{2\beta} + \frac{1}{\beta}\right) \exp\left(\frac{\beta - 1}{2} \frac{kx}{u}\right) \text{ for } x < 0 \quad (21)$$

$$\frac{C}{C_0} = 1 + \left(\frac{1}{\beta} - \alpha \frac{\beta + 1}{2\beta}\right) \exp\left(- \frac{\beta + 1}{2} \frac{kx}{u}\right) \text{ for } x > 0 \quad (22)$$

$$\text{where } \beta^2 = 1 + 4 \frac{u^2}{fEk} \quad (23)$$

Denoting

$$H_k = \frac{u}{k} = \text{height of a transfer unit} \quad (24)$$

and

$$H_E = \frac{fE}{u} = \text{height of an eddy diffusion unit} \quad (25)$$

so that

$$\beta^2 = 1 + 4\frac{H_k}{H_E} \tag{26}$$

it is seen that the concentration profiles are completely determined by the dimensionless parameters α, H_k/H_E and x/H_k.

Figs. 2 and 3 show as examples the cases $H_k/H_E = 6$, $\alpha = 0$, (tracer injection in the dispersed phase) and $H_k/H_E = 6$, $\alpha = 1$ (tracer injection in the dense phase).

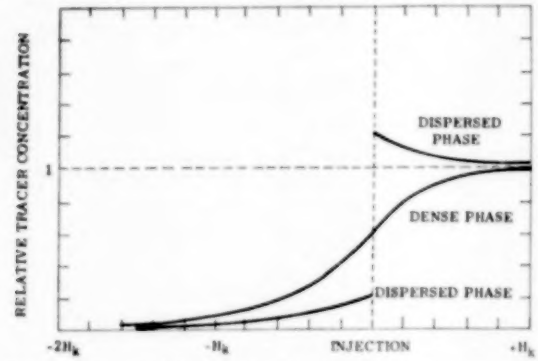

FIG. 2. Tracer injection in the dispersed phase, $\alpha = 0$, $H_k = 6H_E$.

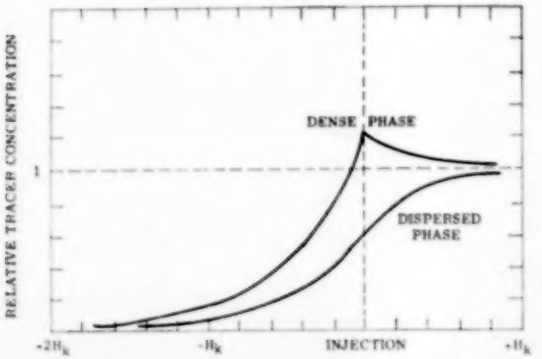

FIG. 3. Tracer injection in the dense phase, $\alpha = 1$, $H_k = 6H_E$.

The value of α appears to have a pronounced influence on the nature of the concentration profiles. The close analogy between Figs. 1 and 2 suggests that tracer injection in the centre is approximately equivalent to tracer injection in the dispersed phase. The high concentrations observed in the centre above the injection point might be the result of sampling from the plume emerging from the injection pipe. Below the injection point the samples drawn in the centre might not be representative of the dispersed phase. These samples will then show too high a concentration. Samples drawn along the wall, however, may be considered to be dense-phase samples.

When Figs. 1 and 2 are compared under these assumptions it would seem that $H_k \simeq 10$ in. and $H_E \simeq 2$ in. for the conditions of Fig. 1. It should be realized, however, that this estimate is rather inaccurate due to the scatter in the experimental results and particularly because of the uncertainty in the value of α, which was assumed to be equal to 0. For instance, the combination $\alpha = 0{\cdot}02$, $H_k = 20$ in. and $H_E = 1$ in. would fit the experimental data just as well. It appears, therefore, that the assumption $\alpha = 0$ would lead to a lower limit for H_k and an upper limit for H_E. These limits may most conveniently be found by plotting the logarithm of the concentration along the wall as a function of the vertical position. Upstream, the experimental points should, according to equation (19), fall on a straight line with a slope

$$S = \frac{\beta - 1}{2H_k} \tag{27}$$

The slope, S, is usually termed the mixing slope. The intercept of this straight line with $x = 0$ is, for $\alpha = 0$, equal to $(\beta - 1)/2\beta$. From slope and intercept the limiting values of H_E and H_k are easily calculated.

In this way some of the older back-mixing experiments [1] where the tracer was injected in the centre have been evaluated. Since the results are rather qualitative details of this evaluation will be omitted. No systematic effect of the superficial gas velocity (0·1–1·1 ft/sec.) or particle diameter (cracking catalyst 55–110 μ) was apparent within the limits of accuracy. The effect of bed diameter may be seen from Table 1 below:

Table 1

Diameter (in.)	H_E *(Maximum) (ft.)*	H_k *(Minimum) (ft.)*
2	0·3–0·5	0·8–1·2
4	0·4–1·2	0·4–1·8
6	1·2–1·9	2·0–2·5

Although only (rather inaccurate) limiting values are obtained it appears from these results that in small-diameter fluidized reactors mass-transfer might be even more important than the effect of eddy diffusion. Bed heights of several feet are required to ensure that mass transfer is not a limiting factor.

In many of MASON's back-mixing experiments [8] the tracer was injected in both the dense and the dispersed phase. For such a case the value of α is too large to allow a similar calculation. It follows, however, from equations (19) and (21) that the mixing slope (27) is the same for the dense and the dispersed phase and, moreover, that it is independent of the value of α. It will be shown in the following how H_E and H_k may be calculated from the mixing slope and a residence time distribution measurement. Fortunately MASON has carried out both types of mixing test for the same systems.

RESIDENCE TIME DISTRIBUTION MEASUREMENTS

For the evaluation of residence time distribution measurements an expression has been derived for the standard deviation, s, in terms of the parameters of the two-phase model (Appendix). To simplify the calculations the assumption has been made that there is no net vertical flow of gas through the dense phase. The expression reads

$$\sigma^2 = \frac{2}{n_k}(1-\phi)^2 + \frac{2}{n_E} + \frac{2q}{n_E^2} \times \times \frac{\{\exp[\tfrac{1}{2}n_k(q-1)]-1\}\{\exp[-\tfrac{1}{2}n_k(q+1)-1\}}{\exp[\tfrac{1}{2}n_k(q-1)] - \exp[-\tfrac{1}{2}n_k(q+1)]} \quad (28)$$

where

$$\sigma = \frac{s}{\bar{\theta}} = \text{relative standard deviation} \quad (29)$$

$$q = \left(1 + 4\frac{n_E}{n_k}\right)^{1/2} \quad (30)$$

$$n_k = \frac{L}{H_k} = \frac{kL}{u} = \text{number of transfer units*} \quad (31)$$

*n_k is equal to the "cross flow ratio" introduced by MAY [6, 7].

$$n_E = \frac{L}{H_E} = \frac{uL}{fE} = \text{number of eddy diffusion units} \quad (32)$$

$$\phi = \frac{F}{F+f} = \text{fraction of gas present as dispersed phase} \quad (33)$$

In Figs. 4, 5, 6 and 7 lines of constant standard deviation are drawn in n_k vs. n_E plots for four values of the parameter ϕ. The positions of the n_k values on the vertical axes were calculated by

$$\frac{2}{n_k}(1-\phi)^2 = \frac{2}{L}(1-\phi)^2 H_k \quad (34)$$

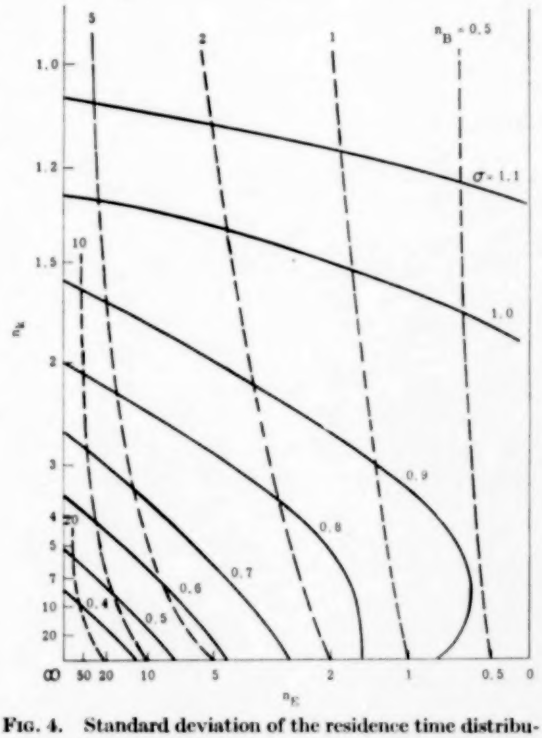

FIG. 4. Standard deviation of the residence time distribution and number of back-mixing units for two-phase fluidization; $\phi = 0{\cdot}2$.

In other words, the vertical co-ordinate is proportional to the height of a transfer unit.

The n_E positions on the horizontal axis are given by

$$\frac{2}{n_E} - \frac{2}{n_E^2}[1 - \exp(-n_E)] = \frac{1}{n} = \frac{H}{L} \quad (35)$$

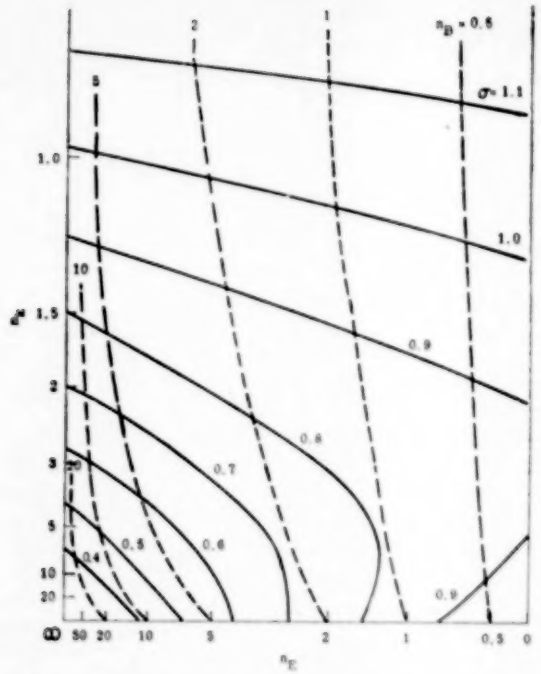

FIG. 5. Standard deviation of the residence time distribution and number of back-mixing units for two-phase fluidization ; $\phi = 0{\cdot}3$.

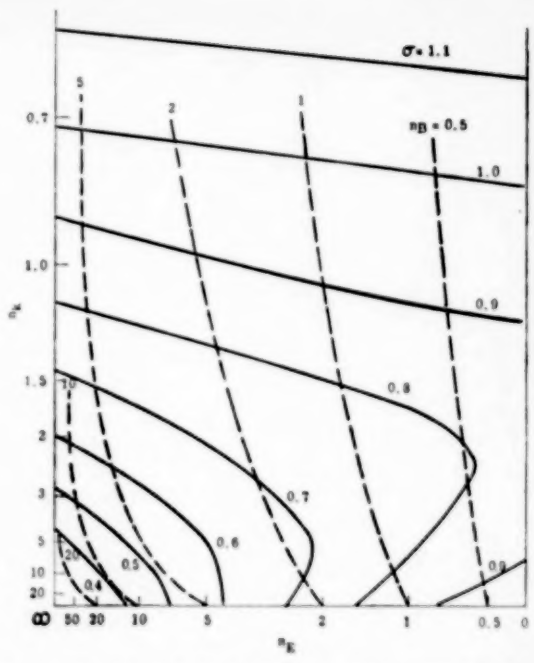

FIG. 6. Standard deviation of the residence time distribution and number of back-mixing units for two-phase fluidization ; $\phi = 0{\cdot}4$.

The expression (35) results from (28) when n_k becomes infinite. n is equal to the number of completely mixed stages giving the same standard deviation (see Ref. 10). The horizontal co-ordinate is, therefore, proportional to the height H, of a mixing stage in the dense phase.

Under the assumption of no net gas flow in the dense phase the expression for the mixing slope

Table 2. Experiments by MASON *in a* 3 in. *diameter,* 37 in. *high bed*

Particles	*Particle size* (μ)	*Superficial velocity* (ft/sec)	*Relative standard deviation*	*Reciprocal mixing slope* (ft)	H_E (ft)	H_k (ft)	H_k/H_E
Cracking catalyst	70	0·4	0·87	0·75	0·40	1·5	4
	70	0·6	0·87	0·78	0·36	1·7	5
	70	0·9	0·87	0·78	0·30	2·0	7
Cracking catalyst	104	0·4	0·84	0·73	0·40	1·5	4
	104	0·6	0·84	0·71	0·33	1·7	5
	104	0·9	0·84	0·68	0·23	2·0	9
Glass beads	102	0·4	0·62	0·29	0·06	0·7	12
	102	0·6	0·62	0·37	0·16	0·7	4
	102	0·9	0·62	0·61	0·27	0·6	2
Glass beads	155	0·6	0·52	0·20	0·06	0·5	8

VOL. 13 1961

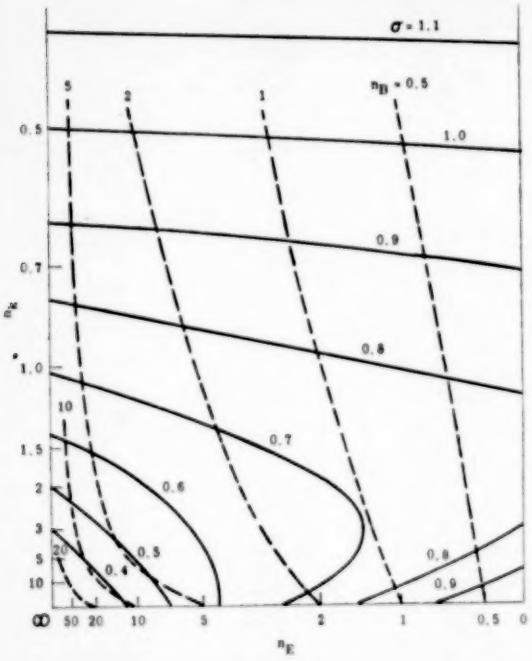

FIG. 7. Standard deviation of the residence time distribution and number of back-mixing units for two-phase fluidization; $\phi = 0.5$.

obtained in a steady-state back-mixing experiment was found to be (cf. equation 27).

$$S = \frac{\sqrt{(1 + 4n_E/n_k)} - 1}{2H_k} \qquad (36)$$

It was pointed out earlier that the theoretical mixing slope (36) is not dependent on the relative amounts of tracer gas injected in each of the two phases.

When both σ and S are measured, n_k and n_E, or H_k and H_E may be determined if the value of ϕ is known. This may be most easily achieved graphically. To this end, lines are drawn in Figs. 4, 5, 6 and 7 on which the product of bed height and mixing slope

$$n_B = L\,S = \tfrac{1}{2}\,n_k\left[\sqrt{(1 + 4\,n_E/n_k)} - 1\right] \qquad (37)$$

is constant. This product may be called the number of back-mixing units. A value much greater than 1 indicates little down-mixing; a value smaller than 1 means considerable down-mixing. The value of ϕ may be estimated from the measured bed expansion or from bed expansion correlations. With the aid of the grid, σ = constant, n_B = constant, the values of n_E and n_k can then be read directly from the corresponding graph. In this way a few of MASON's experiments could be analysed. The results are given in Table 2.

Comparison of Tables 1 and 2 shows that the limiting values of H_E and H_k are reasonably close to the values calculated from the combined information of steady-state and transient mixing tests. Although fluidized beds of glass beads appear to be quieter than cracking catalyst beds the ratio H_k/H_E is roughly the same.

MAY [6, 7] has carried out solid mixing tests with fluid cracking catalyst in vessels of 3 in., 15 in. and 5 ft. diameter. The solid diffusivities were at 0·8 ft/sec. superficial gas velocity 0·6, 1·6 and 5 ft²/sec respectively. The present study indicates that at 0·8 ft/sec superficial gas velocity the gas diffusivity ($E = u\,H_E/f$) is of the same order of magnitude for comparable vessel diameter.

From residence distribution measurements in a 3 in. diameter unit for 12 and 35 ft bed height MAY finds a height of transfer unit of about 3 ft. This value is higher than the values derived from MASON's data, but MAY points out that the experimental conditions are not directly comparable.

Coming now to the question of the physical significance of the present results, some speculation is perhaps justified. To this end, let us go back to the definitions. H_E is a measure of the distance over which the bigger particle aggregates fall before they are broken up into smaller pieces. H_k is the average distance travelled by the dispersed-phase gas between a place where it escapes from disintegrating aggregates to a place where it is trapped by aggregates which are being formed. The ratio H_k/H_E will, therefore, be roughly equal to the ratio of the linear velocity of the dispersed-phase gas and the downward velocity of the bigger aggregates. This conclusion is in agreement with the picture we have of a small-diameter fluidized bed, viz. an internal circulation pattern consisting of fast-moving gas pockets in the centre and a slow downward movement of dense catalyst masses along the wall.

Table 1 suggests that for increasing diameter the ratio H_k/H_E decreases although the absolute values of H_k and H_E increase. It would seem, therefore, that in small-diameter vessels the size of the aggregates is determined by the diameter. This results in lower values for H_E and H_k, but also in a higher value for H_k/H_E because of a reduction in the downward velocity of the aggregates. It may be speculated that for vessels of very large diameter the size of the aggregates is determined by the fluid-dynamical parameters of the fluidized system rather than by wall effects. This would mean that H_E and H_k approach a maximum value if the diameter is increased under otherwise identical conditions. The ratio H_k/H_E, however, will approach a miminum value determined by fluid-mechanical conditions.

HETEROGENEOUS REACTIONS

The two-phase model can directly be applied to the calculation of fluidized bed reactors. MAY [6, 7] has carried out this calculation for a first-order heterogeneous reaction. On the other hand it is possible to evaluate the parameters of the two-phase model from the performance of the fluid bed as a reactor if at the same time a suitable gas-mixing test is carried out. In Fig. 8 the relationship between conversion, n_k and n_E is plotted for a typical case of a first-order heterogeneous reaction.*

In the same Fig. lines of constant relative standard deviation are drawn, taken from Fig. 5. The two families of lines form a grid which determines n_E and n_k when conversion and standard deviation of residence times are known. This procedure may in principle be applied to regenerators of commercial catalytic cracking units since the coke burning is first order in the oxygen concentration and the chemical kinetics are fairly well understood. The main difficulty is the accurate measurement of the spread in residence times. The problems involved with transient mixing tests in large units have been described in the papers of DANCKWERTS *et al.* [11] and

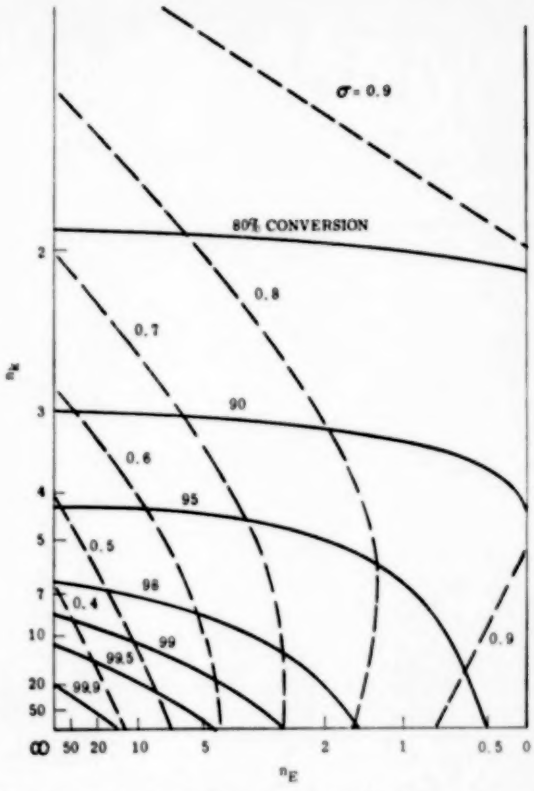

FIG. 8. First-order heterogeneous reaction in a two-phase fluidized bed, $\phi = 0{\cdot}3$.

HANDLOS *et al.* [12]. Some knowledge on the value of the main parameters, H_E and H_k, of the model for large-diameter vessels is, however, absolutely necessary if one ever wants to design large fluidized bed reactors on a more scientific basis.

Acknowledgment—The author wishes to acknowledge the help of several colleagues at Shell Oil Co., Houston Research Laboratory, and at Shell Development Co., Emeryville, during many stimulating discussions. He also would like to express his thanks to the management of Shell Oil Co. for their permission to publish this work.

APPENDIX

For the calculation of the standard deviation of the residence time distribution use will be made of the method indicated by VAN DER LAAN [10].

It will be assumed that the dense-phase gas velocity, v, is so small that the term $v f(\partial c/\partial x)$ in equation (3) can be neglected. The boundary conditions corresponding to a pulse injection of tracer gas are then

*The number of reaction units $KL/u = 10$, where K is the appropriate chemical rate constant. Assumptions: No net vertical gas flow in the dense phase. No catalyst present in the dispersed phase.

VOL. 13 1961

$$\left.\begin{aligned} &t = 0, && C = c = 0 \\ &x = 0, && \frac{\partial c}{\partial x} = 0, \quad C = \delta(t) \\ &x = L, && \frac{\partial c}{\partial x} = 0 \end{aligned}\right\} \qquad (A.1)$$

where $\delta(t)$ is the impulse function.

When the concentration C, is normalized in such a way that $\int_0^\infty \delta(t)\,dt = 1$, then the concentration response at the bed exit, $x = L$, is exactly the residence time distribution function, $R(t)$. Introduction of

$$\phi = \frac{F}{f+F}, \quad \xi = \frac{x}{L}, \quad \tau = \frac{Vt}{L} \qquad (A.2)$$

and application of the Laplace transformations

$$\overline{C} = \int_0^\infty \exp(-p\tau)\,C d\tau, \quad \bar{c} = \int_0^\infty \exp(-p\tau)\,c d\tau$$

reduces the equations (2), (3) and (A.2) to

$$\left.\begin{aligned} &\phi p\overline{C} + \frac{d\overline{C}}{d\xi} + n_k(\overline{C} - \bar{c}) = 0 \\ &(1-\phi)\,p\bar{c} - \frac{1}{n_E}\frac{d^2\bar{c}}{d\xi^2} + n_B(\bar{c} - \overline{C}) = 0 \end{aligned}\right\} \qquad (A.3)$$

$$\left.\begin{aligned} &\xi = 0, \quad \overline{C} = 1, \quad \frac{d\bar{c}}{d\xi} = 0 \\ &\xi = 1, \quad \frac{d\bar{c}}{d\xi} = 0 \end{aligned}\right\} \qquad (A.4)$$

The solution for $\overline{C}$ is obtained by standard methods

$$\overline{C} = \frac{\alpha_1 \exp(\lambda_1\xi) + \alpha_2 \exp(\lambda_2\xi) + \alpha_3 \exp(\lambda_3\xi)}{\alpha_1 + \alpha_2 + \alpha_3} \qquad (A.5)$$

where λ_1, λ_2 and λ_3 are the roots of the equation

$$\lambda^3 + (n_k + \phi p)\lambda^2 - n_E[(1-\phi)p + n_k]\lambda + \\ - \phi(1-\phi)p^2 n_E - p\,n_k\,n_E = 0 \qquad (A.6)$$

and

$$\alpha_1 = \frac{\exp(\lambda_3) - \exp(\lambda_2)}{n_k + \phi p + \lambda_1} \qquad (A.7)$$

$$\alpha_2 = \frac{\lambda_1}{\lambda_2}\frac{\exp(\lambda_1) - \exp(\lambda_3)}{n_k + \phi\,p + \lambda_2} \qquad (A.8)$$

$$\alpha_3 = \frac{\lambda_1}{\lambda_3}\frac{\exp(\lambda_2) - \exp(\lambda_1)}{n_k + \phi\,p + \lambda_3} \qquad (A.9)$$

The Laplace transformation of the residence time distribution is

$$\overline{C}(\xi = 1) = \overline{R}(p) = \\ = \frac{\alpha_1 \exp(\lambda_1) + \alpha_2 \exp(\lambda_2) + \alpha_3 \exp(\lambda_3)}{\alpha_1 + \alpha_2 + \alpha_3} \qquad (A.10)$$

The moments of the residence-time distribution function are found by forming the first, second, etc. differential quotients of $\overline{R}(p)$ with respect to p and letting p go to zero. The calculation for the present case requires differentiation of the expressions (A.6) up to (A.10) inclusive.

In the following differentiation with respect to p will be denoted by a prime and limiting values for $p = 0$ by a subscript 0.

It follows from (A.6) up to (A.10) inclusive

$$\lambda_{10} = 0, \quad \lambda_{21}\,\lambda_{30} = -n_k\,n_E, \quad \lambda_{20} + \lambda_{30} = -n_k,$$

$$n_k\,\alpha_{10} = \exp(\lambda_{30}) - \exp(\lambda_{20}),\ \alpha_{20} = 0,$$

$$\alpha_{30} = 0,\ \overline{R}_0 = 1 \qquad (A.11)$$

(A.10) will be written in the form

$$\overline{R}\,\Sigma\,\alpha_i = \Sigma\,\alpha_i \exp(\lambda_i) \qquad (A.12)$$

Differentiating (A.12) gives

$$\overline{R}'\,\Sigma\,\alpha_i + \overline{R}\,\Sigma\,\alpha_i' = \\ = \Sigma\,\alpha_i' \exp(\lambda_i) + \Sigma\,\alpha_i\,\lambda_i' \exp(\lambda_i) \qquad (A.13)$$

For $p = 0$ (A.13) becomes, considering (A.11)

$$\alpha_{10}\overline{R}' + \alpha'_2 + \alpha_3' = \\ = \alpha_2' \exp(\lambda_{20}) + \alpha_3' \exp(\lambda_{30}) + \alpha_1\lambda_1' \qquad (A.14)$$

By differentiating (A.6), (A.8) and (A.9) and using (A.11) it is found that

$$\lambda_{10}' = -1,$$

$$\alpha_{20}' = \frac{\exp(\lambda_{30}) - 1}{n_E\,n_k}, \quad \alpha_{30}' = \frac{1 - \exp(\lambda_{20})}{n_E\,n_k} \qquad (A.15)$$

and from (A.14) and (A.15)

$$\overline{R}_0' = -1 \qquad (A.16)$$

(the average dimensionless residence time is equal to 1).

Differentiating (A.13) yields

$$\overline{R}''\,\Sigma\,\alpha_i + 2\overline{R}'\,\Sigma\,\alpha_i' + \overline{R}\,\Sigma\,\alpha_i'' = \Sigma\,\alpha_i'' \exp(\lambda_i) + \\ + 2\,\Sigma\,\alpha_i'\lambda_i' \exp(\lambda_i) + \Sigma\,\alpha_i\lambda_i'' \exp(\lambda_i) + \\ + \Sigma\,\alpha_i(\lambda_i')^2 \exp(\lambda_i) \qquad (A.17)$$

For $p = 0$ (A.17) becomes, using (A.11), (A.15) and (A.16)

$$\alpha_{10}\overline{R}_0'' = 2\,\alpha_{20}'[1 + \lambda_{20}' \exp(\lambda_{20})] + \\ + 2\,\alpha_{30}'[1 + \lambda_{30}' \exp(\lambda_{30})] + \\ + \alpha_{20}''[\exp(\lambda_{20}) - 1] + \alpha_{30}''[\exp(\lambda_{30}) - 1] + \\ + \alpha_1\left[1 + \frac{2}{n_E} + \frac{2}{n_k}(1-\phi)^2\right], \qquad (A.18)$$

Expressions for α_{20}'' and α_{30}'' may be derived by differentiating (A.8) and (A.9) twice. It is found that

$$n_E n_k \alpha_{20}'' = 2\alpha_{20}'\lambda_{20}'\lambda_{30} + 2\alpha_{20}'\lambda_{20}(\phi + \lambda_{20}') + \\ + \lambda_{10}''[1 - \exp(\lambda_{30})] + 2[1 + \lambda_{30}'\exp(\lambda_{30})] \quad \text{(A.19)}$$

$$n_E n_k \alpha_{30}'' = 2\alpha_{30}'\lambda_{30}'\lambda_{20} + 2\alpha_{30}'\lambda_{30}(\phi + \lambda_{30}') + \\ + \lambda_{10}''[\exp(\lambda_{20}) - 1] - 2[1 + \lambda_{20}'\exp(\lambda_{20})] \quad \text{(A.20)}$$

When the expressions for α_{20}', α_{20}'', α_{30}' and α_{30}'' are introduced into (A.18) one obtains

$$\alpha_{10}\bar{E}_\theta'' = \alpha_{10}\left[1 + \frac{2}{n_E} + \frac{2}{n_k}(1-\phi)^2\right] + \\ + \frac{2}{n_E^2 n_k^2}[\exp(\lambda_{20}) - 1][\exp(\lambda_{30}) - 1] \times \\ \times (\lambda_{30} - \lambda_{20})(\beta + \lambda_{20}' + \lambda_{30}') \quad \text{(A.21)}$$

It follows from (A.6) that

$$\lambda_1 + \lambda_2 + \lambda_3 = -n_k - \phi p \quad \text{(A.22)}$$

or, by differentiating and letting p go to zero

$$-1 + \lambda_{20}' + \lambda_{30}' = -\phi \quad \text{(A.23)}$$

The use of (A.11) and (A.23) finally reduces (A.21) to

$$\bar{E}_\theta'' = 1 + \frac{2}{n_E} + \frac{2}{n_k}(1-\phi)^2 + \frac{2q}{n_E^2} \times \\ \times \frac{\{\exp[n_k(q-1)/2] - 1\}\{\exp[-n_k(q+1)/2] - 1\}}{\exp[n_k(q-1)/2] - \exp[-n_k(q+1)/2]} \quad \text{(A.25)}$$

The variance of the residence time distribution function is found from

$$\sigma^2 = \bar{E}_\theta'' - 1 = \frac{2}{n_k}(1-\phi)^2 + \frac{2}{n_E} + \frac{2q}{n_E^2} \times \\ \times \frac{\{\exp[n_k(q-1)/2] - 1\}\{\exp[-n_k(q+1)/2] - 1\}}{\exp[n_k(q-1)/2] - \exp[-n_k(q+1)/2]} \quad \text{(A.26)}$$

A few numerical values are found in the following table.

Values of $\sigma^2 - (2/n_k)\{f/(F+f)\}^2$

n_E \ n_k	0·2	0·5	1	2	5	∞
0	0·0333	0·0831	0·1639	0·3131	0·6135	1
0·2	0·0332	0·0822	0·1608	0·3020	0·5758	0·9365
0·5	0·0330	0·0810	0·1563	0·2868	0·5274	0·8522
1	0·0326	0·0791	0·1494	0·2646	0·4614	0·7358
2	0·0321	0·0755	0·1372	0·2292	0·3689	0·5677
5	0·0309	0·0655	0·1103	0·1637	0·2293	0·3280
∞	0	0	0	0	0	0

NOTATION

c, C, C_0	concentration	moles/ft³
E	eddy diffusivity	ft²/sec
f, F	volume fraction	
$H = L/n$	height equivalent to a completely mixed stage	ft
$H_E = fE/u$	height of an eddy diffusion unit	ft
$H_k = u/k$	height of a transfer unit	ft
k	mass-transfer coefficient	sec⁻¹
K	first-order reaction rate constant	sec⁻¹
L	height	ft
n	number of completely mixed stages	
$n_B = LS$	number of back-mixing units	
$n_E = uL/fE$	number of eddy diffusion units	
$n_k = kL/u$	number of transfer units	
$n_R = KL/u$	number of reaction units	
s	standard deviation	sec
S	mixing slope	ft⁻¹
t	time	sec
u	superficial velocity	ft/sec
v, V	linear velocity	ft/sec
x	vertical co-ordinate	ft
α	fraction of tracer injected into the dense phase	
θ	average residence time	
$\sigma = s/\theta$	relative standard deviation	
$\phi = \frac{F}{f+F}$	fraction of gas in the dispersed phase	

REFERENCES

[1] ASKINS J. W., HINDS, G. P. and KUNREUTHER F. *Chem. Engng. Prog.* 1951 **47** 401.
[2] TOOMEY R. D. and JOHNSTONE H. F. *Chem. Engng. Prog.* 1952 **48** 220.
[3] SHEN C. Y. and JOHNSTONE H. F. *Amer. Inst. Chem. Engrs. J.* 1955 **1** 349.
[4] PANSING W. F. *Amer. Inst. Chem. Engrs. J.* 1956 **2** 71.
[5] LEWIS W. K., GILLILAND E. R. and GLASS W. *Amer. Inst. Chem. Engrs. J.* 1959 **5** 419.
[6] MAY W. G. *Dechema-Monogr.* 1959 **32** 261.
[7] MAY W. G. *Chem. Engng. Progr.* 1959 **55** 49.
[8] MASON E. A. Sc.D. Thesis, Chemical Engineering, Massachusetts Institute of Technology 1950.
[9] GILLILAND E. R. and MASON E. A. *Industr. Engng. Chem.* 1952 **44** 218.
[10] VAN DER LAAN E. T. *Chem. Engng. Sci.* 1958 **7** 187.
[11] DANCKWERTS P. V., JENKINS J. W. and PLACE G. *Chem. Engng. Sci.* 1954 **3** 26.
[12] HANDLOS A. E., KUNSTMAN R. W. and SCHISSLER D. O. *Industr. Engng. Chem.* 1957 **49** 25.

VOL 13 1961

Chemical Engineering Science, 1961 Vol. 13, pp. 155 to 166. Pergamon Press Ltd., London. Printed in Great Britain

Heat and mass transfer in the presence of an inert gas

H. F. JOHNSTONE and W. B. RETALLICK*
University of Illinois, Urbana, Illinois, U.S.A.

(*Received* 7 *July* 1960)

Abstract—A new graphical method for solving enthalpy transfer problems is described in which a modified enthalpy is the transfer potential. The condition line is determined by successive approximations. An entire condition line is constructed for each approximation, and the resulting approximate line determines an auxiliary line used for the next construction. The method was used to calculate enthalpy transfer coefficients from experimental data on enthalpy transfer in a grid-packed tower for the tetrachloroethylene–air system, which are reported. Three types of countercurrent operations were studied:

(1) The vapour content of the gas is increased and the gas is heated by hot liquid.

(2) The vapour content of the gas is increased and both the gas and the liquid are cooled.

(3) The liquid is heated by the hot gas and the vapour content of the gas is either increased or decreased.

The enthalpy transfer coefficients for operations of the first type were lower than those for the other two. The existence of fog during dehumidification had no apparent effect on the coefficients.

The application of the graphical method to the design of a cooler-condenser is described.

Résumé—Les auteurs donnent une nouvelle méthode graphique de résolution des problèmes de transfert d'enthalpie dans laquelle le potentiel de transfert est une entropie modifiée. L'équation de la droite opératoire est déterminée par des approximations successives. Une droite opératoire est construite pour chaque approximation et la droite approximative qui en résulte détermine une droite auxiliaire utilisée pour la construction suivante. La méthode est utilisée pour calculer les coefficients de transfert d'enthalpie à partir de données expérimentales sur le transfert d'enthalpie dans une tour à garnissage à grilles pour le système tetrachloroethylene-air. Trois types d'opérations à contre courant ont été étudiées:

1. La teneur en vapeur du gaz est augmentée et le gaz est chauffé par le liquide chaud.
2. La teneur en vapeur du gaz est augmentée et le gaz et le liquide sont tous deux refroidis.
3. Le liquide est chauffé par le gaz chaud et le teneur en vapeur du gaz est soit augmentée, soit diminuée.

Les coefficients de transfert d'enthalpie, pour les opérations du premier type sont inférieurs à ceux des deux autres.

L'existence de brouillard pendant la deshumidification n'a pas d'effet apparent sur les coefficients.

Les auteurs décrivent l'application de la méthode graphique au calcul d'un condenseur.

Zusammenfassung—Es wird eine neue graphische Methode für die Lösung von Enthalpieübergangsproblemen beschrieben, bei der eine modifizierte Enthalpie das Übergangspotential bildet.

Die Zustandskurve wird durch schrittweise Annäherungen bestimmt. Die gesamte Zustandskurve wird bei jeder Annäherung konstruiert und die hieraus sich ergebende Näherungslinie ergibt eine Hilfslinie, die für die Konstruktion der nächstfolgenden Annäherung benutzt wird. Die Methode wurde zur Berechnung von Enthalpie-Übergangskoeffizienten aus experimentellen Ergebnissen des Enthalpieübergangs in einer Füllkörperkolonne für das System Tetrachloräthylen-Luft benutzt, die mitgeteilt werden. Drei Typen von Gegenstromverfahren wurden untersucht:

1. Der Dampfgehalt des Gases wurde erhöht, und das Gas wurde durch die heisse Flüssigkeit erwärmt.
2. Der Dampfgehalt des Gases wurde erhöht, und sowohl das Gas als auch die Flüssigkeit wurden gekühlt.
3. Die Flüssigkeit wurde durch das heisse Gas erwärmt, und der Dampfeghalt des Gases wurde entweder erhölt oder gesenkt.

Die Enthalpie-Übergangskoeffizienten waren bei Versuchen vom Typ (1) niedriger als bei den beiden anderen.

Das Auftreten von Nebeln während der Trocknung hatte keinen augenfälligen Einfluss auf die Koeffizienten.

Die Anwendung der graphischen Methode bei der Auslegung eines Kühler-Kondensators wird beschrieben.

*Present address: Consolidation Coal Company, Library, Pennsylvania.

INTRODUCTION

WHEN heat and mass are transferred simultaneously across a gas–liquid interface it is convenient to consider that enthalpy is the quantity that is transferred [1]. For mixtures of water vapour and air, for which the Lewis relationship, $h_G/k_G = C_s$, is valid, the enthalpy difference is the potential that establishes the rate of transfer. For the general case

$$\frac{h_G}{k_G} = C_s \left(\frac{Sc}{Pr}\right)^{2/3} \frac{P_{BM}}{P_{Bi}} = C_s \psi \qquad (1)$$

and the simple enthalpy potential cannot be used but a modified enthalpy term that includes the Schmidt and Prandtl groups is required, as proposed by MIZUSHINA and KOTOO [2] and MIZUSHINA and NAKAJIMA [3].

ϕ is a modified enthalpy defined by

$$\phi = C_s \psi (t - t_0) + \lambda_0 H \qquad (2)$$

LEWIS and WHITE [4] also use a modified enthalpy potential for enthalpy transfer, but they arrange the groups in another way.

In this paper a graphical method of solving enthalpy transfer problems is described in which the modified enthalpy is included. The method was used to calculated transfer coefficients from experimental data on the tetrachloroethylene–air system, which are also reported here. In the graphical method the condition line for the enthalpy of the gas at any temperature is assumed to start the calculations and the Method of Approximations is used until convergence is obtained for the assumed and calculated condition lines.

THEORETICAL DISCUSSION

In the air–water system the slope of the condition line for any enthalpy transfer process is [1]

$$\frac{di_G}{dt_G} = \frac{i_i - i_G}{t_i - t_G} \qquad (3)$$

For the general case

$$\frac{di_G}{dt_G} = \frac{\phi_i - \phi_G}{t_i - t_G} \cdot \frac{1}{\psi} \qquad (4)$$

The derivation of equation (4) is similar to that given by MICKLEY for the air–water system [1], except that equation (1) is used in the derivation instead of the Lewis relationship. Equation (1) is derived by equating COLBURN's factors for heat and mass transfer and converting the mass transfer coefficient to the use of a potential expressed as pounds of vapour per pound of gas.

To illustrate the graphical method, the coefficients, h_L, k_G and h_G, will be calculated from the data on an adiabatic humidification tower. The initial data include the rates of flow of the gas and liquid, the temperature of the liquid at the ends of the tower, the temperature and humidity of the gas at the ends of the tower and the tower height. The terminal values of i_G and ϕ_G are calculated from the observed temperatures and humidities.

The graphical calculation is shown in Fig. 1. The equilibrium and operating lines are represented by curves of enthalpy, or ϕ, vs. temperature. Only the ϕ equilibrium line is needed.

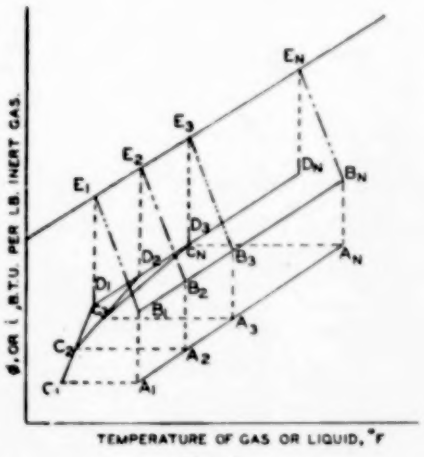

FIG. 1.

The equation for the enthalpy operating line is

$$i_{G_2} - i_{G_1} = \frac{LC_L}{G}(t_{L_2} - t_{L_1}) \qquad (5)$$

This is an enthalpy balance line which connects the points for the enthalpy of the gas and the temperature of the liquid at the ends of the tower. The slope LC_L/G is assumed to be constant so that the line is straight, since small

changes in the liquid rate caused by evaporation or condensation and changes in the heat capacity, C_L, are neglected.

The ϕ operating line on Fig. 1 connects the values of ϕ_G and t_L at every point in the tower. This line is not straight and its construction is complicated because its shape is determined partly by the condition line, which is unknown at first. Only the terminal points on these lines can be calculated from the data, but the curves are uniquely related at all points. Therefore, if a condition line is assumed and plotted on Fig. 2, a single ϕ operating line can be determined and plotted on Fig. 1. Each intersection of this assumed condition line with a line of constant

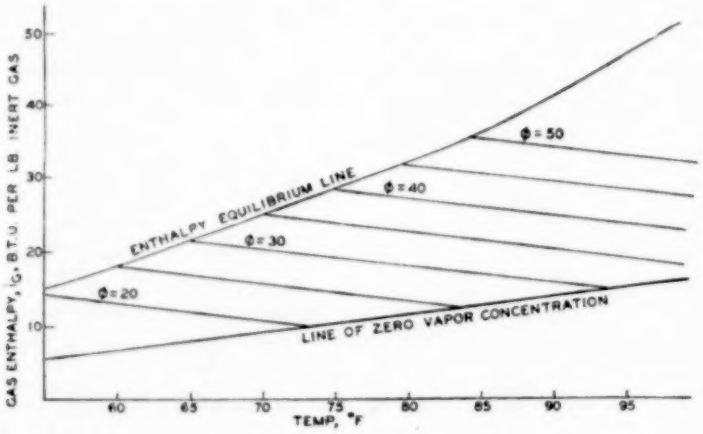

FIG. 2.

ϕ_G on Fig. 2 determines a value for the enthalpy, i_G, which corresponds to a value of t_L on the enthalpy operating line. These values of ϕ_G and t_L determine a point on the ϕ operating line to be constructed on Fig. 1.

A condition line is now constructed to check the one that was assumed. A value for the slope of the tie line, $-h_L a_H/k_G a_M$, is assumed and a series of lines with this slope is drawn on Fig. 1. Vertical lines are drawn through points E and B at which the tie lines intersect the equilibrium and the ϕ operating line. Horizontal lines are then drawn through points A, which are located on the enthalpy operating line, by the vertical lines through points B. The vertical distance between points E and B represents the transfer potential, $\phi_i - \phi_G$, at any point in the tower. The distances, $(1/\psi)(\phi_i - \phi_G)$, are laid off on the vertical lines through points E, upward from their intersections with the horizontal lines through points A. The points D located in this way give the so-called $1/\psi$ – auxiliary line.

According to equation (4) the line $C_1 D_1$ has the slope of the condition line at the gas inlet. The initial slope is assumed to be constant for a short segment of the condition line to C_2 in Fig. 1. By trial and error the condition line is constructed in increments until it reaches C_n. When the correct initial value of $h_L a_H/k_G a_M$ is assumed the condition line passes through point C_n and the line must also coincide with that assumed to start the construction. When convergence has been obtained, $k_G a_M$ is found by graphical integration of

$$k_G a_M = \frac{G}{Z} \int \frac{di_G}{\phi_i - \phi_G} \qquad (6)$$

$h_L a_H$ is found from the slope of the tie line and $h_G a_H$ is found from equation (1), using the mean value of C_s.

The humidification process shown in Fig. 1 is one of the three types of operations that may occur in an enthalpy transfer device. These may be classified as follows:

1. *The gas is heated and the liquid is cooled*

Enthalpy is transferred from the liquid to the gas and the vapour content of the gas increases. For this case the condition line slopes upward and to the right. This is similar to the operation of a humidifier or a water cooling tower. Fig. 5 is an example.

2. *The gas and the liquid are both cooled*

Enthalpy is transferred from the liquid to the gas and the vapour content of the gas increases. The condition line slopes upward and to the left. Fig. 7 is an example.

3. *The gas is cooled and the liquid is heated*

Enthalpy is transferred from the gas to the liquid, and the vapour content of the gas may increase or decrease. The latter case represents the operation of a cooler-condenser. The condition line slopes downward and to the left. Fig. 6 is an example.

The slopes mentioned are the over-all changes in the condition line; the actual slope may change considerably along its path. For example, in operations of the first type the condition line may slope upward to the left initially, cross the operating line and then slope to the right as the difference between the temperature of the gas and of the interface changes signs. In operations of the third type the condition line crosses a line of constant humidity twice when humidification of the gas is followed by dehumidification.

EXPERIMENTAL

Individual film coefficients were determined for the tetrachloroethylene–air system with the apparatus shown in Fig. 3. The tower was 1 ft. square and was packed with six layers (2·25 ft) of No. 6897 drip-point ceramic tiles obtained from the General Refractories Company. Each tile consisted of sixteen parallel rectangular channels separated by corrugated ribs. The tiles were stacked above each other in a non-staggered way. The tower was insulated with 2 in. of 85 per cent magnesia blocks. Glass windows were placed above and below the packing so that the presence of fog in the gas could be observed. The liquid was distributed over the packing by eighteen nozzles made from $\frac{1}{8}$ in. pipe plugs drilled with $\frac{1}{4}$ in. holes. These projected the liquid in low velocity streams onto splash bars. The liquid rate was measured with a calibrated rotameter.

Air at room temperature was blown into the bottom of the tower for the runs in which the air was heated by hot liquid. For runs in which

VOL. 13 1961

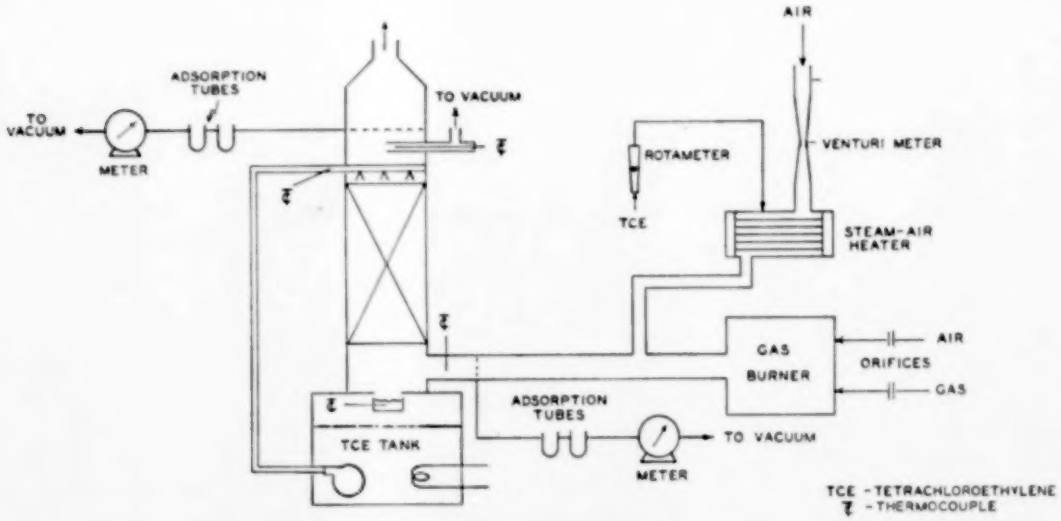

FIG. 3. Apparatus used for enthalpy transfer studies.

the air was cooled the inlet air was heated with a steam-air heat exchanger. When the inlet air was to be humidified, liquid was metered through a calibrated rotameter and sprayed into the exchanger where it was evaporated by the hot tubes. In one run at high temperature (No. 34) combustion gas from a natural gas burner was added to the air stream to raise the temperature. The rate of air flow to the exchanger was measured with a venturi meter and the air and gas to the burner were metered with orifices. The venturi meter and orifices were calibrated against a calibrated nozzle from the Taylor Instrument Company.

The concentrations of vapour in the inlet and exit gas streams were determined by drawing gas samples through two U-tubes in series containing activated charcoal, which were weighed to an accuracy of $\pm$ 0·01 g. The total amount of vapour adsorbed was 5–10 g. The volume of the gas samples, which was measured with calibrated wet-test meters, was about 1 ft³. The increase in weight of a third U-tube in the adsorption train was negligible, showing that adsorption of the vapour in two U-tubes was complete. The sample of the gas at the tower exit was drawn through a perforated stainless steel tube which extended across the tower and was heated electrically to prevent condensation of the vapour. The gas sample at the inlet was drawn through a perforated glass tube which extended across the inlet gas duct. Temperatures were measured with No. 26 gauge chromel–alumel thermocouples and a Leeds and Northrup portable precision potentiometer. The thermocouples used in the four terminal streams were calibrated in place.

The liquid leaving the packing was collected into one stream which flowed into a trough below the gas entry point for the temperature measurement, in order to avoid the effects of a horizontal temperature gradient and of the entering gas stream. The temperature measured in this way was influenced by the tower end-effects, but these were included in the heat balance of the tower. The thermocouple for measuring the temperature of the entering liquid was placed in the feed pipe near the entrance.

The thermocouple for measuring the temperature of the gas leaving the packing was placed about 8 in. above the distributor; the junction was enclosed in a stainless steel tube and the gas was drawn past it at high velocity. The temperature of the entering gas was measured with a bare thermocouple in the gas entry duct. The duct was insulated and heated electrically with resistance wires to a temperature close to the measured temperature of the gas in order to reduce radiation errors.

During a run a steady temperature was necessary in order to obtain a good heat balance because of the large heat capacity of the tower and the relatively small heat exchange across the liquid–gas interface. Temperature and flow rates were recorded at least three times during each run. Samples of the inlet and exit gas were drawn for analysis throughout each run. The duration of the runs was 15–20 min.

The tetrachloroethylene was obtained from the DuPont Company. It boiled between 120·5° and 122·0°C. Other physical properties are listed in Ref. [5].

Results

The results of all experiments with satisfactory heat balances are shown in Fig. 4 and Table 1.

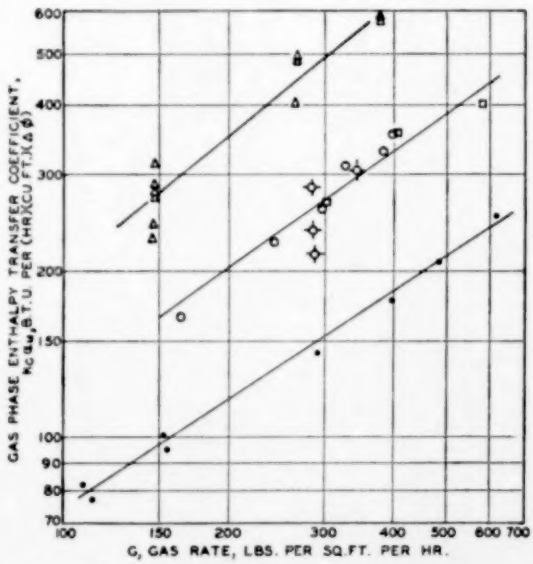

Fig. 4. Enthalpy transfer coefficients for the tetrachloroethylene–air system.

Table 1.

Run no.	Type of operation	$k_G a_M$ for exponent of $\frac{2}{3}$	$k_G a_M$ for exponent of $\frac{1}{2}$	$h_L a_H$ for exponent of $\frac{2}{3}$	$h_L a_H$ for exponent of $\frac{1}{2}$
27	1	178	167	Infinite	− 1335
31	1	251	248	2510	2480
50	2	285	217	462	443
51	2	309	219	495	524
44	3	168	206	545	890
41	3	403	509	2015	Infinite

In the later runs (No. 31 and higher) the technique was improved so that deviations of ± 5 per cent in the heat balance were enough to reject the data. Coefficients were calculated for some runs in which the exit gas was saturated and fog was present in the gas. Calculation of the coefficients in these cases was possible when the slope of the tie-lines could be found, which was not always possible when the exit gas was saturated.

As shown in Fig. 4, all of the coefficients fall on one of two lines. The coefficients for the runs in which the gas was heated and the liquid was cooled are lower than those for all of the other runs. When the liquid was heated and the gas was cooled and its vapour content was higher at the exit than at the inlet condensation could occur in the upper part of the tower. Condensation could occur throughout the tower when the vapour content of the inlet gas was high.

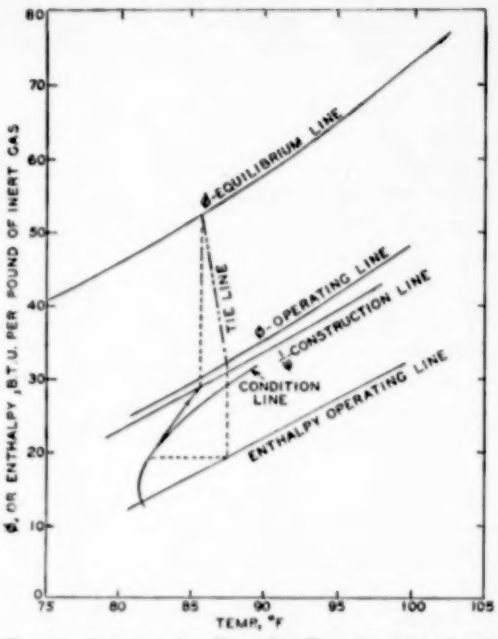

FIG. 5. Construction lines for Run 28, type 1, air heated and humidified tetrachloroethylene–air system.

Figs. 5, 6 and 7 show the graphical construction for calculating the gas- and liquid-film coefficients, $k_G a_M$ and $h_L a_H$, for various operating conditions with the tetrachloroethylene–air system. Figs. 5 and 7 show the construction of an element of the condition line. The former shows the condition when the liquid leaves the tower below

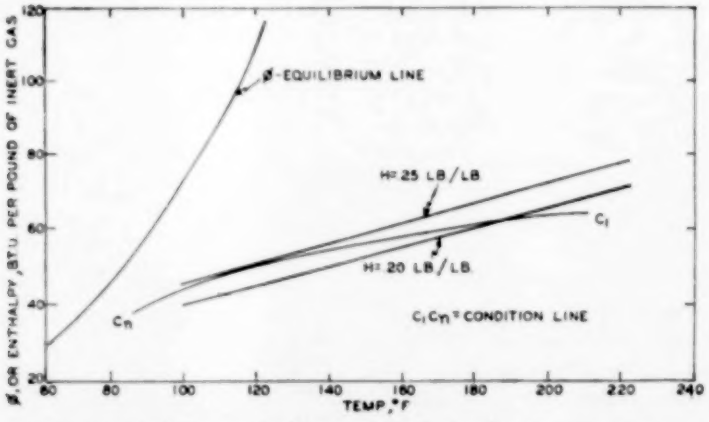

FIG. 6. Condition line for Run 40, type 3, showing alternate humidification and dehumidification tetrachloroethylene–air system.

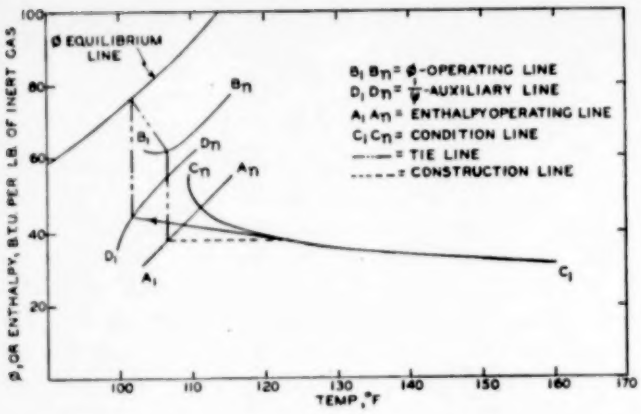

FIG. 7. Construction lines for Run 49, type 2, air cooled and humidified tetrachloroethylene–air system.

$B_1\ B_n$ = ϕ-operating line
$D_1\ D_n$ = $\frac{1}{\phi}$ – auxillary line
$A_1\ A_n$ = enthalpy operating line
$C_1\ C_n$ = condition line
— · · — = tie line
– – – – – = construction line

the temperature of the entering air. The air is cooled at the bottom of the tower but it is reheated rapidly. The minimum temperature occurs where the temperatures of the gas and of the interface are equal.

The runs in which both the gas and the liquid were cooled were made to find why the coefficients fall on two distinct lines. Under these conditions the gas was cooled but its vapour content increased so much that the enthalpy of the gas increased and the liquid was cooled. Heat and mass were transferred in opposite directions across the interface. Since the data for these conditions fall along the upper line, the direction of sensible heat transfer across the interface affects the value of the coefficient more than the direction of mass transfer.

For the conditions shown in Fig. 6 the gas was first humidified in the tower and then dehumidified so that the condition line crosses a line of constant humidity twice. It is possible to have humidification of the gas near the bottom and then dehumidification even when the inlet gas contains no vapour. For Runs 39 and 41 the condition lines show that the vapour content of the gas increased throughout the tower. There should be no fog formation in this case and none was observed. In Run 37 the condition line for the top of the tower is parallel to the constant humidity lines and, as expected, no fog was observed.

In a packed countercurrent tower fog can form only when vapour is transferred from the gas to the liquid. The condition line indicates that dehumidification takes place when its slope is greater than the slope of the lines of constant humidity. This condition alone is not sufficient to cause fog to form but the tendency to form fog increases with the slope of the condition line, that is, with the value of $-dH_G/dt_G$. The effect of fog formation on the values of the anthalpy coefficients was not studied thoroughly because fog was never formed over the entire packing height. However, when fog was formed it had no apparent effect on the values of the coefficients.

For the conditions in Fig. 7 the gas was cooled and its vapour content increased with a net gain in enthalpy. However, about one-third of the total enthalpy transfer occurred after the gas had been cooled below the temperature of the liquid. In this case the transfer coefficient fell nearer those on the lower curve on Fig. 4. The extreme curvature of the ϕ-operating line causes a corresponding curvature in the condition line near the end. The condition line is curved because the gas was cooled rapidly by the large temperature difference near the bottom of the tower. The rapid cooling of the gas below the liquid temperature indicates that the interface was cooler than the liquid. This suggests a measurable resistance to heat transfer in the liquid film.

MCKINLEY [6] made some runs in which the same apparatus was used for cooling and dehumidifying very hot combustion gas. His results are shown in Fig. 4 for comparison of the coefficients for the tetrachloroethylene-air system with those

for the water–air system. The coefficients are approximately proportional to the square root of the vapour diffusivity. The exponent is not constant but increases slightly with the mass velocity as shown by the divergence of the lines of $k_G a_M$ at high gas velocities.

Discussion

Errors in the calculated coefficients are caused by errors in the approximations made in the method of calculation, as follows:

1. The coefficients are based on the actual volume of packing, but there was actually some heat and mass transfer above and below the packing. The local transfer at the distributor head was small because of the low velocity of the gas and liquid streams. McAdams *et al.* [7] and Hensel and Treybal [8] show that the assumption that the packing has the same area for heat and mass transfer is correct only when it is completely wet. When the inside surface of a packing ring is partially dry and the outside is wet heat is transferred through the dry wall by conduction as well as across the liquid–gas interface. In the present study the tile packing resembled a bundle of vertical flues and it is not likely that a part of the surface was dry as is apt to be the case in randomly packed rings. The packing was observed visually through the windows and was thoroughly wet at the liquid rates used.

2. Fog formation did not have a noticeable effect on the individual enthalpy transfer coefficients shown in Table 1 or on the over-all coefficients for the water–air system at high temperatures. This conclusion was also reached by Mizushina and Nakajima [3] from experiments in a double tube cooler-condenser. They found that the same enthalpy transfer coefficient applied for all three cases: no fog, fog formation only in the film and fog formation in the main gas stream.

3. For calculating the modified enthalpy, the exponent on the Schmidt and Prandtl groups was assumed to have the conventional value of 2/3. This value was verified experimentally in a wet and dry bulb apparatus [5]. For 28 runs on the tetrachloroethylene–air system the exponent n varied between the extremes of 0·51 and 0·74 with an average value of 0·64. The exponent was calculated from

$$\left(\frac{\mathrm{Sc}}{\mathrm{Pr}}\right)^n = \frac{166\,\lambda\,p_{WB}}{(29)\,(0{\cdot}24)\,(t_{DB}-t_{WB})\,p_{BM}} \qquad (7)$$

where the wet and dry bulb temperatures t_{WB} and t_{DB} are the experimental data. The equation is derived by equating Colburn's factors for heat and mass transfer. The numbers 166 and 29 are the molecular weights of tetrachloroethylene and air, and 0·24 is the heat capacity of air. The Schmidt and Prandtl groups were taken as 2·15 and 0·74 in all of this work. Different coefficients are calculated when the exponent is reduced to ½, but they still do not fall along a single line in Fig. 4.

The negative value for $h_L a_H$ in Run 27 is impossible because it implies that heat is transferred against the temperature potential.

4. At high vapour concentrations neither enthalpy nor the modified enthalpy represents the transfer potential accurately because the true potential causing transfer is proportional to $\Delta p/p_{BM}$. When the vapour pressure and the concentration are low p_{BM} approaches unity and ΔH is proportional to Δp. Cribb and Nelson [9] have evaluated the error at high vapour concentrations and give the correction as a function of temperature.

5. In deriving the basic equations it was assumed that the values of C_s and of ψ at the interface are the same as those in the main gas stream. This is an approximation for which the correction factor is not a simple function of temperature. It was assumed further that p_{BM}/p_{Bi} is unity. This is justified over the range where vapour concentration can be used for the transfer potential. At higher concentrations, the correction of Cribb and Nelson must be applied.

6. The experimental values of $h_L a_H$ are sensitive to errors and approximations in the graphical calculation because an error in the slope of the tie line affects the value of $h_L a_H$ more than $k_G a_M$, particularly at high values of the slope. Therefore h_L was calculated theoretically to check the experimental values. At any point along the falling film of liquid, the point

value of the liquid phase heat transfer coefficient is

$$h_L = \frac{(dt/dx)_{x=0}}{t_{x=0} - t_{\text{Bulk}}} k_L = \frac{\text{B.Th.U.}}{\text{hr ft}^2\,^\circ\text{F}} \qquad (8)$$

where

$\left(\frac{dt}{dx}\right)_{x=0}$ = the temperature gradient at the gas–liquid interface

k_L = the thermal conductivity of the liquid.

t_{Bulk} = the integrated average temperature over the thickness of the film.

The experimental coefficient is identified with the value obtained by integrating the point coefficient over the height of the falling film. This is also equivalent to integrating over the life span of the falling film, which is the time for the film to descend a single block of packing 4·5 in. high. The assumption here is that the liquid is completely mixed before forming a film on the next lower block of packing. The life span was calculated from the surface velocity V_s of the falling film [10].

$$V_s = \frac{3}{2}\left(\frac{g\,\rho_L}{3\,\mu_L}\right)^{1/3}\left(\frac{L}{\rho_L\, y}\right)^{2/3} = \frac{\text{ft}}{\text{sec}} \qquad (9)$$

where μ_L and ρ_L are the viscosity and density of the liquid and y is the total wetted perimeter in 1 ft² of tower section, 40 ft in this case, and includes the wetted walls of the tower. Then for the conditions of Run 51 :

t_L (average) = 108 °F.

μ_L = 1·75 lb mass/ft hr

ρ_L = 99 lb/ft³.

k_L = 0·073 (B.Th.U/hr.) ft² (°F/ft).

V_s = 0·54 ft/sec.

Film thickness = 0·00040 ft.

Life span of film = 0·695 sec.

Now if the temperature profile across the film is known at any instant during the life span of the film, the instantaneous (point) value of h_L can be found from equation (8). The profiles were calculated by Schmidt's method of finite increments, which requires that the quantity $(\Delta x)^2/2\alpha\Delta\theta$ be set equal to unity, where

Δx = the increment of film thickness, $4{\cdot}0 \times 10^{-5}$ ft or one tenth of the total thickness

$\alpha = \dfrac{k_L}{L\,\rho_L}$

$\Delta\theta$ = the increment of time for a single step, $8{\cdot}18 \times 10^{-4}$ sec, giving a total of 850 steps.

In using equation (8), $(dt/dx)_{x=0}$ was approximated as $t_{x=0} - t_x = 4 \times 10^{-5} = {}^\circ F/\text{ft}$ and $t_{x=0}$ was given an arbitrary constant value. Assuming a constant value for $t_{x=0}$ will not affect the value of the calculated coefficients [11]. The point value of h_L was calculated for every other step, giving 425 values whose arithmetic mean is identified with the experimental value. Here is a selection of the calculated coefficients :

Elapsed fraction of the life span	*Point coefficient* (B.Th.U/hr) ft² °F	*Coefficient integrated over elapsed life span*
0·013	570	760
0·034	460	590
0·129	450	465
0·354	450	460
1·000	445	440

The calculations were done on an IBM 650 digital computer.

We ignored the effect of a velocity gradient across the film, but the error is small because the temperature profile flattens out rather quickly when a constant value is assumed for $t_{x=0}$. The flow was laminar since the Reynolds number was only 120. As a final result the integrated value of $h_L\,a_H$ is 440 × 40 = 17,600 (B.Th.U/hr) ft³ °F. Similar values would be obtained for the other runs because the liquid velocity was nearly constant between runs and the viscosity has a small effect. The lower experimental values for $h_L\,a_H$ must result from experimental error and approximations in the method of calculation.

7. The gas phase coefficient was also calculated theoretically, from a diffusional model [11].

$$k_G = \frac{2 \times 29\,P}{RT}\sqrt{\frac{Dv}{\pi Z}} \qquad (10)$$

where

v = velocity of gas through the slots in the packing
T = absolute temperature
P = system pressure
29 = molecular weight of air
D = diffusion coefficient

for an arbitrary run in which

G = 300 (lb/hr) ft²
T = 550° Rankin
v = 2·74 ft/sec
D = 0·0770 cm²/sec
P = 1 atm
Z = 4·5 in., for a single block of packing

The calculated coefficient is

$$7{\cdot}2\ \frac{\text{lb vapour}}{(\text{lb vapour/lb air})\ \text{hr ft}^2} \quad \text{or}$$

$$7{\cdot}2\ \frac{\text{B.Th.U.}}{(\text{B.Th.U/lb air})\ \text{hr ft}^2}$$

so that $k_G a_M$ is $7{\cdot}2 \times 40 = 288$.

Equation (10) applies only when the gas is in non-turbulent plug flow. In all of the runs the gas velocity was low enough to prevent turbulence. Plug flow is more likely to occur when the gas is being cooled, which corresponds to the middle line of Fig. 4. From the middle line at G = 300, the value of $k_G a_M$ is 270. Such a close check may be fortuitous because in the calculation it was assumed that the gas is remixed between the blocks of packing. Nevertheless, the coefficient will be lower when the profile has curvature because even when the profile is flat, the vapour barely penetrates to the centre plane of the slots during the passage through a single block of packing. This may explain the lower coefficients obtained experimentally when the gas was heated. A mathematical model has been designed to explore the effect of the velocity profile, and this will be presented in a later paper.

Comparison with Other Methods of Calculation

The graphical calculation described here differs from the graphical methods described previously in that an assumed, or a corrected, condition line is used to start each trial calculation. MIZUSHINA and KOTOO [2] and LEWIS and WHITE [4] construct the condition lines directly from an assumed slope of the tie line. Consequently, they eliminate the preliminary calculations before the actual construction of the condition line starts. The present method requires the use of Fig. 2 and the $1/\phi$ – auxiliary line in Fig. 1 to start the calculations. However, fewer operations are required for constructing the condition line.

Design of a Cooler-Condenser

An important application of the modified enthalpy potential method is illustrated by the design of a cooler condenser for the recovery of vapours from an inert gas.

Consider the design of a direct-contact cooler condenser for which the following are specified :

1. Temperature, vapour content and flow rate of the entering gas.
2. Vapour content of the exit gas.
3. Temperature of the inlet liquid.

The exit gas will have a temperature slightly above that of the entering liquid ; the difference will be indicated by the first trial calculation. The exit temperature of the gas, therefore, is known approximately as well as its enthalpy which is determined by its vapour content and temperature. Thus, only the liquid flow rate or the temperature of the exit liquid is unknown. The flow rate should be sufficient to wet the packing completely, while the temperature of the exit liquid must be low enough to cause dehumidification at the bottom of the tower. Within these limits either the flow rate or the temperature of the exit liquid is assumed and the other quantity is fixed.

The graphical design procedure is illustrated in Fig. 8. With the assumptions made so far it is possible to plot the enthalpy operating line, $A_1 - A_n$, the terminal points on the ϕ – operating line, B_1 and B_n, and the terminal points on the condition line, C_1 and C_n. The shape of the condition line is assumed and the corresponding ϕ-operating line is determined by the method described under THEORETICAL DISCUSSION. The coefficients for the liquid and gas films are known

VOL. 13 1961

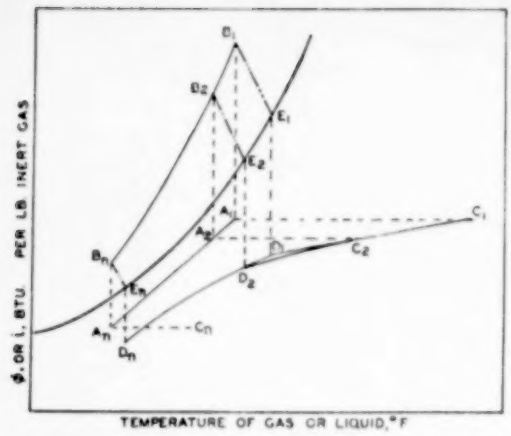

FIG. 8. Graphical construction for the design of a cooler condenser using the modified enthalpy potential.

for the chosen operating conditions and likewise the slope of the tie lines, $-h_L a_H/k_G a_M$. The $1/\psi$ – auxiliary line is laid out on Fig. 8, and a trial condition line is constructed to some point C_n' with the same enthalpy as point C_n. The vapour content of the gas at point C_n' is higher than the assumed value if C_n' lies to the left of C_n, and vice versa. Fig. 9 illustrates these possibilities and the situations causing them. A new exit liquid temperature is assumed for the construction of another condition line, the shape of which is estimated from the one just constructed. A new

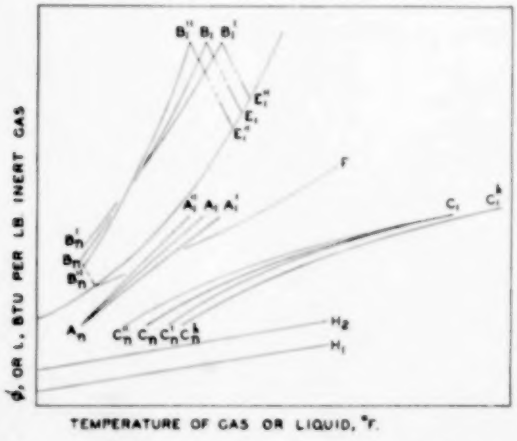

FIG. 9. Graphical design of a cooler condenser, showing the effect of varying the effluent liquid temperature.

ϕ-operating line and a new $1/\psi$ – auxiliary line are used.

It is not necessary to retain the temperature of the exit gas assumed originally since only the vapour content is important. If a trial condition line terminates at a point representing a higher gas temperature and a lower vapour content than those assumed originally, this is accepted for the final calculations and this condition line is used to determine the ϕ-operating line and the $1/\psi$ – auxiliary line for the next trial. A new temperature for the exit liquid need not be assumed, but the liquid flow rate must be adjusted to close the heat balance. In the final calculation it is only necessary for the assumed and constructed condition lines to coincide reasonably well and terminate at a point representing a satisfactory vapour content.

The tower height is found by graphical integration of

$$Z = \frac{G}{k_G a_M} \int \frac{di}{\phi_G - \phi_i} \qquad (11)$$

The term, $\phi_G - \phi_i$, is the vertical component of the tie line.

The design should be checked to ensure that no fog will form in the condenser. It is possible for fog to form at the gas–liquid interface or within the gas film even when supersaturation does not occur in the gas. This is possible because both temperature and concentration gradients exist across the gas film. Fog can form within the film when the profiles of actual temperature and saturation temperature intersect or become tangent within the film. JOHNSTONE *et al.* [12] give equations for the fog limitation lines such as the one shown in Fig. 9. These are the loci of all bulk gas conditions which cause incipient fog formation at the interface. If the conditions of the gas lie above this line fog can form ; if they lie below the line fog cannot form. For constructing a condition line on Fig. 9 conditions at the interface and in the main gas stream are defined at all levels in the tower. If any point on the condition line lies above the fog limitation line constructed from the corresponding point at the interface fog can form at the interface.

Fog formation will always occur first at the top

of the tower. If there is no fog here there can be none elsewhere, either in the gas film or in the main gas stream. The fog limitation line shown in Fig. 9 is the critical line for the interface temperature at the top of the tower. If the condition line terminates below the line no fog will form in the tower. If the condition line terminates above the line the distance between the line and the point representing the exit gas conditions is a measure of the potential to form fog. When the potential is small fog can be prevented by raising the temperature of the inlet gas, as shown in Fig. 9. If the inlet gas is heated at constant humidity its new conditions may be represented by some point, such as C^h_1. The new exit gas conditions will be represented by some point, such as C^h_n. The displacement of point C^h_n is smaller than that of C^h_1, and considerable heating may be required to avoid fog. The fog limitation lines depend very much on the liquid temperature so that sometimes fog may be prevented by a slight increase in the inlet liquid temperature. This increase must be small because a low inlet liquid temperature is necessary for thorough dehumidification.

Fog will not necessarily form in the gas film when supersaturation exists. For a small degree of supersaturation the presence of condensation nuclei is necessary for a finite rate of fog formation [12]. BRAS [13] points out that in the absence of nuclei a large supersaturation is necessary for a finite rate of fog formation. For water vapour the rate of nucleation is negligible when the dimensionless ratio p_r/p_∞ is less than 3. The rate increases by a factor of 10^9 when p_r/p_∞ is increased from 4 to 5. Furthermore, small film thicknesses or high turbulence decrease the tendency to form fog in the film.

VOL. 13 1961

REFERENCES

[1] MICKLEY H. S. *Chem. Engng. Progr.* 1949 **45** 739.
[2] MIZUSHINA T. and KOTOO T. *Chem. Engng.* (*Japan*) 1949 **13** 75.
[3] MIZUSHINA T. and NAKAJIMA M. *Mem. Fac. Engng., Kyoto Univ.* 1951 **13** No. 1.
[4] LEWIS J. G. and WHITE R. R. *Industr. Engng. Chem.* 1953 **45** 486.
[5] RETALLICK W. B., Ph.D.Thesis, University of Illinois 1953. (Microfilm available from University Microfilms, Inc., Ann Arbor, Michigan. Publication No. 6976).
[6] MCKINLEY D. L., Ph.D.Thesis, University of Illinois 1952.
[7] MCADAMS W. H., POHLENZ J. B. and ST. JOHN R. C., *Chem. Engng. Progr.* 1949 **45** 241.
[8] HENSEL L. H., Jr. and TREYBAL R. E. *Chem. Engng. Progr.* 1952 **48** 362.
[9] CRIBB C. S. and NELSON E. T. *Chem. Engng. Sci.* 1956 **5** 20.
[10] NIJSING R. A. T. O., HENDRIKS R. M. and KRAMERS H. *Chem. Engng. Sci.* 1959 **10** 88.
[11] DREW T. B. *Trans. Amer. Inst. Chem. Engrs.* 1931 **26** 26.
[12] JOHNSTONE H. F., KELLEY M. D. and MCKINLEY D. L. *Industr. Engng. Chem.* 1950 **42** 2298.
[13] BRAS G. H. P. *Industr. Chem. Mfg.* 1955 **31** 22.

Chemical Engineering Science, 1961, Vol. 13, pp. 167 to 172. Pergamon Press Ltd., London. Printed in Great Britain

The unrestricted engineering Bernoulli equation

R. A. GAGGIOLI
Edwin W. Rice, Jr., Fellow of the General Electric Foundation,
Department of Mechanical Engineering, University of Wisconsin, U.S.A.

(*Received* 13 *May* 1960 ; *in revised form* 18 *June* 1960)

Abstract—Based on a force analysis, BIRD recently derived restricted " engineering Bernoulli equations." The procedure consisted of forming the scalar product of the velocity with the Navier–Stokes equations of motion and then integrating over the volume of the open system to obtain first a general mechanical-energy balance. For the restricted cases of isothermal and isentropic flow at constant composition (or else at chemical equilibrium), and with each species experiencing the same conservative body forces, BIRD converted the mechanical-energy balance into " engineering Bernoulli equations." In the present paper a Bernoulli equation will be derived by a generalized method ; the only condition will be that of identical body forces upon the constituents.*

Résumé—BIRD a récemment obtenu une équation réduite qu'il appelle " Engineering Benoulli équation " basée sur une analyse des forces. Le procédé consiste à faire le produit scalaire de la vitesse avec les équations de mouvement de Navier-Stokes, et d'intégrer ensuite au volume du système ouvert pour obtenir un bilan général de l'énergie mécanique. Dans le cas particulier d'écoulement isentrope et isotherme à composition constante (ou a l'équilibre chimique) BIRD expérimente pour chaque espèce les mêmes liaisons internes et convertit le bilan énergie mécanique en " équation mécanique de Bernoulli." Dans la présente étude on obtient une équation de Bernoulli par une méthode généralisée, la seule condition étant que des forces identiques s'exercent sur les constituants.

Zusammenfassung—Auf der Grundlage einer Vektoranalyse hat Bird kürzlich spezielle " engineering Bernoulli equations " abgeleitet. Diese Ableitung bestand aus der Bildung des skalaren Produktes aus der Geschwindigkeit mit der Navier-Stokes'schen Bewegungsgleichung und anschliessender Integration über das Volumen des offenen Systems, wodurch zunächst eine allgemeine mechanische Energiebilanz erhalten wurde. Für die auf isotherme und isentrope Strömung beschränkten Fälle bei konstanter Zusammensetzung (oder auch bei chemischem Gleichgewicht) und in jedem Falle, in dem dieselben Massenkräfte ausgeübt werden, formte Bird die mechanische Energiebilanz in " engineering Bernoulli equations " um.

In der vorliegenden Arbeit wird eine Bernoulli-Gleichung mit Hilfe einer verallgemeinerten Methode abgeleitet ; die einzige Bedingung ist die der gleichen Massenkräfte auf die einzelnen Komponenten.

*The treatment is readily extended to the case where the body forces are not identical : In BIRD's equations (20) and (21) replace $\rho \mathbf{F}_\phi$ by $\Sigma \rho_i \mathbf{F}_i = \Sigma \rho_i [\mathbf{F}_{i\phi} + \mathbf{F}_{ii}]$ where $\mathbf{F}_{i\phi}$ are conservative body forces [equal to $-\nabla \phi_i (x, y, z)$], and $\mathbf{F}_{ii}$ are time-dependent body forces. Then, the integration $\int_{\mathscr{V}} [\mathbf{v} \cdot (\Sigma \rho_i \mathbf{F}_{i\phi})]\, d\mathscr{V}$ may be carried out in a manner entirely analogous to that of BIRD (his equation 26). This results in

$$\int_{\mathscr{V}} \mathbf{v} \cdot (\Sigma \rho_i \mathbf{F}_i)\, d\mathscr{V} = -\frac{dE_\phi}{dt} - \int_{\mathscr{S}} \rho e_\phi [(\mathbf{v} - \mathbf{v}_{\mathscr{S}}) \cdot \mathbf{n}]\, d\mathscr{S} - \Sigma \int_{\mathscr{S}} \phi_i (\mathbf{j}_i \cdot \mathbf{n})\, d\mathscr{S} + \Sigma + \int_{\mathscr{V}} r_i \phi_i\, d\mathscr{V} + \Sigma \int_{\mathscr{V}} (\mathbf{j}_i \cdot \nabla \phi_i)\, d\mathscr{V} + \int_{\mathscr{V}} \mathbf{v} \cdot (\Sigma \rho_i \mathbf{F}_{ii})\, d\mathscr{V} \qquad \text{(f.1)}$$

where ϕ_i is the potential energy of the i-th constituent, the energy resulting from the location of i in the potential field $\phi_i (x, y, z)$. Also $E_\phi = \Sigma \int_{\mathscr{V}} \rho_i \phi_i\, d\mathscr{V}$ and $e_\phi = (1/\rho) \Sigma \rho_i \phi_i$: r_i is the rate of production of constituent i, per unit volume. The last four terms of this equation are zero when all the body forces are identical and conservative; inclusion of these terms renders the equations to follow unrestricted. By rewriting equation (f.1) as an expression for dE_ϕ/dt, each of the other terms may be rationalized into a specific contribution to the total change in E_ϕ.

1. MECHANICAL-ENERGY BALANCE, AND BERNOULLI EQUATION

THE general mechanical-energy balance developed by BIRD [1] (the integral of his equation 21 with the substitutions of equations 22, 23 and 26) is equivalent to

$$\frac{dE_k}{dt} + \frac{dE_\phi}{dt} = -\int_{\mathscr{S}} \rho\,(e_k + e_\phi)[(\mathbf{v} - \mathbf{v}_{\mathscr{S}}) \cdot \mathbf{n}]\,d\mathscr{S} - \int_{\mathscr{V}} (\mathbf{v} \cdot \nabla p)\,d\mathscr{V} - \int_{\mathscr{S}} [(\boldsymbol{\tau} \cdot \mathbf{v}) \cdot \mathbf{n}]\,d\mathscr{S} + \int_{\mathscr{V}} (\boldsymbol{\tau} : \nabla\mathbf{v})\,d\mathscr{V} \qquad (1.1a)$$

This balance may be transformed into one that facilitates solution. Rewrite, using the Gauss divergence theorem,

$$-\int_{\mathscr{V}} (\mathbf{v} \cdot \nabla p)\,d\mathscr{V} = \int_{\mathscr{V}} (\nabla \cdot p\mathbf{v})\,d\mathscr{V} + \int_{\mathscr{V}} p\,(\nabla \cdot \mathbf{v})\,d\mathscr{V} = -\int_{\mathscr{S}} (p\mathbf{v} \cdot \mathbf{n})\,d\mathscr{S} + \int_{\mathscr{V}} p\,(\nabla \cdot \mathbf{v})\,d\mathscr{V}$$

In the equation

$$\int_{\mathscr{S}} (p\mathbf{v} \cdot \mathbf{n})\,d\mathscr{S} = \int_{\mathscr{S}} [p\,(\mathbf{v} - \mathbf{v}_{\mathscr{S}}) \cdot \mathbf{n}]\,d\mathscr{S} + \int_{\mathscr{V}} (p\mathbf{v}_{\mathscr{S}} \cdot \mathbf{n})\,d\mathscr{S} \qquad (1.2a)$$

the first term on the right-hand side is the pressure *flow-energy** transferred across the boundary of the system; the second term is the work rate resulting from pressure forces on the system boundary (and is designated dW_p/dt). Similarly, the right-hand side of

$$\int_{\mathscr{S}} [(\boldsymbol{\tau} \cdot \mathbf{v}) \cdot \mathbf{n}]\,d\mathscr{S} = \int_{\mathscr{S}} \{[\boldsymbol{\tau} \cdot (\mathbf{v} - \mathbf{v}_{\mathscr{S}})] \cdot \mathbf{n}\}\,d\mathscr{S} + \int_{\mathscr{S}} [(\boldsymbol{\tau} \cdot \mathbf{v}_{\mathscr{S}}) \cdot \mathbf{n}]\,d\mathscr{S} \qquad (1.2b)$$

consists of the shear flow energy and the work rate of shear (dW_v/dt). Thus, equation (1.1a) yields another mechanical-energy balance:

$$\frac{dE_k}{dt} + \frac{dE_\phi}{dt} = -\frac{dW_p}{dt} - \frac{dW_v}{dt} + \int_{\mathscr{V}} (\boldsymbol{\tau} : \nabla\mathbf{v})\,d\mathscr{V} + \int_{\mathscr{V}} p\,(\nabla \cdot \mathbf{v})\,d\mathscr{V} - \int_{\mathscr{S}} \{\rho\,(e_k + e_\phi + p/\rho)[(\mathbf{v} - \mathbf{v}_{\mathscr{S}}) \cdot \mathbf{n}] + [\boldsymbol{\tau} \cdot (\mathbf{v} - \mathbf{v}_{\mathscr{S}})] \cdot \mathbf{n}\}\,d\mathscr{S} \qquad (1.1b)$$

Yet another variation of equation (1.1) is obtained if, using the equation of continuity $\partial\rho/\partial t + \nabla \cdot \rho\mathbf{v} = 0$ and the definition of the Stokes derivative, one rewrites $p\,(\nabla \cdot \mathbf{v})$ as $-(p/\rho)\,(D\rho/Dt)$.

The extension of BIRD's procedure to obtain an unrestricted Bernoulli equation depends solely upon the evaluation of the integral $\int_{\mathscr{V}} (\mathbf{v} \cdot \nabla p)\,d\mathscr{V}$ in equation (1.1a). A generalized procedure will be treated here. With the thermodynamic relationship

$$v\,dp = dh - T\,ds - \Sigma\,\mu_i\,dx_i,$$

and the definition of the Stokes derivative,

$$-\int_{\mathscr{V}} (\mathbf{v} \cdot \nabla p)\,d\mathscr{V} = \int_{\mathscr{V}} \left[\frac{\partial p}{\partial t} - \frac{Dp}{Dt}\right] d\mathscr{V} = \int_{\mathscr{V}} \frac{\partial p}{\partial t}\,d\mathscr{V} + \int_{\mathscr{V}} \rho \left[T\frac{Ds}{Dt} - \frac{Dh}{Dt} + \Sigma\,\mu_i \frac{Dx_i}{Dt}\right] d\mathscr{V} = \int_{\mathscr{V}} \rho \left[T\frac{Ds}{Dt} + \Sigma\,\mu_i \frac{Dx_i}{Dt}\right] d\mathscr{V} - \int_{\mathscr{V}} \rho \left[\frac{\partial h}{\partial t} + \mathbf{v} \cdot \nabla h\right] d\mathscr{V} + \int_{\mathscr{V}} \frac{\partial p}{\partial t}\,d\mathscr{V}$$

*BIRD (and others) often call equations (1.2 a, b) the pressure work and the shear work, respectively; in this paper all forms of energy transferred across the boundary because of material flow are defined *flow energy*. This procedure and most of the symbolism follows the terminology of OBERT [2].

VOL. 13 1961

By invoking the three-dimensional Leibniz theorem,

$$
\begin{aligned}
-\int_{\mathscr{V}} (\mathbf{v}\cdot\nabla p)\,d\mathscr{V} &= \int_{\mathscr{V}} \rho\left[T\frac{Ds}{Dt} + \Sigma\mu_i\frac{Dx_i}{Dt}\right]d\mathscr{V} \\
&\quad - \frac{d}{dt}\int_{\mathscr{V}} \rho h\,d\mathscr{V} + \int_{\mathscr{V}} h\frac{\partial\rho}{\partial t}\,d\mathscr{V} \\
&\quad + \int_{\mathscr{S}} \rho h\,(\mathbf{v}_{\mathscr{S}}\cdot\mathbf{n})\,d\mathscr{S} \\
&\quad - \int_{\mathscr{V}} \rho\,(\mathbf{v}\cdot\nabla h)\,d\mathscr{V} + \frac{d}{dt}\int_{\mathscr{V}} p\,d\mathscr{V} \\
&\quad - \int_{\mathscr{S}} p\,(\mathbf{v}_{\mathscr{S}}\cdot\mathbf{n})\,d\mathscr{S} \qquad \text{(a)}
\end{aligned}
$$

The continuity equation, along with thed ivergence theorem, allows

$$
\begin{aligned}
\int_{\mathscr{V}}\left[h\frac{\partial\rho}{\partial t} - \rho\,(\mathbf{v}\cdot\nabla h)\right]d\mathscr{V} &= \int_{\mathscr{V}}\left[-h\,(\nabla\cdot\rho\mathbf{v}) - \rho\,(\mathbf{v}\cdot\nabla h)\right]d\mathscr{V} \\
&= -\int_{\mathscr{V}} (\nabla\cdot\rho\mathbf{v}h)\,d\mathscr{V} \\
&= -\int_{\mathscr{S}} \rho h\,(\mathbf{v}\cdot\mathbf{n})\,d\mathscr{S}
\end{aligned}
$$

Also,

$$
\frac{d}{dt}\int_{\mathscr{V}} (p-\rho h)\,d\mathscr{V} = -\frac{d}{dt}\int_{\mathscr{V}} \rho u\,d\mathscr{V} = -\frac{dU}{dt}
$$

and

$$
\int_{\mathscr{S}} p\,(\mathbf{v}_{\mathscr{S}}\cdot\mathbf{n})\,d\mathscr{S} \equiv \frac{dW_p}{dt}
$$

With these substitutions in equation (a),

$$
\begin{aligned}
-\int_{\mathscr{V}} (\mathbf{v}\cdot\nabla p)\,d\mathscr{V} &= \int_{\mathscr{V}} \rho\left[T\frac{Ds}{Dt} + \Sigma\mu_i\frac{Dx_i}{Dt}\right]d\mathscr{V} \\
&\quad - \int_{\mathscr{S}} \rho h\left[(\mathbf{v}-\mathbf{v}_{\mathscr{S}})\cdot\mathbf{n}\right]d\mathscr{S} \\
&\quad - \frac{dU}{dt} - \frac{dW_p}{dt} \qquad (1.3)
\end{aligned}
$$

Upon introducing equations (1.3) and (1.2b) into equation (1.1a), the general equation is obtained

$$
\begin{aligned}
\frac{dE}{dt} - \int_{\mathscr{V}} \rho T\frac{Ds}{Dt}\,d\mathscr{V} &= \\
&\quad - \int_{\mathscr{S}} \{\rho(h+e_k+e_\phi)\left[(\mathbf{v}-\mathbf{v}_{\mathscr{S}})\cdot\mathbf{n}\right] \\
&\quad + \left[\tau\cdot(\mathbf{v}-\mathbf{v}_{\mathscr{S}})\right]\cdot\mathbf{n}\}\,d\mathscr{S} + \int_{\mathscr{V}} (\tau:\nabla\mathbf{v})\,d\mathscr{V} \\
&\quad + \Sigma\int_{\mathscr{V}} \rho\mu_i\frac{Dx_i}{Dt}\,d\mathscr{V} - \frac{dW_p}{dt} - \frac{dW_v}{dt} \qquad (1.4)
\end{aligned}
$$

And this represents the unrestricted " engineering Bernoulli equation "—a generalization of those presented by Bird—which is desirable since science strives to formulate descriptions of the most general situations (this equation does have the condition that the body forces on each species are identical and conservative, but see footnote on p.1).

Equation (1.4) is readily restricted to the isothermal and isentropic constant-composition (or chemical equilibrium) flow treated by Bird. To specialize equation (1.4) for the case when temperature is independent of position, consider first the term

$$
\begin{aligned}
-\int_{\mathscr{V}} \rho T\frac{Ds}{Dt}\,d\mathscr{V} &= -\int_{\mathscr{V}} \rho T\left[\frac{\partial s}{\partial t} + \mathbf{v}\cdot\nabla s\right]d\mathscr{V} \\
&= -T\int_{\mathscr{V}} \left[\rho\frac{\partial s}{\partial t} + (\nabla\cdot\rho s\mathbf{v}) - s\,(\nabla\cdot\rho\mathbf{v})\right]d\mathscr{V}\Bigg|_{T=T(t)}
\end{aligned}
$$

With the divergence theorem, the continuity equation $\partial\rho/\partial t = -\nabla\cdot\rho\mathbf{v}$, and the Leibniz theorem,

$$
\begin{aligned}
-T\int_{\mathscr{V}} \rho\frac{Ds}{Dt}\,d\mathscr{V} &= -T\int_{\mathscr{S}} \rho s\,(\mathbf{v}\cdot\mathbf{n})\,d\mathscr{S} \\
&\quad - T\frac{d}{dt}\int_{\mathscr{V}} \rho s\,d\mathscr{V} + T\int_{\mathscr{S}} \rho s\,(\mathbf{v}_{\mathscr{S}}\cdot\mathbf{n})\,d\mathscr{S} \\
&= -T\int_{\mathscr{S}} \rho s\left[(\mathbf{v}-\mathbf{v}_{\mathscr{S}})\cdot\mathbf{n}\right]d\mathscr{S} - T\frac{dS}{dt}
\end{aligned}
$$

Upon substituting in equation (1.4),

$$\frac{dE}{dt} - T\frac{dS}{dt} = -\int_{\mathscr{S}} \{\rho(h - Ts + e_k + e_\phi)[(\mathbf{v} - \mathbf{v}_{\mathscr{S}}) \cdot \mathbf{n}] + [\boldsymbol{\tau} \cdot (\mathbf{v} - \mathbf{v}_{\mathscr{S}})] \cdot \mathbf{n}\} d\mathscr{S} + \int_{\mathscr{V}} (\boldsymbol{\tau} : \nabla \mathbf{v})\, d\mathscr{V} + \Sigma \int_{\mathscr{V}} \rho \mu_i \frac{Dx_i}{Dt}\, d\mathscr{V} - \frac{dW_m}{dt} \Bigg] \begin{matrix} \mathbf{F}_i = -\nabla\phi \\ T = T(t) \end{matrix} \quad (1.5)$$

where $W_m = W_p + W_v$ is the mechanical work of the system. Also, $(h - Ts)$ equals the Gibbs free energy g. Since $(\mathbf{v} - \mathbf{v}_{\mathscr{S}})$ is zero except at a flow boundary of the system, the surface integral represents the transport associated with material flow across the boundary. For the isothermal case with one flow stream of constant composition (or chemical equilibrium) and negligible change in shear flow energy, equation (1.5) reduces to

$$\frac{dA}{dt} + \frac{dE_k}{dt} + \frac{dE_\phi}{dt} = -\Delta\left[\dot{m}_f(\bar{g} + \bar{e}_k + \bar{e}_\phi)\right] + \int_{\mathscr{V}} (\boldsymbol{\tau} : \nabla \mathbf{v})\, d\mathscr{V} - \frac{dW_m}{dt} \Bigg] \begin{matrix} \mathbf{F}_i = -\nabla\phi \\ T = \text{constant} \\ \Sigma \mu_i \dfrac{Dx_i}{Dt} = 0 \\ \Delta \dot{m}_f e_\tau = 0 \end{matrix} \quad (1.6)$$

where $A = U - TS$ is the Helmholtz free energy (and this form is equivalent to BIRD's equation 28). For isentropic flow equation (1.4) becomes

$$\frac{dE}{dt} = -\int_{\mathscr{S}} \{\rho(h + e_k + e_\phi)[(\mathbf{v} - \mathbf{v}_{\mathscr{S}}) \cdot \mathbf{n}] + [\boldsymbol{\tau} \cdot (\mathbf{v} - \mathbf{v}_{\mathscr{S}})] \cdot \mathbf{n}\} d\mathscr{S} + \int_{\mathscr{V}} (\boldsymbol{\tau} : \nabla \mathbf{v})\, d\mathscr{V} + \Sigma \int_{\mathscr{V}} \rho \mu_i \frac{Dx_i}{Dt}\, d\mathscr{V} - \frac{dW_m}{dt} \Bigg] \begin{matrix} \mathbf{F}_i = -\nabla\phi \\ s = \text{constant} \end{matrix} \quad (1.7)$$

And, with one flow stream of constant composition (or chemical equilibrium) and negligible shear flow energy change

$$\frac{dE}{dt} = -\Delta\left[\dot{m}_f(\bar{h} + \bar{e}_k + \bar{e}_\phi)\right] + \int_{\mathscr{V}} (\boldsymbol{\tau} : \nabla \mathbf{v})\, d\mathscr{V} - \frac{dW_m}{dt} \Bigg] \begin{matrix} \mathbf{F}_i = -\nabla\phi \\ s = \text{constant} \\ \Sigma \mu_i \dfrac{Dx_i}{Dt} = 0 \\ \Delta \dot{m}_f e_\tau = 0 \end{matrix} \quad (1.8)$$

And this form is equivalent to BIRD's equation (29).

2. FRICTION EQUATION

As a matter of interest, equation (1.4) can be transformed into what might aptly be called the Friction Equation. Notice that

$$\rho\mu_i \frac{Dx_i}{Dt} = \mu_i \frac{D\rho_i}{Dt} - \mu_i x_i \frac{D\rho}{Dt} = \mu_i \frac{\partial \rho_i}{\partial t} + \mu_i \mathbf{v} \cdot \nabla \rho_i - \mu_i x_i \frac{D\rho}{Dt}$$

With the continuity equation for constituent i,

$$\partial \rho_i / \partial t = r_i - \nabla \cdot \rho_i \mathbf{v} - \nabla \cdot \mathbf{j}_i,$$

where $(\mathbf{j}_i/\rho_i) = (\mathbf{u}_i - \mathbf{v})$ is the difference between the velocity of constituent i and the mass-average velocity (Ref. [3], pp. 295–6, 344–5),

$$\rho\mu_i \frac{Dx_i}{Dt} = r_i \mu_i - \mu_i \nabla \cdot \mathbf{j}_i - \mu_i \rho_i (\nabla \cdot \mathbf{v}) - \mu_i x_i \frac{D\rho}{Dt}$$

so

$$\begin{aligned} \Sigma \rho\mu_i \frac{Dx_i}{Dt} &= \Sigma\, r_i \mu_i - \Sigma\, \mu_i \cdot \nabla \mathbf{j}_i \\ &\quad - \rho g (\nabla \cdot \mathbf{v}) - g \frac{\partial \rho}{\partial t} - g\mathbf{v} \cdot \nabla \rho \\ &= \Sigma\, r_i \mu_i - \Sigma\, \mu_i \nabla \cdot \mathbf{j}_i \\ &\quad - g(\rho \nabla \cdot \mathbf{v} - \nabla \cdot \rho \mathbf{v} + \mathbf{v} \cdot \nabla \rho) \\ &= \Sigma\, r_i \mu_i - \Sigma\, \nabla \cdot \mu_i \mathbf{j}_i + \Sigma\, \mathbf{j}_i \cdot \nabla \mu_i \end{aligned} \quad (a)$$

Also, with $\mu_i = h_i - Ts_i$, where h_i and s_i are partial specific quantities

$$\frac{1}{T} \Sigma\, \mu_i \mathbf{j}_i \cdot \nabla T - \frac{1}{T} \Sigma\, h_i \mathbf{j}_i \cdot \nabla T + \Sigma\, s_i \mathbf{j}_i \cdot \nabla T = 0$$

Subtracting this from equation (a), and noting

VOL. 13 1961

$$T\,\mathbf{j}_i \cdot \nabla(\mu_i/T) = \mathbf{j}_i \cdot \nabla\mu_i - (1/T)\,\mu_i \mathbf{j}_i \cdot \nabla T,$$

$$\Sigma\,\rho\mu_i \frac{Dx_i}{Dt} = \Sigma\, r_i\,\mu_i - \Sigma\,\nabla \cdot \mu_i\,\mathbf{j}_i + \Sigma\, T\mathbf{j}_i \cdot \nabla(\mu_i/T) + \frac{1}{T}\,\Sigma\, h_i \mathbf{j}_i \cdot \nabla T - \Sigma\, s_i\,\mathbf{j}_i \cdot \nabla T + \frac{\boldsymbol{\epsilon}}{T} \cdot \nabla T - \frac{\boldsymbol{\epsilon}}{T} \cdot \nabla T \qquad \text{(b)}$$

Finally, substituting (b) in equation (1.4), and rearranging,

$$-\frac{dE}{dt} - \frac{dW_m}{dt} - \Sigma \int_{\mathscr{V}} (\nabla \cdot \mu_i\,\mathbf{j}_i)\,d\mathscr{V} + \int_{\mathscr{V}} \rho T \frac{Ds}{Dt}\,d\mathscr{V} - \int_{\mathscr{V}} \left[\left(\frac{\boldsymbol{\epsilon}}{T} + \Sigma\, s_i\,\mathbf{j}_i\right) \cdot \nabla T\right] d\mathscr{V} - \int_{\mathscr{S}} \{\rho\,(h + e_k + e_\phi)\,[(\mathbf{v} - \mathbf{v}_{\mathscr{S}}) \cdot \mathbf{n}] + [\boldsymbol{\tau} \cdot (\mathbf{v} - \mathbf{v}_{\mathscr{S}})] \cdot \mathbf{n}\}\,d\mathscr{S} = \int_{\mathscr{V}} -\{(\boldsymbol{\tau} : \nabla\mathbf{v}) + \frac{\boldsymbol{\epsilon}}{T} \cdot \nabla T + \Sigma\,[(h_i/T)\,\mathbf{j}_i \cdot \nabla T + T\mathbf{j}_i \cdot \nabla(\mu_i/T)] + \Sigma\, r_i\,\mu_i\}\,d\mathscr{V} \qquad (2.1)$$

The integrand of the right-hand side of equation (2.1) here called the local friction rate, $\dot{f}$, is equal to T times the rate of entropy production per unit volume (HIRSCHFELDER, *et al.* [4], p. 702).* The integral can be interpreted as being the total friction of the irreversible flow process. The first term represents the degradation of mechanical energy into thermal energy—the mechanical friction accompanying fluid motion. The second term is the friction from heat transfer through temperature gradients—an evaluation of the mechanical energy which could have been obtained had the heat passed through reversible cycles rather than through irreversible temperature gradients. The third term is the friction of diffusion and the last is the degradation of chemical energy because of irreversible reaction.

*The term $n_i \mathbf{V}_i \cdot \mathbf{X}_i = \Sigma\,\mathbf{j}_i \cdot \mathbf{F}_i$ of Ref. 4 is zero here, since all body forces were assumed equal, and $\Sigma \mathbf{j}_i = 0$.

Acknowledgment—The help and suggestions of Professors EDWARD F. OBERT and R. BYRON BIRD of the University of Wisconsin are gratefully acknowledged. This work was made possible by a fellowship granted by the General Electric Foundation.

NOTATION

$A(t)$ = Helmholtz free energy of mass contained in the system, at time t
$E(t)$ = energy (internal + kinetic + potential) of mass contained in the system at time t
$e_f(x, y, z, t)$ = flow energy per unit mass at position (x, y, z) and at time t
$e_k(x, y, z, t)$ = kinetic energy per unit mass
$E_k(t)$ = kinetic energy of mass contained in the system, at time t
$e_\phi(x, y, z, t)$ = potential energy per unit mass
$E_\phi(t)$ = potential energy of mass enclosed, at time t
e_τ = shear component of flow energy
$\dot{f}(x, y, z, t)$ = local friction per unit volume and unit time
$g(x, y, z, t)$ = Gibbs free energy $= (1/\rho)\,\Sigma\,\rho_i g_i = (1/\rho)\,\Sigma\,\rho_i\mu_i$
$h(x, y, z, t)$ = enthalpy at (x, y, z) and at time t
$h_i(x, y, z, t)$ = contribution of the i-th constituent to $h(x, y, z, t)$: the partial specific enthalpy
$\mathbf{j}_i(x, y, z, t)$ = mass flux of constituent i relative to mass-average flux
$m(t)$ = mass contained in the system at time t
$\dot{m}_f(t)$ = mass flow rate
$\mathbf{n}$ = unit vector normal to a surface pointing outward from the enclosed volume
$p(x, y, z, t)$ = pressure
$s(x, y, z, t)$ = entropy per unit mass
$s_i(x, y, z, t)$ = contribution of the i-th species to $s(x, y, z, t)$: the partial specific entropy
$S(t)$ = entropy of mass in the system at t
$\mathscr{S}(t)$ = surface of system at t
t = time
$T(x, y, z, t)$ = temperature
$u(x, y, z, t)$ = internal energy per unit mass
$U(t)$ = internal energy contained at t
$\mathbf{u}_i(x, y, z, t)$ = absolute velocity of the i-th constituent
$\mathbf{v}(x, y, z, t)$ = velocity relative to (x, y, z) at t
$\mathscr{V}(t)$ = volume of system at time t
$W(t)$ = the total work of the system from time zero
(x, y, z) = co-ordinate fixed in space
$x_i(x, y, z, t)$ = concentration of the i-th constituent at (x, y, z) and t; $x_i = (\rho_i/\rho)$

Greek Symbols

ΔX = the difference between the quantity X at the entrance and exit of an open system with one flow stream
$\boldsymbol{\epsilon}(x, y, z, t)$ = heat flux at (x, y, z) and time t
$\rho(x, y, z, t)$ = density
$\mu_i(x, y, z, t)$ = chemical potential of the i-th constituent at (x, y, z) and t: partial specific Gibbs free energy

$\boldsymbol{\tau}(x, y, z, t)$ = shear stress tensor (see Ref. [4], p. 699)
$\phi_i(x, y, z, t)$ = potential for i-th constituent

Subscripts

i	i-th constituent
k	kinetic
m	mechanical
p	pressure
$\mathscr{S}$	surface

$\mathbf{v}, \boldsymbol{\tau}$	shear
ϕ	potential

Marks above symbols

—	cross-section average
·	derivative with respect to time

Stokes (substantial) derivative

$$\frac{Df(x, y, z, t)}{Dt} = \frac{\partial f}{\partial t} + \mathbf{v} \cdot \nabla f$$

References

[1] Bird R. B. *Chem. Engng. Sci.* 1957 **6** 123.

[2] Obert E. F. *Concepts of Thermodynamics* Sections 2–13, 5–3. McGraw-Hill, New York 1960.

[3] Bird R. B., Stewart W. E. and Lightfoot E. N. *Notes on Transport Phenomena*, Appendix A, Sections 18.1, 3, 4 ; 16.1 ; 7.3 ; 15.2, John Wiley, New York 1958.

[4] Hirschfelder J. O., Curtiss C. F. and Bird R. B. *Molecular Theory of Gases and Liquids*, p. 699, 700–702, John Wiley, New York 1954.

Chemical Engineering Science, 1961, Vol. 13, pp. 173 to 179. Pergamon Press Ltd., London. Printed in Great Britain

Thermal cracking of acetone—I.

Influence of the process variables on the product distribution

G. Froment, H. Pijcke and G. Goethals

Laboratorium voor Organische Technische Chemie, Rijksuniversiteit Gent, Belgium

(*Received September* 15, 1960)

Abstract—The thermal cracking of acetone into ketene was studied by flow-experiments. The effect of the feed-rate on the product distribution was investigated in the temperature range 710–750 °C and for residence times below 1 sec. The conversions and selectivities are correlated vs. the total acetone conversion in a diagram valid for the whole temperature range investigated.

Résumé—La décomposition thermique de l'acétone en cétène a été étudiée par des essais en régime dynamique. On a déterminé principalement l'influence du débit d'alimentation sur la distribution des produits à des températures allant de 710 à 750 °C et pour des temps de séjour en-dessous d'une seconde. Les différentes conversions et sélectivités ont été portées par rapport à la conversion totale de l'acétone dans un diagramme valable dans le domaine entier des températures considérées.

Zusammenfassung—Der thermische Krackprozess von Azeton ins Keten wurde durch Fliessexperimente studiert. Der Einfluss der Dosierung auf die Produkt-verteilung zwischen den Temperaturgrenzen von 710–750 °C, und für Reaktionszeiten unter eine Sekunde, wurde untersucht. Der Zusammenhang zwischen Umwandlungen und Selektivitäten im Verhältnis zu der totalen Umwandlung von Azeton ist in einem, für den ganzen untersuchten Temperaturbereich gültigen Diagramm, dargestellt.

1. Introduction

Acetic anhydride is used in large quantities in the cellulose acetate plants and is produced by reaction of ketene on acetic acid. Until recently ketene has been obtained exclusively by the thermal cracking of acetic acid. In recent years however increased attention has been paid to the use of acetone as a starting material as a result of its present surplus.

When submitted to pyrolytic conditions acetone decomposes according to an endothermic apparent over-all reaction:

$$CH_3\,CO\,CH_3 \rightarrow CH_2 = CO + CH_4 \qquad (1)$$

that may be considered irreversible in the range of practical interest (700–750 °C). Ketene and methane are not the only products, however: in the rang considered ethylene, carbon monoxide and dioxide, hydrogen and carbon are also obtained. The mechanism of formation of these byproducts is far from being elucidated. The presence of ethylene and of part of the carbonmonoxide has been explained by the apparent over-all reaction [1]:

$$2CH_2 = CO \rightarrow CH_2 = CH_2 + 2CO \qquad (2)$$

Whatever the mechanism or the intermediate steps of this reaction may be, the decomposition of ketene is a fact, that is reflected in the very short residence times and the consequent low conversions per pass ($\leqslant 25$ per cent) that have been adopted in industrial practice [1].

The formation of hydrogen and of cokes has been attributed [1] to the reaction

$$CH_3COCH_3 \rightarrow 3H_2 + CO + 2C \qquad (3)$$

which consumes acetone in parallel with (1). The prevention of this coke formation, which is strongly catalysed by the presence of nickel, has received considerable attention in the patent literature.

If, for reasons of strength, the usual types of

stainless steel are preferred to the nickel free chromium steels, a special pretreatment that forms a carbide film [2] or the addition of small quantities of a sulphur containing compound, e.g. carbon disulphide [3], is required to reduce substantially the carbon formation.

Practically no quantitative data have been published on the influence of the process variables on the rate of the reactions and the product distribution. The data available were obtained in static systems and under conditions that are not useful for industrial practice. It was not the purpose of the work reported here to study the reaction mechanism in detail: a chemical engineering approach turned toward design was adopted. A flow apparatus was used and the conditions of temperature and residence times were chosen to be as close as possible to industrial conditions.

2. Apparatus and Experimental Procedure

A scheme of the apparatus is given in Fig. 1. The acetone is fed by gravity and under a constant head through a flowmeter to the pyrolysis-tube. This is a chromium steel (16 per cent Cr, no Ni) spiral-wound tube of 10 mm outside diameter, 6 mm inside diameter and of length 1·20 m, a detailed scheme of which is given in Fig. 2. This tube is placed in an electric oven, filled for the sake of equalizing the temperature with copper shots. Besides of the main heating wire, proper to the oven, secondary resistances are provided around the inlet and outlet sections of the tube, in order to compensate heat losses to the exterior and to reduce the preheating section to a minimum.

The inlet temperature of the acetone vapours is

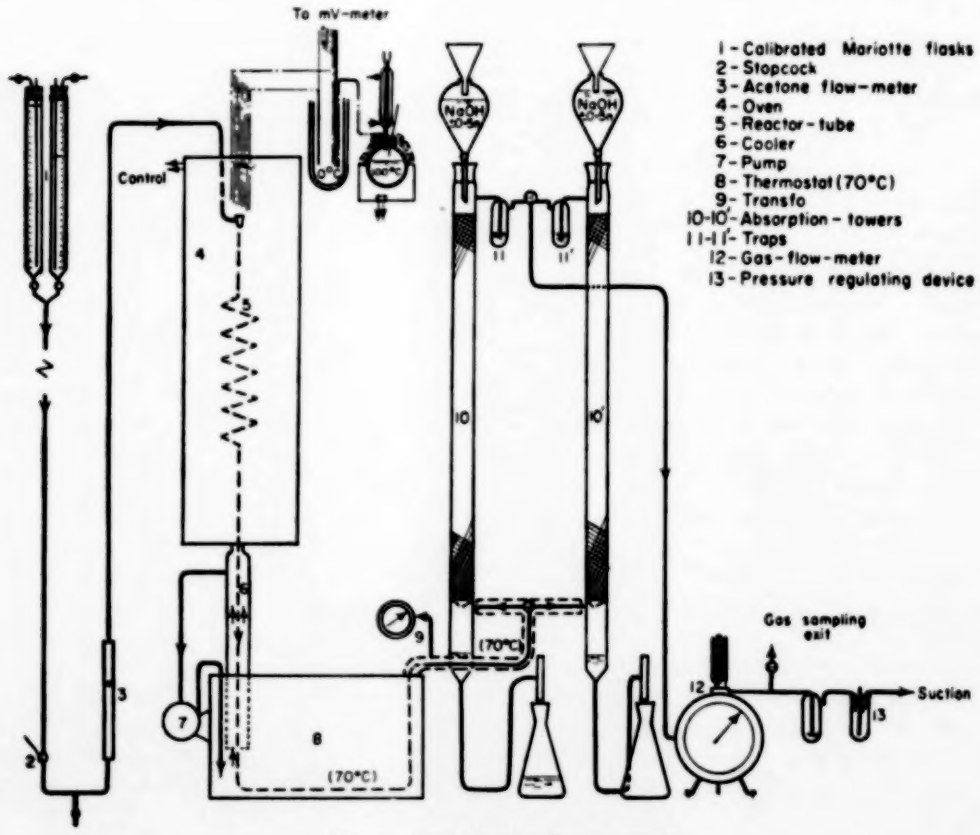

FIG. 1. Flow sheet of the apparatus.

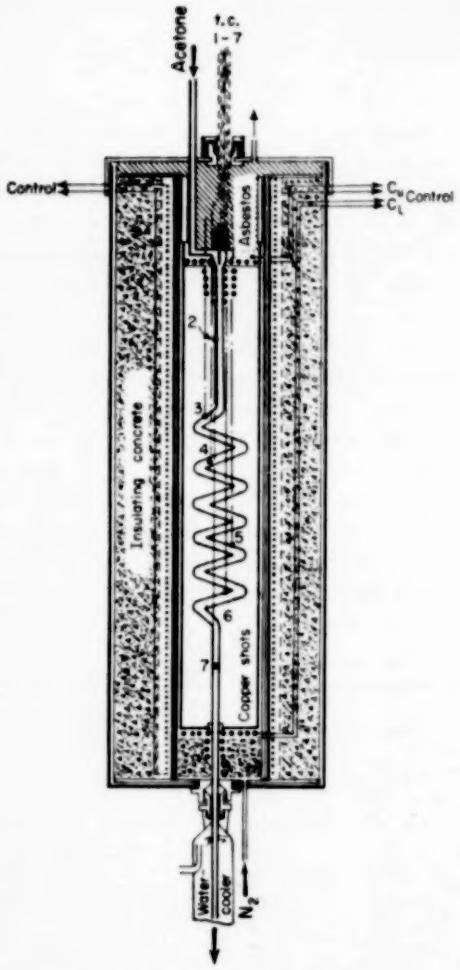

FIG. 2. Oven with reactor tube.

measured by thermocouple 1, while the wall temperature of the tube is measured at six different spots by Ni–NiCr–thermocouples.

At the outlet the gases are drastically cooled in order to limit as much as possible the conversion to the reactor itself. Because ketene polymerizes rapidly in liquid acetone the temperature is not lowered beneath the dew-point of acetone in the gases. To be safe the lines were kept at 70° by a thermostat or by heating wires. The gases than enter one of the two absorption towers where they are scrubbed by a known volume of standard sodium hydroxide. The acetone is absorbed while the ketene reacts under the formation of sodium acetate.

A trap filled with 0·01 N sodium hydroxide serves as an indicator that no ketene escapes. The volume of the remaining gases is measured in a wet gas meter. The pressure in the apparatus is controlled by a pump and the bottle 13.

The unreacted acetone present in the sodium hydroxide liquor was titrated by Messinger's method, based on the iodoform reaction. The ketene present in the gases was determined by titration of the excess sodium hydroxide in the absorption liquor. The gases were analysed with an Orsat apparatus, while additional information was obtained from gas chromatography and mass spectrometry.

In spite of the absence of nickel, carbon deposition did occur and it was necessary to burn it off from time to time. After this operation the apparatus had to run some time before reproducible data could be obtained. After this start-up period neither the conversion, nor the product distribution were dependent on time.

3. Definitions

The conversions and the product distribution of this complex system have been characterized as follows:

The total conversion of acetone has been defined as:

$$x_{at} = \frac{\text{moles of acetone decomposed}}{\text{moles of acetone fed}} \qquad (4)$$

The conversion of acetone in side-reactions (e.g. equation 3) as

$$x_{as} = \frac{\text{moles of acetone decomposed by side-reactions}}{\text{moles of acetone fed}} \qquad (5)$$

The conversion of acetone to ketene, according to (1) as

$$x_{ak} = \frac{\text{moles of ketene formed}}{\text{moles of acetone fed}} \qquad (6)$$

The conversion of ketene itself, according to (2) as

$$x_{kd} = \frac{\text{moles of ketene decomposed}}{\text{moles of acetone fed}} \qquad (7)$$

The net ketene concentration, as measured effectively, is also obtained through a conversion, defined as

$$x_{ke} = \frac{\text{moles of ketene measured}}{\text{moles of acetone fed}} \quad (8)$$

(4), (5) and (6) are related by

$$x_{at} = x_{ak} + x_{as} \quad (9)$$

(6), (7) and (8) by

$$x_{ak} = x_{ke} + x_{kd} \quad (10)$$

Furthermore, we define the yield by

$$\eta = \frac{x_{ke}}{x_{at}} \leqslant 1 \quad (11)$$

the acetone selectivity by

$$y = \frac{\text{moles of ketene formed}}{\text{moles of acetone decomposed}} = \frac{x_{ak}}{x_{at}} \leqslant 1 \quad (12)$$

the ketene selectivity by

$$z = \frac{\text{moles of ketene measured}}{\text{moles of ketene formed}} = \frac{x_{ke}}{x_{ak}} \leqslant 1 \quad (13)$$

x_{at} is obtained from the measured amount of acetone fed and from titration of the acetone in the absorption liquor; x_{ke} from the titration of NaOH in this liquor; x_{kd} from the ethylene content of the gases and their volume, according to reaction (2); x_{ak} from (10); x_{as} from (9).

4. Experimental Results

The results of the series of experiments at 710, 730 and 750 °C are given in Table 1 and Figs. 3, 4 and 5 respectively. The conversions are given in function of the time factor V_R/F, rather than of the residence time itself, which is a complicated function because of expansion. The V_R/F values are such that the residence times varied between 0·1 and 0·6 sec.

VOL. 13 1961

Table 1. *Experimental results*

No.	V_R/F	x_{at}	x_{ke}	x_{kd}	x_{ak}	y	z	η
				750 °C				
1	9·17	0·175	0·126	0·011	0·137	0·78	0·92	0·72
2	11·20	0·240	0·160	0·0245	0·1845	0·77	0·87	0·68
3	14·65	0·322	0·212	0·034	0·252	0·78	0·84	0·65
4	23·80	0·4625	0·2685	0·080	0·3565	0·77	0·775	0·60
5	28·90	0·516	0·282	0·1025	0·3845	0·75	0·73	0·55
6	43·10	0·610	0·3085	0·163	0·472	0·77	0·65	0·51
7	71·50	0·716	0·330	0·237	0·566	0·79	0·58	0·46
				730 °C				
8	12·95	0·219	0·159	0·019	0·170	0·78	0·89	0·69
9	18·60	0·273	0·1795	0·0275	0·207	0·76	0·87	0·66
10	25·00	0·308	0·195	0·038	0·233	0·76	0·84	0·63
11	41·40	0·515	0·280	0·096	0·376	0·74	0·74	0·545
12	41·80	0·516	0·280	0·0975	0·377	0·73	0·74	0·54
				710 °C				
13	11·70	0·110	0·085	0·0065	0·092	0·83	0·93	0·78
14	20·55	0·165	0·122	0·018	0·1395	0·82	0·87	0·74
15	25·15	0·203	0·142	0·024	0·165	0·81	0·86	0·70
16	36·20	0·314	0·214	0·046	0·260	0·82	0·82	0·68
17	51·75	0·406	0·249	0·061	0·310	0·76	0·80	0·61
18	74·90	0.478	0·278	0·103	0·381	0·80	0·73	0·58

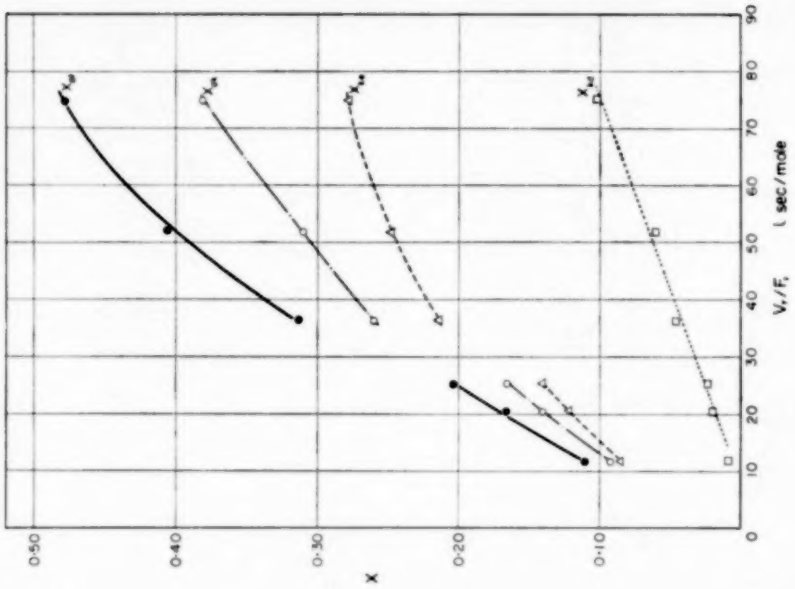

FIG. 3. Experiments at 710 °C.

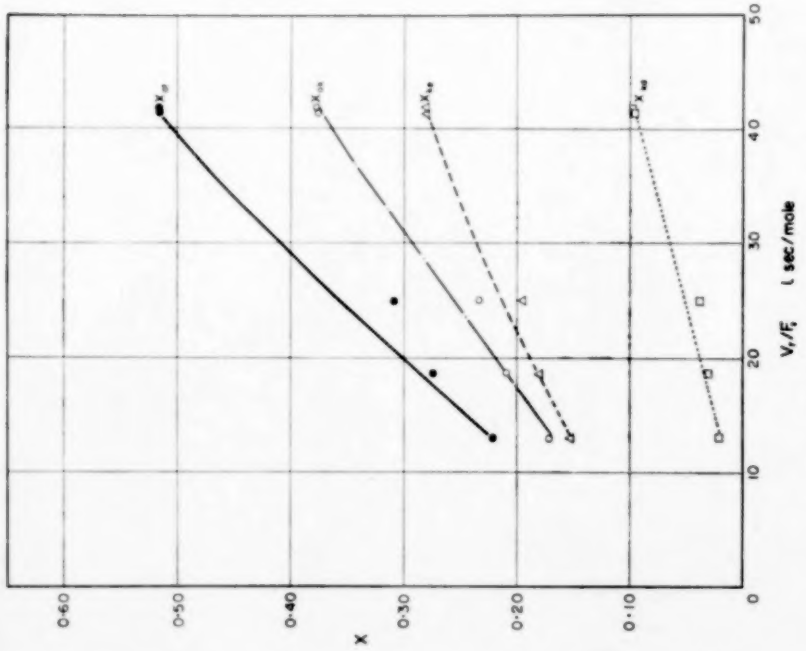

FIG. 4. Experiments at 730 °C.

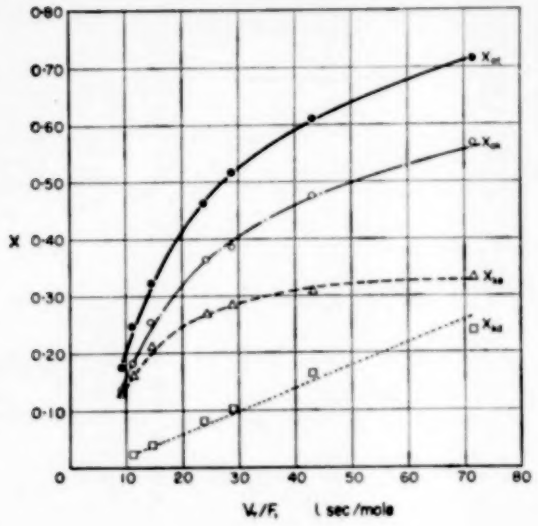

Fig. 5. Experiments at 750 °C.

5. Discussion

Qualitatively the results agree with the picture given by equations (1), (2) and (3): x_{at}, x_{as}, x_{ak} increase with V_R/F; x_{ke} tends to a maximum, that is best seen from the data at 750 °C, where the conversions are highest and will probably decrease at higher V_R/F because of the increasing importance of the decomposition reaction (2).

The attention should be drawn on the incomplete picture of the consumption of acetone in side-reactions given by equation (3).

Indeed, material balances on the acetone consumed in side-reactions may be obtained in two ways: either from the acetone and residual sodium hydroxide content of the absorption liquor or from the CO content of the gases after deduction of the CO generated by the ketene decomposition.

These balances do not check, although the apparatus was controlled for tightness before every experiment. Clearly then, equation (3) does not account for all the acetone decomposed in the side-reaction, either because other reactions also occur or because it is only the last of a series of steps which have not come completely to their achievement.

For the experiments at 750 °C for example, the percentage of acetone consumed in side-reactions, based on the content of the gas, showed a very definite trend and increased from 28 per cent of the value obtained by titration at $V_R/F = 9{\cdot}17$ to 70·4 per cent at $V_R/F = 71{\cdot}50$. This seems to support the latter hypothesis.

It is seen also how the curves of the Figs. 3, 4 and 5 do not extrapolate through the origin. This is characteristic for homogeneous reactions carried out in a flow reactor and results from the fact that not all of the volume accounted for is at the reference temperature considered. This will be discussed in detail in Part II, where the curves will be corrected for this effect.

In a first attempt to eliminate this effect and also to relate the different conversions to one another, these have been plotted in Fig. 6, together with the yield and the selectivities, vs. the total acetone conversion.

It is seen how x_{ak}, x_{ke} and consequently η may be correlated as unique functions of x_{at}. The diagram indicates clearly how the yield η decreases as the acetone conversion increases. The diagram is limited to the ascending part of the curve $x_{ke} - V_R/F$. If values past the maximum were considered a very sharp decrease in the η-x_{at} is to be expected. As is to be expected also from a system of consecutive reactions, the ketene selectivity z decreases as x_{at} increases and z vs. x_{at} is very nearly independent of the temperature. A closer look however shows how the values at 710 °C are somewhat below those at 750 °C. This seems to indicate that the activation energy of the ketene decomposition (2), although not too different from that of the formation (1), is lower.

The values of y, the acetone selectivity, at 710 °C are also slightly higher than at 750 °C. Nevertheless, these differences are very small and the diagram, which covers the field of interest for industrial practice, is therefore believed to be general, i.e. not limited to the apparatus used with its characteristic temperature and conversion profiles.

Presented as they are the results permit the prediction of the product distribution when the total conversion of acetone is known. The prediction of this conversion is a problem of kinetics which makes use of x vs. V_R/F data.

VOL 13 1961

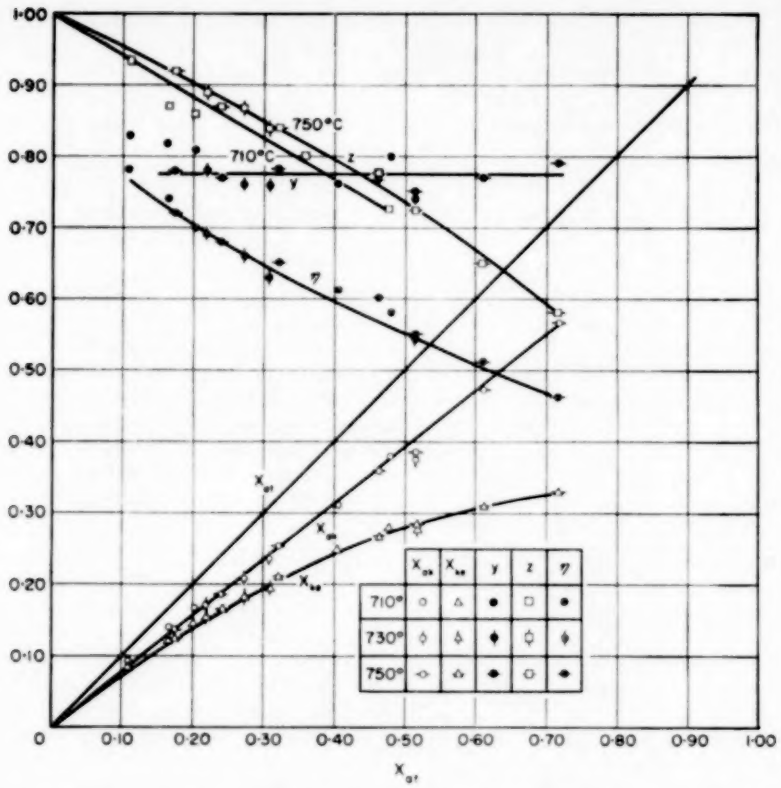

FIG. 6. Conversions, yields and selectivities vs. the total acetone conversion.

It is not possible however to derive a rate equation from the data as they are presented in the Figs. 3, 4 and 5, since they are too specific for the apparatus used. The derivation of rate equations from experiments of the type reported here will be tackled in Part II of this paper.

NOTATION

C_p = specific heat
E = activation energy
F = feed rate
k_h = thermal conductivity of the gas
k = rate-constant
L = length
m = mass feed rate
n = order of a reaction
p = partial pressure
r = reaction rate
R = gas constant
s_r^2 = error-variance
t_m = temperature of the gases at a distance L
t_0 = entrance temperature of the gases
t_s = wall temperature
T = temperature
V_R = reactor volume
V_R' = equivalent reactor volume
x_{ak} = conversion of acetone to ketene
x_{as} = conversion of acetone in side reactions
x_{at} = total acetone conversion
x_{kd} = ketene conversion
x_{ke} = net acetone conversion to ketene
y = acetone selectivity $\frac{x_{ak}}{x_{at}}$
z = ketene selectivity $\frac{x_{ke}}{x_{ak}}$
η = yield

REFERENCES

[1] DAROUX W. G. *J. Appl. Chem.* 1953 **3** 241.
[2] MOÏSE J. E. *U.S. Pat.* 2537687 1951.
[3] TYLER D. L. *Brit. Pat.* 629211 1949.

Chemical Engineering Science, 1961, Vol. 13, pp. 180 to 189. Pergamon Press Ltd., London. Printed in Great Britain

Thermal cracking of acetone—II.

Deriving rate-equations from non-isothermal flow experiments*

G. Froment, H. Pijcke and G. Goethals
Laboratorium voor Organische Technische Chemie, Rijksuniversiteit Gent, Belgium.

(*Received September* 15, 1960)

Abstract—When homogeneous reactions are carried out in a flow apparatus a clear-cut separation between preheat and reaction sections is impossible, so that the latter shows in fact a longitudinal temperature gradient. This situation greatly complicates the derivation of kinetic data. With the help of the equivalent reactor volume concept and a proposed method for estimating the activation energy prior to the knowledge of the rate constants, the conversion vs. V_R/F data of Part I, which are too specific for the apparatus used, have been corrected. This enabled rate equations to be derived for the ketene formation and decomposition and from these rate equations for the net ketene production. Used in conjunction with the selectivity diagram of Part I this result permits the prediction of a fairly complete product distribution.

Résumé—Lorsque des réactions homogènes sont exécutées en régime dynamique il est impossible de définir nettement les sections de préchauffage et de réaction. Il existe donc en cette dernière un gradient longitudinal de température qui complique sérieusement l'étude cinétique. A l'aide du concept du volume équivalant et d'une méthode originale permettant d'évaluer l'énergie d'activation, avant même de connaitre les constantes de vitesse, les données conversion $- V_R/F$ de la 1ère partie, trop spécifiques, ont été corrigées. On peut alors dériver des équations cinétiques pour la formation et la décomposition du cétène et donc pour la production effective : utilisé en conjonction avec le diagramme des sélectivités de la 1ère partie ce résultat permet de prédire la distribution quasi complète des produits du cracking.

Zusammenfassung—Wenn in einem Fliess-apparat homogene Reaktionen durchgeführt wird, eine vollständige Trennung der Vorwärme- und Reaktions-sektionen ist unmöglich, so dass die Reaktions-sektion in der Tat einem longitudinalen Temperatur-gradient aufweist. Dieser Umstand kompliziert sehr die Ableitung von kinetischen Daten. Mit der Hilfe des Begriffes des äquivalenten Reaktions-volumens und einer vorgeschlagenen Methode zur Abschätzung der Aktivierungs-energie, bevor man die Geschwindigkeits-konstanten der Umwandlung kennt, V_R/F Daten im ersten Teil, welche viel zu spezifisch für den verwendeten Apparat sind, wurden korrigiert. In dieser Weise es ist möglich die kinetischen Gleichungen für die Formung und Zerlegung der effektiven Keten-produktion abzuleiten. Verwendet zusammen mit dem Selektivität-diagramm vom ersten Teil, dieses Ergebnis ermöglicht die ziemlich gute vorherige Abschätzung der Krackprozess-verteilung.

1. Introduction

The design of a chemical reactor requires in the most general case the simultaneous integration of the continuity, energy and momentum equations. Even if the physical properties are taken to be constant analytical integration of this system is excluded, because of the non-linearity of the equations. Numerical integration however is straightforward.

The reverse problem, namely, the derivation of kinetic data is far more involved. This comprises the determination of the form of the rate equation itself and of a number of constants-for homogeneous reactions: the order, the rate constant and the activation energy, which gives the temperature dependence of the rate constant. This can be done by successive trials, postulating rate equations and trying values of the constants until the calculated conversion, temperature and pressure profiles reproduce the experimental. Even with the help of statistical methods and computers this is a formidable task however,

*Part I: This issue, p. 173.

especially when no first approximations are at hand. The procedure most often used is than to simplify the physical picture. If, by reducing the size to a convenient scale, the pressure drop becomes negligible, then the momentum equation need not be considered and if it is possible to eliminate all temperature gradients, the energy equation need not be taken into account. The mathematical model has then become sufficiently simple to permit, in most cases, the derivation of a satisfactory rate equation.

The condition of isothermicity is a very drastic one, however: the heat effect of the reaction is often considerable and cannot always be compensated entirely.

Furthermore, in some cases it is inevitable that part of the reactor is used to bring the feed to the desired temperature. This is the case with flow reactors for homogeneous reactions, where, in contrast to catalytic reactors, no clear-cut separation between preheat and reaction section is possible. If the rate is to be determined at a reference temperature, say T_1, and if the reaction volume is counted from the point where T_1 is reached, then the conversion in the preheat section, that cannot be excluded, is not accounted for. Similarly at the outlet there is a section where, while being cooled, the conversion continues to some extent.

This situation, from which there is no way out, complicates seriously the task of deriving rate equations for homogeneous reactions. The idea of this paper is to take the situation as it is and nevertheless to find a method for deriving at least approximate values for the rate constant, the order and the activation energy, the refinement of which, if necessary, would be left to the computer.

The essential features of the method are the use of an equivalent reactor volume, as introduced by HOUGEN and WATSON [2] and of a proposed short-cut procedure for a preliminary determination of the activation energy. This will be illustrated on the data of Part I.

2. THE EQUIVALENT REACTOR-VOLUME

The equivalent reactor volume has been defined as that volume, V'_R, which, at the reference temperature T_1, would give the same conversion as the actual reactor, with its temperature profile.*

It follows that

$$dV'_R = \frac{r_T}{r_{T1}}\, dV_R$$

from which

$$V'_R = \int_0^{V_R} \exp\left[-\frac{E}{R}\left(\frac{1}{T} - \frac{1}{T_1}\right)\right] dV_R \qquad (1)$$

Once V'_R has been derived the calculation of the rate constant is straight-forward, as for isothermal experiments and solely based on the continuity equation

$$F\, dx = r\, dV'_R \qquad (2)$$

The calculation of V'_R requires the knowledge of the temperature profile along the tube and of the activation energy E.

Note also that where several reactions are occuring simultaneously the dependence of V'_R on E leads to different values of V'_R for each of the reactions considered.

3. ESTIMATION OF THE ACTIVATION ENERGY

However, as the activation energy is not known *a priori*, the use of the equivalent reactor volume concept leads to a trial and error procedure: a value of E is guessed and with this value and the measured temperature profile, V'_R is derived from (1) by graphical integration. Then, from (2), the rate constant is derived.

This procedure is carried out at several temperature levels and from the temperature dependence of the rate constant, expressed by Arrhenius' formula, a value of E is obtained. If this value is not in accordance with that used in the calculation of V'_R the whole procedure has to be repeated with a better approximation for E and thus for V'_R.

In this paragraph a short-cut method for the first estimate of E, not based on Arrhenius' formula and therefore not requiring knowledge of the rate constant, is proposed. It is based on the following considerations.

Consider two experiments carried out in a flow

*The notation used is given at the end of part I.

reactor, one at a reference temperature T_1, the other at the reference temperature T_2 and let the conditions be such that the temperature difference $\Delta T = T_1 - T_2$ is the same over the whole length of the reactor. The reaction taking place is homogeneous and of the type $A \rightarrow B$. If the feed-rates are adjusted so that equal conversions are obtained, then the x, i.e. the p_A vs. V_R profiles are identical in both cases. Then

$$\frac{dx_1}{dV_R} = \frac{dx_2}{dV_R}, \quad (p_A)_1 = (p_A)_2$$

at all points, while ΔT is independent of V_R. From the continuity equation,

$$F\,dx = \alpha \exp\left(-\frac{E}{RT}\right)(p_A)^n\,dV_R$$

applied to both experiments, it follows that

$$\frac{F_1}{F_2} = \exp\left[-\frac{E}{R}\left(\frac{1}{T_1} - \frac{1}{T_2}\right)\right] = \exp\left[\frac{E}{R}\cdot\frac{\Delta T}{T_1 \cdot T_2}\right]$$

from which $$E = 2{\cdot}3\,R\,\frac{T_1\,T_2}{\Delta T}\log\frac{F_1}{F_2} \qquad (3)$$

This means that the activation energy may be derived from two experiments at different temperatures without even knowing the rate constants, provided the conversions are the same and the temperature profiles, plotted vs. V_R, are parallel.

The latter condition is not always fulfilled in practice. It requires that the heat effect of the reaction is negligible or entirely compensated for by the heat flux from or to the surroundings or (and) that the specific heat of the gases is very large.

If the reactant A is consumed by more than one reaction than, at equal conversion to the product of interest, B, p_A is only equal in both experiments when the activation energies of the parallel reactions are equal. If not, the approximation is better the more the principal reaction prevails over the side reaction(s).

4. Kinetic analysis of the cracking of acetone

It was mentioned in part I how the data, presented as they are, permit the prediction of the product distribution provided that one of the main conversions is known. Extrapolation of the conversions from the Figs. 3, 4 and 5, Part I, is not allowed, however, as they were obtained with temperature profiles too typical for the apparatus used. The correct procedure is to extract from these data what is general: i.e. the rate equations.

The data available permit a kinetic analysis of reactions (1) and (2) of Part I. The prediction of the total acetone conversions would also require, strictly speaking an analysis of the acetone consuming side reaction for which reaction (3) of Part I was shown to be a far too simplified scheme. In the range investigated however, the total acetone conversion may be related uniquely through the ketene selectivity parameter to the conversion to ketene (Fig. 6, Part I) so that a fairly complete picture is obtained with rate equations for reactions (1) and (2) of Part I, only.

Prior to the derivation of the rate-equations, however, the temperature profile of the reaction mixture itself had to be calculated. Measuring the gas temperature itself would have required an inner tube to hold the thermocouples, leaving an annular reaction space, which is not likely to be adopted for pilot-plant work, a stage that was continuously kept in mind in this investigation.

With the wall temperature and the flow regime known and the physical properties of acetone and reaction mixtures of different compositions taken from the literature or estimated, it is a classical problem of heat transfer to calculate the temperature of the gases at any point along the tube. As the flow regime was laminar, use was made of the experimental Sieder–Tate equation, represented in a convenient form as

$$\phi = \frac{t_0 - t_m}{t_0 - t_s} \text{ vs. } \frac{mc_p}{k_R L} \qquad [3]$$

In the reaction section the heat effect of the reaction was not taken into account. There is experimental evidence however that the heat flux from outside was so high that the effect of the endothermicity of the reaction (18600 cal/mol at

VOL. 13 1961

700–750 °C) was easily compensated, so that the computed profile is not too far off. In the exit section, where the wall temperature decreases sharply as a result of the sudden cooling, small increments were chosen. In Fig. 2 a typical temperature profile (experiment 6) measured in the wall and the computed profile of the flowing reaction gases are shown. Now rate equations for reactions (1) and (2) of Part I may be derived.

4 (a). *The formation of ketene*

The first step in the kinetic analysis of the ketene formation consists of calculating the equivalent reactor volume. The method proposed in section 3 was used to estimate the activation energy. In the reaction and exit sections the temperature profiles at different reference temperatures and feed rates were very nearly parallel. The largest deviations were observed in the preheat section, but their importance is relatively minor for the present calculation as little reaction is taking place in this section.

In Fig. 1, x_{ak} and p_{ac} are plotted vs. log F for two series of experiments, one at 750°, the other at 710 °C. The two x_{ak} lines are parallel, while although side-reactions do occur, equal p_{ac} correspond very nearly to equal x_{ak}, as is shown by the dotted lines. The conditions for a satisfactory estimate of E are fulfilled.

The horizontal distance between the two parallel x_{ak} lines leads to a unique value of the activation energy: 51800 cal/mole. This value compares quite favourably with the activation energies of a number of cracking reactions mentioned by HINSHELWOOD [1] and MURDOCH and HOLLAND [4].

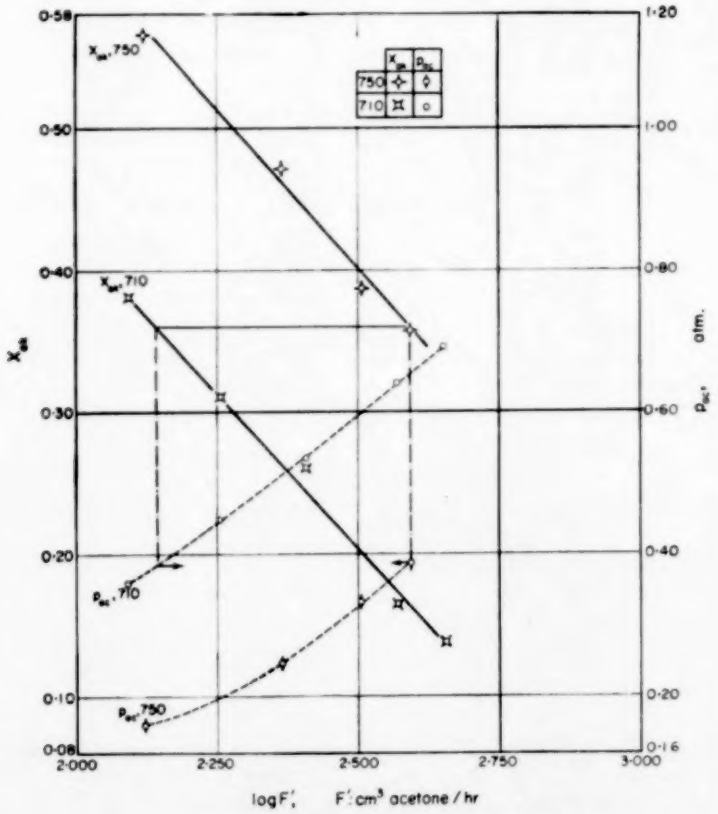

FIG. 1. Estimation of the activation energy.

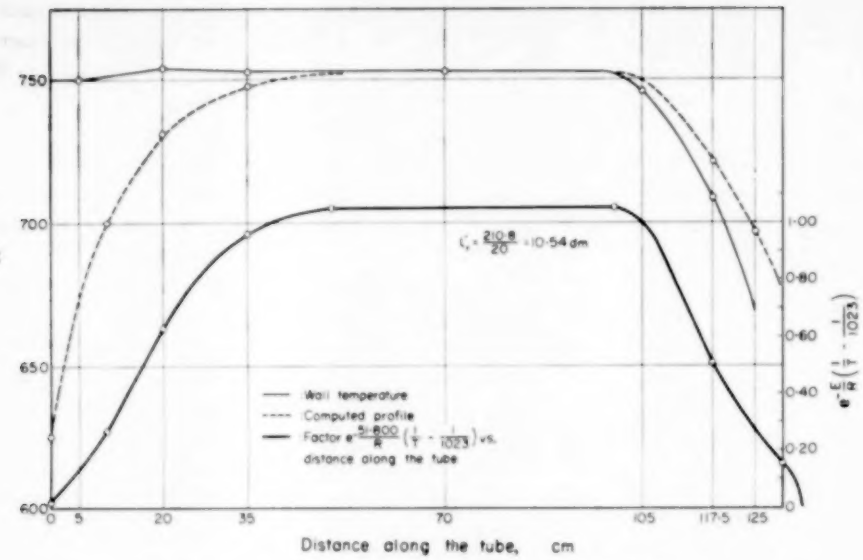

Fig. 2. Wall temperatures, computed temperature profile of the gases and equivalent reactor length for experiment 6.

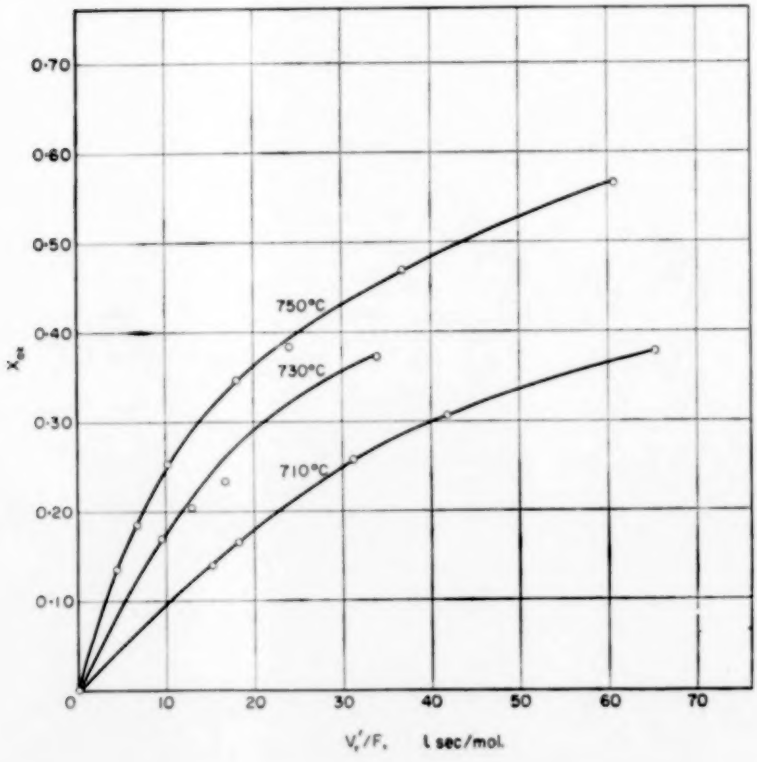

Fig. 3. x_{ak} vs. corrected V_r/F.

VOL. 13 1961

Cracking of:

dipropylether	: 60,500 cal/mole	[1]
diethylether	: 53,500 cal/mole	
methylethylether	: 47,000 cal/mole	
acetaldehyde	: 45,500 cal/mole	
propane	: 51,300 cal/mole	[4]

With this value of E and the temperature profiles of the experiments approximated as described above, the equivalent reactor volume may be obtained by graphical integration as indicated in Fig. 2. With the V_R/F reported in Part I corrected for each experiment it is possible to draw corrected curves for the x_{ak} vs. V_R/F data of the Figs. 3, 4 and 5 of Part I. The result of this is shown in Fig. 3. Compared with Fig. 5 (Part I) it is seen how there is no longer any break in the curve corresponding to the experiments at 710 °C and how the curves may now be extrapolated through the origin. The other conversions shown in Figs. 3–5 (Part I) are also better correlated vs. V_R'/F, but they are not shown in Fig. 3 as they refer to reactions with activation energies which may differ from that used in computing V_R'/F. With this corrected x_{ak} vs. V_R'/F-diagram established, the derivation of a rate equation may be tackled. Two ways were followed here: the integral and the differential method.

When a rate equation of the form

$$r = k\, p_{ac}^{n} \tag{4}$$

is postulated, the continuity equation becomes

$$\frac{V_R'}{F} = \frac{1}{k} \int_0^x \frac{dx_{ak}}{p_{ac}^{\,n}} \tag{5}$$

The differential method is based on (4), the integral on (5).

Integral method. Before the integral in equation (5) may be worked out it is necessary to express p_{ac} as a function of x_{ak}. A rigorous expression would only be possible if all reactions taking place were exactly known. Therefore an empirical fit of the function p_{ac} vs. x_{ak} was undertaken. In Fig. 4 it is shown how, at the three temperatures considered, p_{ac} may be expressed as a unique function of x_{ak}:

$$p_{ac} = 1 - 2{\cdot}1\, x_{ak} + 1{\cdot}1\, x_{ak}^2 = (1 - 1{\cdot}05\, x_{ak})^2 \tag{6}$$

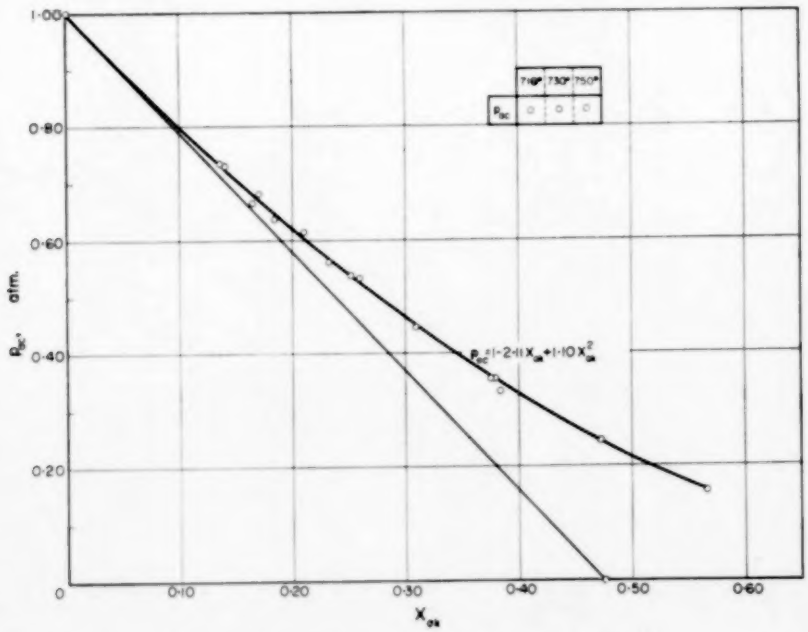

Fig. 4. Empirical equation for the p_{ac} vs. x_{ak} data.

Equation (5) then becomes

$$\text{for } n \neq \frac{1}{2} : k = \frac{1}{1{\cdot}05\,(V'_R/F)\,(2n-1)} \left[\frac{1}{(1-1{\cdot}05\,x_{ak})^{2n-1}} - 1\right] \quad (7)$$

$$\text{for } n = \frac{1}{2} : k = \frac{1}{1{\cdot}05\,V'_R/F} \ln \frac{1}{1-1{\cdot}05\,x_{ak}} \quad (8)$$

It follows that, when the values of x_{ak} and V'_R/F corresponding to the different experiments are substituted in equations (7) or (8), k becomes, for

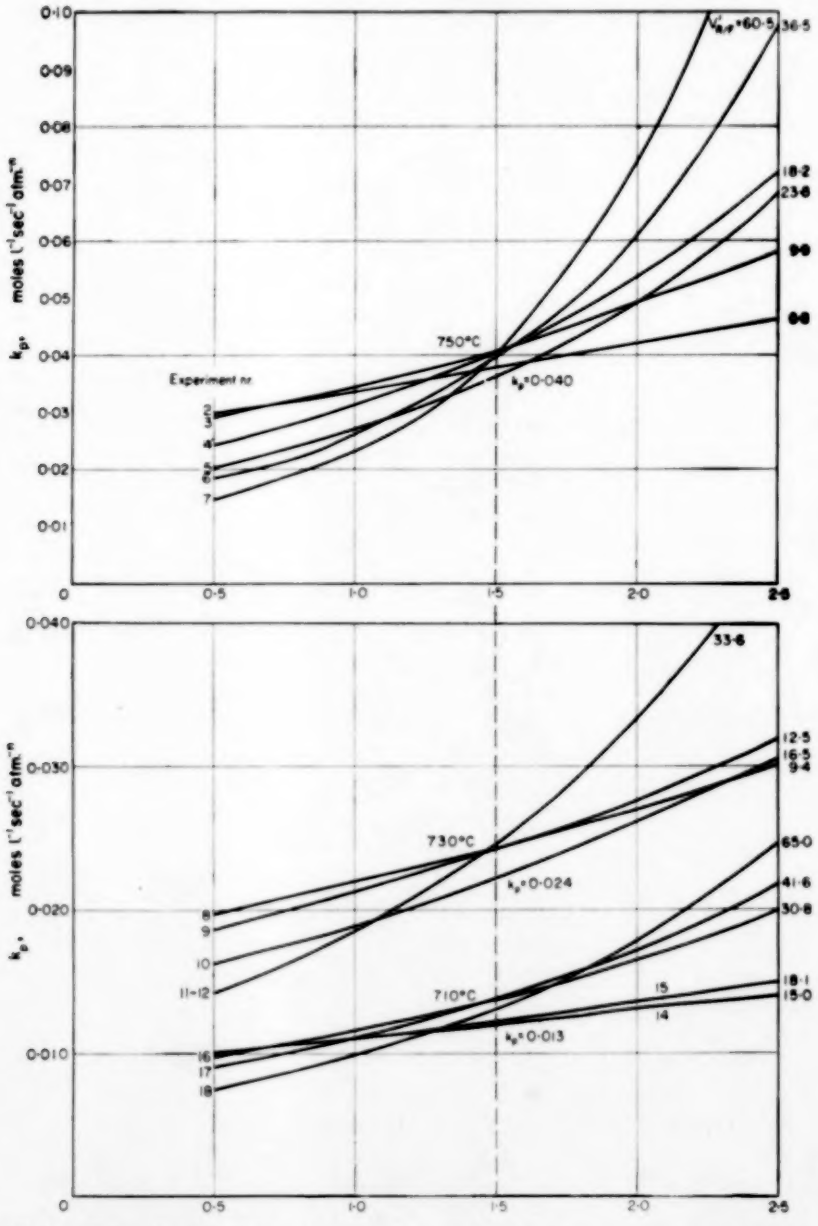

FIG. 5. Determination of the rate-constant, k_p, and of the order, n, of the reaction.

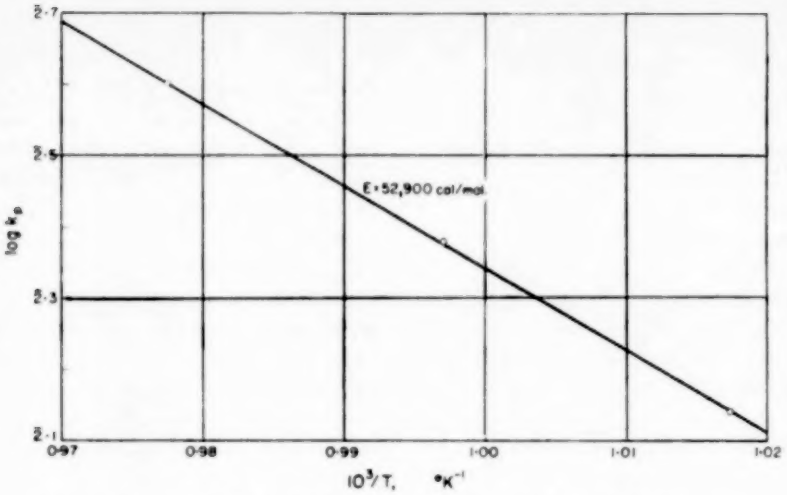

FIG. 6. Arrhenius plot for the final determination of the activation energy.

each experiment, a function of n only. The point of intersection of the k vs. n curves should give the value of k at the temperature considered and the unique value of n. The k vs. n curves are shown in Fig. 5. It is seen how the experiments at 750° and 730 °C lead to an order of 1·50 and values for k of 0·040 and 0·024 moles/l. sec atm.$^{1·5}$ The largest deviations amount to 0·005 at 750° (12 per cent) and 0·0025 moles/l. sec atm$^{1·5}$ at 730 °C (10 per cent). The curves relating to the experiments at 710°, which are not so steep, do not intersect in one point and do not permit the accurate determination of the order at that temperature. It can only be stated that the relative spread on k is lowest between $n = 1·0$ and 1·5. However, if n is also taken to be 1·5 the value of 0·013 moles/l. sec. atm$^{1·5} \pm$ 0·001 (8 per cent) is obtained for k. When these k values are plotted vs. the reciprocal of the absolute temperature, $1/T$, as in Fig. 6, they fall on a straight-line from which an activation energy of 52,900 cal/mole is derived. It may be concluded that the mechanism of formation of ketone from acetone is not altered between 710° and 750 °C and that the rate of this process may be described by

$$r = \exp\left(22·780 - \frac{26,600}{T}\right) p_{ae}^{1·5} \qquad (9)$$

The value of 52,900 cal/mole for E is very close to that obtained by the short-cut method of section 3, i.e. 51,800 cal/mole, so that no iteration is required. This proves the value of the proposed method.

Differential method. This method is based upon equation (4). The rate r, has to be derived from a p_{ae} vs. V_R'/F plot, e.g. by graphical differentiation.

The values of k and n are then obtained from a logarithmic plot of equation (4) by means of a least-square fit of the points to a straight line. The results are given in Table 1 together with the error variance on n.

Table 1

°C	k	n	$s_e^2(n)$
750	0·041	1·48	0·01
730	0·023	1·37	0·01
710	0·014	1·54	0·04

This method, in contrast to the integral method, leads to a clearly defined value for n at 710°. The value at 730° is less reliable however, because due to the deviation of the point related to experiment 10 ($V_R'/F = 16·5$; $x_{ak} = 0·233$) noticed in the integral method (Fig. 5), the x vs. V_R'/F curve cannot be drawn accurately for the higher

V_R'/F region. Nevertheless, these results confirm entirely those obtained by the integral method.

4(b). *The decomposition of ketene*

The prediction of the effective ketene content at the outlet of the reactor requires a rate equation for the decomposition of ketene (reaction 2, Part I) in addition to the equation for the rate of formation (equation 9, Part II).

The procedure described above may be repeated here. Again a value of E has to be estimated. In an investigation of the ketene-decomposition by static experiments ($p = 100$ mm Hg; 510–590 °C) Young found that at the higher temperatures the activation energy was about 50,000 cal/mole [5]. From the correlation of the results as given in Fig. 6, Part I, it was deduced that the activation energy was not too much different from that of the ketene formation. Therefore E was estimated to be 51,800 cal/mole, which is the value used for the determination of the equivalent reactor volume of the ketene formation. In this way the V_R'/F reported in section 4(a) could be used again as a first estimate, saving thus a substantial amount of calculations.

In Fig. 7 x_{kd} is plotted vs. V_R'/F at the three reference temperatures investigated. The data may be represented by straight lines through the origin. This means that the decomposition is zero order with respect to ketene. The rate constants are then 0·0044, 0·00262 and 0·00153 moles/l. sec at 750, 730 and 710 °C respectively. These values lead to an activation energy of 51,000 cal/mole, which is sufficiently close to the estimated value to render a second approximation superfluous. This activation energy is also very close to that for the ketene formation, as predicted. From the standpoint of kinetics, however, no definitive conclusions should be drawn from these results. The linear change of x_{kd} with V_R'/F which leads to an order zero, is probably due only to the rather narrow range over which the partial pressure of ketene was varied. It is a fact however that, in the range of practical interest investigated in this work, the decomposition of ketene may be described with excellent accuracy by

$$r = \exp\left(19{\cdot}617 - \frac{25{,}660}{T}\right) \quad \left(\frac{\text{moles}}{\text{l. sec}}\right) \qquad (10)$$

Substitution of the rate equations (9) and (10) into the continuity equation leads to

$$F\,dx_{kc} = \exp\left[\left(22{\cdot}780 - \frac{26{,}600}{T}\right) p_{ac}^{1{\cdot}5} - \right.$$
$$\left. - \exp\left(19{\cdot}617 - \frac{25{,}660}{T}\right)\right] dV_R' \qquad (11)$$

where p_{ac} is given by (6).

In this equation the same value of V_R' was used for both the formation and decomposition of ketene, although this is only an approximation as already explained

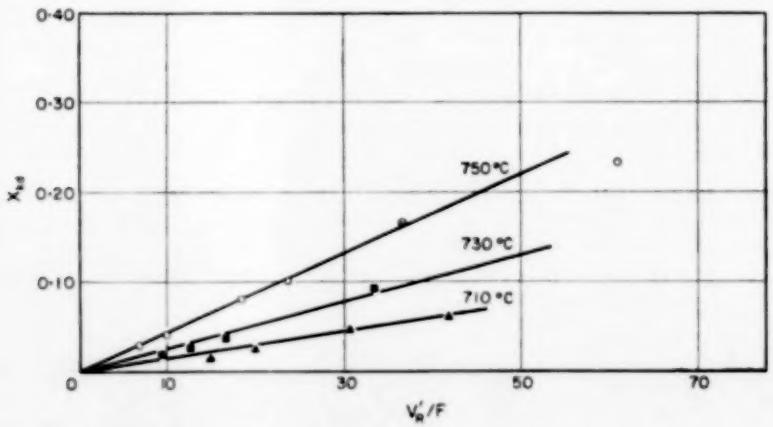

Fig. 7. x_{kd} vs. V_R'/F data.

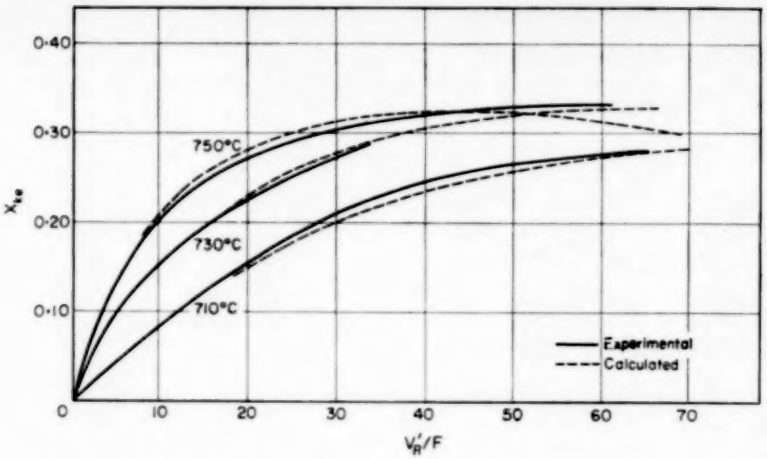

FIG. 8. x_{ke} vs. V_R'/F. Comparison of experimental and calculated profiles.

When integrated simultaneously with the energy- and eventually the momentum equation, the net ketene conversion is obtained. From Fig. 6, part I, the corresponding total acetone conversion, the acetone lost in side-reactions and a fairly good estimate of the amount and composition of the cracking gas are obtained.

For isothermal conditions or non-isothermal conditions which have been corrected by means of the equivalent reactor-volume concept, equation (11) may be integrated, remembering (7), to give

$$x_{ke} = 0{\cdot}955\left[1 - \left(2{\cdot}1\frac{k_1 V_R'}{F} + 1\right)^{-1/2}\right] - k_2\frac{V_R'}{F} \quad (12)$$

Fig. 8, finally, is a graphical representation of equation (12) which illustrates how the kinetic constants derived lead to an excellent reproduction of the corrected experimental results.

REFERENCES

[1] HINSHELWOOD C. *Kinetics of Chemical Change*. Oxford University Press, New York 1941.

[2] HOUGEN O. A. and WATSON K. M. *Chemical Process Principles* Part III, p. 884. John Wiley, New York 1947.

[3] JAKOB M. *Heat Transfer* Part I, p. 461. John Wiley, New York 1958.

[4] MURDOCH P. G. and HOLLAND C. D. *Petrol. Refin.* 1954 **33** 6.

[5] YOUNG J. R. *J. Chem. Soc.* 1958 2909.

Chemical Engineering Science, 1961, Vol. 13, pp. 190 to 191. Pergamon Press Ltd., London. Printed in Great Britain

Shorter Communications

Skewed holding time distributions

(*Received* 18 *June* 1960)

THE use of the holding or residence time distribution to characterize continuous-flow equipment, such as chemical reactors, percolators, chromatographic columns, has been discussed in the studies of DANCKWERTS [1] and KLINKENBERG and SJENITZER [2].

DANCKWERTS' paper introduces the problem in its general form to the chemical engineer. KLINKENBERG and SJENITZER investigate under what conditions a normal or Gaussian distribution is obtained. It appears that this type of distribution is found in many instances where the spread in holding times becomes relatively small, such as in pipe flow, flow in packed beds, flow through a series of identical units.

This note deals with a few typical cases, where the holding time distribution may possess a considerable skewness. Furthermore it will be investigated whether the skewness is characteristic of the physical properties of the system.

The skewness, g, is defined by

$$g^3 = \int_0^\infty (t - \theta)^3 \, R(t) \, dt,$$

where $R(t)$ is the holding time distribution function and θ is the average holding time. Standard deviation and skewness may be calculated from the Laplace-transformed holding time distribution function by a differentiation procedure [4].

The accompanying table and graph summarize the results of the calculations.

Only for the first case is the skewness, γ, proportional to the standard deviation, σ. For all other cases γ is proportional to $\sigma^{4/3}$, at least for low values of σ. The first distribution is skewed for all values of σ, the others become symmetrical as σ approaches zero. It has been

Table 1

	Relative standard deviation $\sigma = \frac{s}{\theta}$	*Relative skewness* $\gamma = \frac{g}{\theta}$
1. One completely mixed stage in series with a piston flow stage	$\frac{\theta_M}{\theta_M + \theta_p}$	$2^{1/3}\sigma$
2. Equal completely mixed stages in series	$\frac{1}{\sqrt{n}}$	$2^{1/3}\,\sigma^{4/3}$
3. Eddy diffusion in the direction of flow*	$\frac{1}{n_E}\{2n_E - 2[1 - \exp(-n_E)]\}^{1/2}$ $= \frac{2}{n_E}$ for large n_E	$\frac{2}{n_E}\left[\frac{3}{2}n_E - 3 + 3(\frac{1}{2}n_E + 1)\exp(-n_E)\right]^{1/3}$ $= 3^{1/3}\,\sigma^{4/3}$ for large n_E
4. Mass transfer between a moving and a stationary phase†	$\frac{fK}{fK + F}\sqrt{\frac{2}{n_k}}$	$\left(\frac{3}{2}\frac{fk + F}{fK}\right)^{1/3}\sigma^{4/3}$

*The expression for the standard deviation has been given by VAN DER LAAN [4].
†Solutions to the underlying differential equations are available from the literature [3].
The Laplace transformed holding time distribution function for this case reads

$$\exp\left[-\frac{Lp}{u} - \frac{fkKLp}{Fu\,(k + fKp)}\right] \quad (p \text{ corresponds to } t).$$

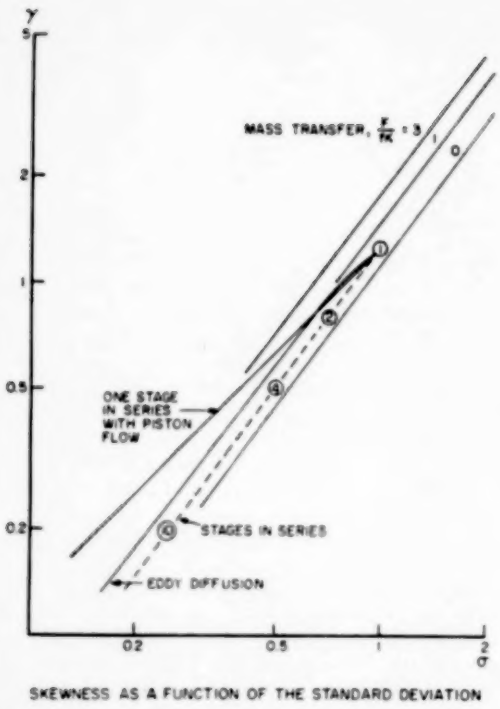

FIG. 1. Skewness as a function of the standard deviation.

pointed out earlier [2] that the latter distributions become Gaussian under this condition.

For the case of mass transfer, values of $\sigma > 1$ are possible when n_k becomes very small. Physically this means that the stationary phase acts as a dead zone. This leads to tailing of the holding time distribution and consequently to large values for σ and γ. Furthermore the skewness increases for increasing capacity F/fK of the stationary phase.

When the higher values of F/fK are left out of consideration, it appears that between $\sigma = 0.5$ and $\sigma = 1$ (1–4 mixed stages) the differences in relative skewness at equal σ between the various cases become small. This means that under many practical conditions the skewness is not very characteristic of the physical process in the system. It also follows that in many cases the standard deviation (or, alternatively, the number of mixed stages) as a single parameter is sufficient to characterize a skewed holding time distribution up to the third moment.

NOTATION

E	eddy diffusivity	m^2/sec
f	volume fraction of stationary phase	
F	volume fraction of moving phase	
g	skewness	sec
k	mass transfer coefficient	sec^{-1}
K	$\left(\frac{\text{concentration in stationary phase}}{\text{concentration in moving phase}}\right)$ at equilibrium	
L	height of vessel	m
n	number of completely mixed stages	
$n_E = \frac{Lu}{E}$	number of diffusion units	
$n_k = \frac{kL}{Fu}$	number of transfer units	
$R(t)$	holding time distribution function	
s	standard deviation	sec
t	time	sec
u	linear velocity	m/sec
$\gamma = \frac{g}{\theta}$	relative skewness	
θ	average holding time	sec
θ_M	average holding time of completely mixed stage	sec
θ_P	residence time of piston flow stage	sec
$\sigma = \frac{s}{\theta}$	relative standard deviation	

J. J. VAN DEEMTER*

Shell Oil Company,
Houston Research Laboratory
Houston, Texas, U.S.A.

*Present address: Koninklijke/Shell-Laboratorium, Amsterdam, Badhuisweg 3, Amsterdam-Noord.

REFERENCES

[1] DANCKWERTS P. V. *Chem. Engng. Sci.* 1953 **2** 1.
[2] KLINKENBERG, A. and SJENITZER F. *Chem. Engng. Sci.* 1956 **5** 258.
[3] KLINKENBERG A. *Industr. Engng. Chem.* 1948 **40** 1992.
[4] VAN DER LAAN E. T. *Chem. Engng. Sci.* 1958 **7** 187.

Chemical Engineering Science, 1961, Vol. 13, pp. 192 to 193. Pergamon Press Ltd., London. Printed in Great Britain

Book Reviews

LEJAREN A. HILLER and ROLFE A. HERBER: **Principles of Chemistry.** McGraw-Hill, New York 1960. xv + 735 pp. $7.75.

THIS textbook has been written for use in courses emphasizing the quantitative aspects of modern chemistry. It is intended primarily for students whose major interest is in the physical sciences and engineering. As stated in the preface, it is planned for that particular type of student who will have had an above-average course in high school chemistry, will understand – and be prepared to use – first-year college-level mathematics and will be interested in both the "how" and "why" of chemistry. The organization and presentation of the subject seems, in general, well-suited for the type of student described. Students without superior background and enthusiasm for the subject would probably find the work too difficult. This reviewer believes that, at the present time, the courses in mathematics and chemistry taught in many secondary schools fail to provide adequate background for the rigorous treatment presented in this book.

The material covered is divided into two major parts: "The Properties of Chemical Substances" and "The Dynamics of Chemical Change." Study of the properties of matter includes emphasis on understanding underlying principles. These principles are developed primarily as logical conclusions based on theoretical considerations. The second part of the text emphasizes mechanisms by which changes in matter are brought about. Related subjects are grouped together within chapters which are relatively self-contained.

Following a brief review of simpler fundamental concepts the periodic classification of the elements is derived from the orderly sequence of atomic numbers. The distribution of electrons surrounding atomic nuclei into shells and subshells, or orbitals, is deduced by reasoning based on the periodic repetition of properties among the elements. The probabilities of location and the properties of electrons in atomic orbitals are described and explained by four quantum numbers defined by a solution of the Schrödinger wave equation.

Electron pairing and the nature of different types of covalent bonds are discussed with emphasis on orbital theory. This is followed by a chapter dealing with the structures of organic compounds and types of reactions they exhibit. This section is descriptive in nature, with little emphasis on underlying principles. Electron transfer and the electrovalent bond, together with the properties and reactions of ionic substances are next considered.

Chapter 5, which follows, is devoted to the discussion of a limited number of elementary substances and inorganic compounds. The reason for the selection of these particular compounds in preference to others is not evident. Theoretical considerations are not stressed.

Chapters 6, 7 and 8 deal with the states of matter and changes in state. Crystal structure and lattice energy are emphasized in the discussion of solids. The properties of gases are related to randomness of distribution in space and the kinetic energy of the particles of which gases are composed. The liquid state is pictured as intermediate in structure and properties. The treatment of the subject matter in these chapters is excellent.

Part 2 – "The Dynamics of Chemical Change" – deals in successive chapters with: the nature of chemical equilibrium; heterogeneous equilibrium and the properties of solutions; ionic equilibria in aqueous solution; chemical thermodynamics; oxidation—reduction reactions; chemical kinetics and catalysis; and radiochemistry and the nuclear properties of matter.

The discussion in each of these topics is clear and comprehensive. Underlying principles are utilized in the logical development of the subject matter. The student will find that sustained concentration is required to secure sound understanding of the material presented; and in a few instances the mathematical demands may prove excessive for first-year college students. This reviewer thinks it probable that some of the advanced topics, particularly in the chapters dealing with chemical thermodynamics and chemical kinetics, will prove to be beyond the grasp of many students at this stage of their work.

Questions and problems at the end of each chapter will be helpful to students in the preparation of their work. A review of mathematical operations and a selected bibliography, grouped according to chapters in the text, will be found in the appendix.

This book is an important contribution among the textbooks available for a rigorous course in general chemistry. In addition to its suitability for use as a textbook in courses for students with superior background, it will be of great value to many teachers in the organization of their own courses.

STUART R. BRINKLEY

W. L. WILKINSON: **Non-Newtonian Fluids.** London: Pergamon Press, Oxford, 1960. 138 pp. 37s. 6d.

AN ELEMENTARY textbook on non-Newtonian fluid flow is o erdue, and it is pleasing to review a book that does not cover ground already adequately covered.

Because of the immense range of non-Newtonian effects and the very real distinctions between various types of behaviour, any author must restrict himself to a small number of topics: this book is built round the mechanics of pipe and channel flow, on the assumption that this is

VOL. 13 1961

the facet of greatest importance to chemical engineers. On this topic the book is sound, readable and up-to-date for both laminar and turbulent flow.

On other topics, the author is on less sure ground. Although his classification of non-Newtonian fluids follows conventional lines, it fails to make any reference to the necessarily tensorial character of any generally-applicable equation of state; for teaching purposes, however, his restriction to *plane shear* will probably be welcomed by students in that it avoids undue mathematical complexity. The sections devoted to linear models for visco-elastic materials (more solid than fluid in their behaviour) prove to be of little practical use, and might well have been left out—though physicists might argue that this apparent lack of utility is the fault of engineers who are slow to use the mechanical properties of high polymers in design.

The chapters on experimental characterization and on viscometric apparatus will probably be useful to those who are not familiar with the standard physical measurements that are commonly made.

Although well printed and bound, the book is rather expensive for the student, who might well expect a more comprehensive volume for 37s. 6d.

J. R. A. Pearson

C. W. Beckett, W. S. Benedict, L. Fano, J. Hilsenrath, H. J. Hoge, J. F. Masi, R. L. Nuttall and Y. S. Touloukian: **Tables of Thermodynamic and Transport properties of Air, argon, carbon-dioxide, carbon monoxide, hydrogen, nitrogen and Steam.** Pergamon Press, London 1960. pp. xiii + 479. £7.

The present volume is, according to the fly-leaf, a revised edition of a series of compilations by the American National Bureau of Standards and was originally published by the U.S. Department of Commerce as N.B.S. Circular 564.

The material presented here, which appears to be identical in practically all respects with that of Circular 564, is the compressibility factor, density, specific heat, enthalpy, entropy and velocity of sound at pressures of 0·01, 0·1, 1, 10, 40, 70 and 100 atm from low temperatures up to temperatures of 3000–5000 °K. Also given are the viscosity, thermal conductivity and values of the vapour pressure for all the materials except air, over a wide range of temperatures and at close temperature intervals. The thermodynamic properties have been obtained using spectroscopic data to give the ideal gas state functions and the virial equation of state to calculate the real gas functions. Tables of ideal gas state thermodynamic functions and virial coefficients suitable for further calculations are included.

The figures presented refer to correlated experimental data and have been arrived at by careful weighting of experimental measurements. In a number of cases use is made of the Lennard–Jones intermolecular potential as an interpolation and extrapolation formula, and the best experimental results are fitted to this. The tabulated values of the thermodynamic properties of steam have been obtained by correlating experimental data with the aid of the Keyes equation. The figures given in the Tables are expressed as ratios of the properties under standard conditions (e.g. 0 °C and 1 atm) and the absolute values of the standard quantities are then clearly given in both c.g.s. and engineering units, so that a single multiplication gives any property in the desired units.

The Tables, which first appeared in 1955, have been found of great value by the reviewer for physical and chemical laboratory work and they should be of considerable use in design calculations of all sorts for engineers. The production and lay-out of the material is good.

The original text was sold at 34s. and though this presumably represented a subsidised price it is difficult to see how the publishers justify an increase to £7 for a re-printed book identical in practically all tabular matter with the original. Owners of the earlier volume appear to have made a substantial capital gain.

Although the publishers mention revisions, these are difficult to find. However, one revision in particular arises in a table of temperature conversions at the end of the book which has been altered to bring it into accord with the convention 0 °C = 273·15 °K, the previous convention in the earlier text being 0 °C = 273·16 °K. It is unfortunate however, that all the enthalpy tables of the earlier text have been reproduced in the present work divided by RT_0 where the value of T_0 = 0 °C = 273·16 °K.

One can only regret that the U.S. Department of Commerce which has given us a number of worthwhile Tables of thermodynamic data at reasonable cost should have found it necessary to discontinue their financial support for this valuable set of Tables.

J. C. McCoubrey.

Chemical Engineering Science, 1961, Vol. 13, pp. 194. Pergamon Press Ltd., London. Printed in Great Britain

Letters to the Editors

I REFER to the paper "Transfer from a Sphere into a Fluid in Laminar Flow" by LINTON and SUTHERLAND [1]. In their paper, the authors refer to an "inferior approximation" in my paper [2] to a method used by AKSEL'RUD. More careful consideration will show that my method, developed independently of ASKEL'RUD's approximation, was actually used to solve a different problem and should be judged in that context. My approach permitted the determination of the complete N_{SH} N_{PE} curve rather than the limiting behaviour for $N_{PE} \to \infty$, alone. Hence it allowed an estimate of the region where the limiting law begins to break down.

I have also been told [3] that in his book, LEVICH [4] has obtained an "exact" expression for $N_{PE} \to \infty$ using a thin boundary layer approximation. His result is $N_{SH} = 0{\cdot}997\, N_{PE}^{1/3}$.

S. K. FRIEDLANDER

Department of Chemical Engineering
The Johns Hopkins University
Baltimore 18
Maryland
U.S.A.

VOL. 13 1961

REFERENCES

[1] LINTON M. and SUTHERLAND K. L. *Chem. Engng. Sci.* 1960 **12** 214.

[2] FRIEDLANDER S. K. *Amer. Inst. Chem. Engrs. J.* 1957 **3** 43.

[3] NATANSON G. L. Personal communication.

[4] LEVICH. *Physicochemical Hydrodynamics* Moscow 1952.

SELECTION OF CURRENT PAPERS OF INTEREST TO CHEMICAL ENGINEERS

P. C. Sholten and K. J. Mysels: Random walk theory of electrodiffusion. *Trans. Farad. Soc.* 1960 **56** 994–1000.

F. J. W. Roughton: Diffusion through membranes followed by diffusion with rapid irreversible immobilization in another medium (e.g. transfer between phases followed by chemical reaction). *Trans. Farad. Soc.* 1960 **56** 1085–1094.

R. S. Schechter and E. H. Wissler: Photochemical reactions in an isothermal laminar-flow chemical reactor. *Appl. Sci. Res.* 1960 **A9** 334–344.

L. N. Tao: Heat transfer of combined free and forced convection in circular and sector tubes. *Appl. Sci. Res.* 1960 **A9** 357–368.

N. C. J. Ros: An analysis of simultaneous gas/liquid flow through a restriction and its application to flowmetering. *Appl. Sci. Res.* 1960 **A9** 374–388.

E. Thornton: Viscosity and thermal conductivity of binary gas mixtures: xenon–krypton, xenon–neon and xenon–helium. *Proc. Phys. Soc. Lond.* 1960 **76** 104–112.

E. W. Billington: Some measurements of the elastic and viscous properties of thixotropic fluids (wax-containing oils). *Proc. Phys. Soc. Lond.* 1960 **76** 127–136.

H. C. Gupta: Diffusion in the presence of barriers. *J. Math. Phys.* 1960 **39** 58–63.

T. Bohlin: On the drag of a rigid sphere moving in a viscous liquid inside a cylindrical tube. *Trans. Royal Inst. Tech., Stockholm.* 1960 Nr. 155.

E. H. Brown: Expansion engines for hydrogen liquefaction. *J. Res. Nat. Bur. Stand.* 1960 **64C** 25–36.

W. H. P. Leslie, J. J. Hunter and D. Robb: Precision temperature measurement outside the laboratory. *Research* 1960 **13** 250–256.

A. Acrivos, M. J. Shah and E. E. Petersen: On the flow of a non-Newtonian liquid on a rotating disk. *J. Appl. Phys.* 1960 **31** 963–968.

A. E. de Vries and M. F. Laranjeira: Thermal diffusion of ternary mixtures. *J. Chem. Phys.* 1960 **32** 1714–1716.

R. S. Brokaw: Thermal conductivity of gas mixtures in chemical equilibrium—II. *J. Chem. Phys.* 1960 **32** 1005–1006.

S. Weissman and S. E. Wood: Vapour-liquid equilibrium of benzene 2, 2, 4-trimethylpentane mixtures. *J. Chem. Phys.* 1960 **32** 1153–1160.

J. J. Clarke and R. Gordon: Thermal conductivity of condensed films. *J. Chem. Phys.* 1960 **32** 705–707.

B. N. Srivastava and S. K. Barua: Thermal conductivity of binary mixtures of diatomic and monatomic gases. *J. Chem. Phys.* 1960 **32** 427–435.

R. E. Walker and A. A. Westenberg: Molecular diffusion studies in gases at high temperatures—IV. Result and interpretation of the CO_2–O_2, CH_4–O_2, H_2–O_2, CO–O_2 and H_2O–O_2 systems. (See also *J. Chem. Phys.* 1958 **29** 1139, 1147 and 1959 **31** 519.) *J. Chem. Phys.* 1960 **32** 436–442.

R. L. Potter and W. Vanderkulk: Computation of the equilibrium composition of burnt gases. *J. Chem. Phys.* 1960 **32** 1304–1307.

R. E. Walker, N. de Hass and A. A. Westenberg: Measurements of multicomponent diffusion coefficients for the CO_2–He–N_2 system, using the point source technique. *J. Chem. Phys.* 1960 **32** 1314–1316.

S. E. Wood and C. H. Masland: Refractive index and dispersion of the benzene–carbon tetrachloride system. *J. Chem. Phys.* 1960 **32** 1385–1388.

S. E. Wood, S. Langer and R. Battine: Refractive index and dispersion of the benzene–methanol system. *J. Chem. Phys.* 1960 **32** 1389–1393.

C. R. Mueller and A. J. Ignatowski: Equilibrium and transport properties of the carbon tetrachloride–methylene chloride system. *J. Chem. Phys.* 1960 **32** 1430–1434.

N. C. Blais and J. B. Mann: Thermal conductivity of Helium and Hydrogen at high temperatures. *J. Chem. Phys.* 1960 **32** 1459–1465.

SELECTION OF CURRENT SOVIET PAPERS OF INTEREST TO CHEMICAL ENGINEERS*

I. V. Mazyukevich: Experimental investigation of heat transfer in condensation of ammonia vapour from its mixture with air on a horizontal tube. *Zh. prikl. Khim.* 1960 **33** 1060–1068.

V. N. Sokolov and A. S. Reshanov: On the effect of time on the dispersion of drops in a stream made turbulent by bubbling gas. *Zh. pruikl. Khim.* 1960 **33** 1068–1075.

M. S. Nemtsov: On chemical processes in heterogeneous systems. *Zh. prikl. Khim.* 1960 **33** 1075–1084.

A. S. Vigdorov and V. V. Kafarov: Generalized expression for the coefficient of useful work of a rectification plate. *Zh. prikl. Khim.* 1960 **33** 1091–1101.

A. I. Rodionov and V. F. Marchenkov: Study of sieve plates with two types of perforations. *Zh. prikl. Khim.* 1960 **33** 1101–1108.

L. Ya. Kolyanor and L. Z. Gorelova: Purification of crude benzene. *Zh. Vses. Khim. Obshch. Mend.* 1960 **5** (1) 18–27.

L. A. Tumarkin and L. A. Toptigin: Main trends in automation of chemical plants in coke-oven works. *Zh. Vses. Khim. Obshch. Mend.* 1960 **5** (1).

I. N. Kuzmunikh, D. M. Popov and B. I. Gorbachev: Bubbler absorption of sulphur dioxide with production of strong solution of ammonium bisulphite. *Khim. Prom.* 1960 (2) 128–132.

V. V. Aronovich and R. S. Patushinskaya: Automatic control of the process of straight hydration of ethylene. *Khim. Prom.* 1960 (2) 143–147.

A. N. Planovski, O. S. Chekov and D. S. Artamonov: On hydraulic resistance of plates of different construction. *Khim. Prom.* 1960 (2) 151–152.

V. A. Malyusov, N. A. Malafeev and N. M. Zhavoronkov: Film rectification of styrene–ethyl benzene mixtures. *Khim. Prom.* 1960 (2) 153–157.

B. S. Bogdanov: Investigation of aerosols in radiochemical reactions. *Zh. fiz. Khim.* 1960 **34** 1044–1049.

S. S. Dhukin: Kinetics of the attachment of mineral particles to air bubbles in flotation. *Zh. fiz. Khim.* 1960 **34** 1053–1059.

B. V. Ioffe: Determination of refractive index of volatile liquid mixtures by means of the Pulfrich refractometer. *Zh. fiz. Khim.* 1960 **34** 1133–1135.

A. F. Anisimov, A. G. Samarski and Yu. A. Alekseev: Automation of the caralyst circulation system on a catalytic cracking plant. *Khim. Tekh. Topl. Masel.* 1960 **5** (6) 1–6.

V. G. Bergo and V. M. Platonov: Calculation of rectification processes on digital computing machines. *Khim. Tekh. Topl. Masel* 1960 **5** (6) 39–44.

V. P. Motylevich: Heat transfer at any point of obtuse bodies washed by a stream of liquid. *Inzh. -Fiz. Zh.* 1960 **3** (5) 17–23.

A. I. Risovich: Experimental investigation of the efficiency of streamlined ribs for GTY regenerators. *Inzh. -Fiz. Zh.* 1960 **3** (5) 24–30.

R. Z. Alimov: Heat and mass transfer in cooling by evaporation of surfaces heated to a high temperature. *Inzh. -Fiz. Zh.* 1960 **3** (5) 31–39.

I. P. Vichnev and N. K. Elukin: Heat transfer in boiling of liquids in tubes. *Inzh. -Fiz. Zh.* 1960 **3** (5) 74–80.

S. Y. Lovkov: Determination of optimum conditions of initial tuning of a Mach-Zehnder type interferometer when used under experimental conditions. *Inzh. -Fiz. Zh.* 1960 **3** (5) 103–105.

V. D. Ermolenko: Application of methods involving the thermo-dynamics of irreversible processes to mass transfer phenomena in colloids. *Inzh. -Fiz. Zh.* 1960 **3** (5) 124–126.

V. N. Adrianov: Certain problems in the theory of radiant heat exchange. *Teploenergetika* 1960 **7** (6) 63–67.

V. G. Fastovski and U. V. Petrovski: Heat transfer and resistance of tube bundles in staggered arrangement. *Teploenergetika* 1960 **7** (6) 69–72.

U. P. Shlikov, E. A. Ganin and N. B. Demkin: Investigation into contact heat transfer. *Teploenergetika* 1960 **4** (6) 72–77.

N. V. Tsederberg, V. N. Popov and N. A. Morozova: Experimental investigation into heat conduction of argon. *Teploenergetika* 1960 **7** (6) 82–86.

Note: The journal *Khimicheskaya Nauki a Promyshlennost* (Chemical Science and Industry) has been renamed *Zhurnal Vsesoyuznego Khimicheskego Obshchestva im. Mendeleeva* (Journal of the All-Union Mendeleev Chemical Society).

---

*To assist readers, translations of any article appearing in the above list can be obtained at a reasonable charge. All orders should be addressed to the Administrative Secretary of the Pergamon Institute at either Headington Hill Hall, Oxford or 122 East 55th Street, New York 22, whichever is more convenient.